

## ***B*-physics observables and electroweak precision data in the CMSSM, mGMSB and mAMSB**

**S. Heinemeyer,<sup>a</sup> X. Miao,<sup>b</sup> S. Su<sup>b</sup> and G. Weiglein<sup>c</sup>**

<sup>a</sup>*Instituto de Fisica de Cantabria (CSIC-UC),  
Avenida de los Castros s/n, 39005 Santander, Spain*

<sup>b</sup>*Department of Physics, University of Arizona,  
1118 E. 4th St., Tucson, AZ 85721, U.S.A.*

<sup>c</sup>*Department of Physics, IPPP University of Durham, Science Laboratories,  
South Rd., Durham DH1 3LE, U.K.*

*E-mail: Sven.Heinemeyer@cern.ch, miao@physics.arizona.edu,  
shufang@physics.arizona.edu, Georg.Weiglein@durham.ac.uk*

**ABSTRACT:** We explore electroweak precision observables (EWPO) and *B*-physics observables (BPO) in the CMSSM, the mGMSB and the mAMSB. We perform a  $\chi^2$  analysis based on the combination of current EWPO and BPO data. For the first time this allows the comparison of the mGMSB and mAMSB in terms of EWPO and BPO with the CMSSM. We find that relatively low mass scales in all three scenarios are favored. However, the current data from EWPO and BPO can hardly exclude any parameters at the level of  $\Delta\chi^2 = 9$ . Remarkably the mAMSB scenario, despite having one free GUT scale parameter less than the other two scenarios, has a somewhat lower total minimum  $\chi^2$ . We present predictions for the lightest Higgs boson mass, based on the  $\chi^2$  analysis of current data, where relatively good compatibility with the bounds from Higgs searches at LEP is found. We also present the predictions for other Higgs sector parameters and SUSY mass scales, allowing to compare the reach of the LHC and the ILC in the three scenarios. We furthermore explore the future sensitivities of the EWPO and BPO for the current best-fit results and for a hypothetical point with somewhat higher mass scales that results in a similar Higgs and SUSY spectrum in the three scenarios. We find that the future improvement of the accuracy of the EWPO and BPO will lead to a significant gain in the indirect parameter determination. The improvement is similar in the CMSSM, mGMSB and mAMSB and will yield constraints to the parameter space even for heavy Higgs and SUSY mass scales.

**KEYWORDS:** Supersymmetry Phenomenology, Higgs Physics, GUT, Electromagnetic Processes and Properties.

---

## Contents

<b>1. Introduction</b>	<b>1</b>
<b>2. The soft SUSY-breaking scenarios</b>	<b>3</b>
<b>3. The precision observables</b>	<b>5</b>
3.1 The $W$ boson mass	6
3.2 The effective leptonic weak mixing angle	7
3.3 The anomalous magnetic moment of the muon	9
3.4 The mass of the lightest $\mathcal{CP}$ -even MSSM Higgs boson	11
3.5 The decay $b \rightarrow s\gamma$	13
3.6 The branching ratio for $B_s \rightarrow \mu^+\mu^-$	14
<b>4. <math>\chi^2</math> analysis for CMSSM, mGMSB, mAMSB</b>	<b>16</b>
4.1 Analysis of high-scale parameters	18
4.1.1 CMSSM	18
4.1.2 mGMSB	18
4.1.3 mAMSB	19
4.2 Low-energy analysis	19
<b>5. Future sensitivities</b>	<b>32</b>
5.1 Analysis of high-scale parameters	33
5.1.1 CMSSM	33
5.1.2 mGMSB	34
5.1.3 mAMSB	35
5.2 Low-energy analysis	39
<b>6. Conclusions</b>	<b>40</b>

---

## 1. Introduction

The dimensionality of the parameter space of the minimal supersymmetric extension of the Standard Model (MSSM) [1, 2] is so high that phenomenological analyses often make simplifying assumptions that reduce drastically the number of parameters. One assumption that is frequently employed is that (at least some of) the soft SUSY-breaking parameters are universal at some high input scale, before renormalization. One model based on this simplification is the constrained MSSM (CMSSM), in which all the soft SUSY-breaking scalar masses  $m_0$  are assumed to be universal at the GUT scale, as are the soft SUSY-breaking gaugino masses  $m_{1/2}$  and trilinear couplings  $A_0$ . The assumption that squarks and

sleptons with the same gauge quantum numbers have the same masses is motivated by the absence of identified supersymmetric contributions to flavor-changing neutral interactions and rare decays (see ref. [3] and references therein). Universality between squarks and sleptons with different gauge interactions may be motivated by some GUT scenarios [4]. Other “simplified” versions of the MSSM that are based on (some) unification at a higher scale are (minimal) Gauge mediated SUSY-breaking (mGMSB) [5–7] and (minimal) Anomaly mediated SUSY-breaking (mAMSB) [8–10].

One approach to analyze the reduced parameter spaces of the CMSSM, mGMSB, mAMSB or other GUT-based models is a combined  $\chi^2$  analysis of electroweak precision observables (EWPO) and of  $B$ -physics observables (BPO). Those analyses have yet been restricted to the CMSSM or the non-universal Higgs mass (NUHM) model [11–18] (see also refs. [19–22]). In these analyses also the cold dark matter density constraint imposed by WMAP and other cosmological data [23] has been taken into account. In this case the lightest SUSY particle (LSP), assumed to be the lightest neutralino, is required to give rise to the correct amount of cold dark matter (CDM).

The aim of this paper is to perform a  $\chi^2$  analysis to compare the predictions of the CMSSM, mGMSB and mAMSB. The mechanisms to fulfill the CDM constraints are less clear in mGMSB and mAMSB as compared to the CMSSM. In order to treat the three soft SUSY-breaking scenarios on the same footing, we do not impose the CDM constraint in our analysis and scan over the full parameter space of the three models. Concerning the impact of CDM constraints, it should be kept in mind that small modifications of the physics scenario that concern neither the theory basis nor the collider phenomenology could have a strong impact on the CDM derived bounds. If the amount of CDM appears to be too small, other DM candidates can provide the necessary amount to reach the measured density (see also ref. [24] for a recent analysis). If, on the other hand, the CDM density appears to be too large, a small amount of  $R$ -parity violation [25], not affecting the collider phenomenology, could remove the CDM bound completely. Other possibilities not invoking  $R$ -parity violation are “thermal inflation” [26] or “late-time entropy injection” [27]. They could offer a mechanism for bringing a high CDM density into agreement with the WMAP measurements. Applying the WMAP constraints always assumes “standard cosmology”. Therefore the choice of not imposing the CDM constraints, as we do, can be motivated in the wider class of models under investigation here. For the CMSSM we have checked that including the CDM constraint previous results could be reproduced.

The set of EWPO included in our analysis is the  $W$  boson mass  $M_W$ , the effective leptonic weak mixing angle  $\sin^2 \theta_{\text{eff}}$ , the anomalous magnetic moment of the muon  $(g-2)_\mu$ , and the mass of the lightest  $\mathcal{CP}$ -even MSSM Higgs boson mass  $M_h$ . In addition, we also include two BPO: the branching ratios  $\text{BR}(b \rightarrow s\gamma)$  and  $\text{BR}(B_s \rightarrow \mu^+\mu^-)$ . Other BPO such as  $\text{BR}(B_u \rightarrow \tau\nu_\tau)$  and the  $B_s$  mass mixing parameter  $\Delta M_{B_s}$  have shown to possess only a low sensitivity with the current precision in this kind of  $\chi^2$  analysis [13]. For the evaluation of the BPO we assume minimal flavor violation (MFV) at the electroweak scale. Non-minimal flavor violation (NMFV) effects can be induced by RGE running from the high scale, see e.g. ref. [28], that may amount to  $\sim 10\%$  of the SUSY corrections. These additional contributions are neglected throughout the paper. For each observable,

we construct the  $\chi^2$  function including both theoretical and experimental systematic uncertainties, as well as statistical errors. Our analysis should be seen as an exploratory study, with the main goal to compare the three soft SUSY-breaking scenarios. A more elaborate investigation using more precision data and a refined  $\chi^2$  analysis, see e.g. ref. [18], can be performed in a later stage and is beyond the scope of this paper.

The rest of the paper is organized as follows. We first briefly review the three soft SUSY-breaking scenarios and the investigated parameter space. In section 3 we shortly describe the current status of the EWPO and BPO that we use, our treatment of the available theoretical calculations and their uncertainties, as well as their present experimental values. The analysis within the three soft SUSY-breaking scenarios using current experimental data can be found in section 4. In a final step we assume an improvement of the various EWPO and BPO accuracies from future experimental data and theory calculations and analyze in section 5 the improvement in the parameter determination. The conclusions can be found in section 6.

## 2. The soft SUSY-breaking scenarios

The fact that no SUSY partners of the SM particles have so far been observed means that low-energy SUSY cannot be realized as an unbroken symmetry in nature, and SUSY models thus have to incorporate additional Supersymmetry breaking interactions. This is achieved by adding to the Lagrangian (defined by the  $SU(3)_C \times SU(2)_L \times U(1)_Y$  gauge symmetry and the superpotential  $W$ ) some further interaction terms that respect the gauge symmetry but break Supersymmetry (softly, i.e. no quadratic divergences appear), so called “soft SUSY-breaking” (SSB) terms. Assuming that the  $R$ -parity symmetry [25] is conserved, which we do in this paper for all SUSY breaking scenarios, reduces the amount of new soft terms allowed in the Lagrangian. Choosing a particular soft SUSY-breaking pattern allows further reduction of the number of free parameters and the construction of predictive models. The three most prominent scenarios for such models are

- *CMSSM* (constrained Minimal Supersymmetric Standard Model) [29, 30].<sup>1</sup>

Apart from the SM parameters (for the experimental values of the SM input parameters we use ref. [33]), 4 parameters and a sign are required to define the CMSSM scenario:

$$\{ m_0, m_{1/2}, A_0, \tan \beta, \text{sign}(\mu) \}. \quad (2.1)$$

While  $m_0$ ,  $m_{1/2}$  and  $A_0$  define the scalar and fermionic masses and the trilinear couplings at the GUT scale ( $\sim 10^{16}$  GeV),  $\tan \beta$  (the ratio of the two vacuum expectation values) and the  $\text{sign}(\mu)$  ( $\mu$  is the supersymmetric Higgs mass parameter) are defined at the low-energy scale. For our numerical analyses, see sections 4 and 5, we

---

<sup>1</sup>For reviews see also ref. [1] and the first article in ref. [2].

have scanned over the following parameter space

$$\begin{aligned}
 50 \text{ GeV} &\leq m_0 \leq 2 \text{ TeV} , \\
 50 \text{ GeV} &\leq m_{1/2} \leq 2 \text{ TeV} , \\
 -3 \text{ TeV} &\leq A_0 \leq 3 \text{ TeV} , \\
 1.5 &\leq \tan \beta \leq 60 , \\
 \text{sign } \mu &= \pm 1.
 \end{aligned}
 \tag{2.2}$$

- *mGMSB* (minimal Gauge Mediated SUSY-Breaking) [7].

A very promising alternative to the CMSSM is based on the hypothesis that the soft SUSY-breaking occurs at relatively low energy scales and is mediated mainly by gauge interactions through the so-called “messenger sector” [5–7, 31, 32]. Also in this scenario, the low-energy parameters depend on 4 parameters and a sign,

$$\{ M_{\text{mess}}, N_{\text{mess}}, \Lambda, \tan \beta, \text{sign}(\mu) \} ,
 \tag{2.3}$$

where  $M_{\text{mess}}$  is the overall messenger mass scale;  $N_{\text{mess}}$  is a number called the messenger index, parameterizing the structure of the messenger sector;  $\Lambda$  is the universal soft SUSY-breaking mass scale felt by the low-energy sector. The phenomenology of mGMSB is characterized by the presence of a very light gravitino  $\tilde{G}$  with mass given by  $m_{3/2} = m_{\tilde{G}} = \frac{F}{\sqrt{3}M_P} \simeq \left(\frac{\sqrt{F}}{100 \text{ TeV}}\right)^2 2.37 \text{ eV}$  [34], where  $\sqrt{F}$  ( $\sim M_{\text{mess}}$ ) is the fundamental scale of SSB and  $M_P = 2.44 \times 10^{18} \text{ GeV}$  is the reduced Planck mass. Since  $\sqrt{F}$  is typically of order 100 TeV, the  $\tilde{G}$  is always the LSP in these theories. The numerical analysis in sections 4 and 5 is based on the following scatter ranges:

$$\begin{aligned}
 10^4 \text{ GeV} &\leq \Lambda \leq 2 \times 10^5 \text{ GeV} , \\
 1.01 \Lambda &\leq M_{\text{mess}} \leq 10^5 \Lambda , \\
 1 &\leq N_{\text{mess}} \leq 8 , \\
 1.5 &\leq \tan \beta \leq 60 , \\
 \text{sign } \mu &= \pm 1.
 \end{aligned}
 \tag{2.4}$$

Values of  $N_{\text{mess}}$  larger than  $\sim 8$  result in problems with perturbativity of the gauge interactions at very high scales [7].

- *mAMSB* (minimal Anomaly Mediated SUSY-Breaking) [8–10].

In this model, SUSY breaking happens on a separate brane and is communicated to the visible world via the super-Weyl anomaly. The particle spectrum is determined by 3 parameters and a sign:

$$\{ m_{\text{aux}}, m_0, \tan \beta, \text{sign}(\mu) \}.
 \tag{2.5}$$

The overall scale of SUSY particle masses is set by  $m_{\text{aux}}$ , which is the vacuum expectation value of the auxiliary field in the supergravity multiplet.  $m_0$  is introduced

as a phenomenological parameter to avoid negative slepton mass squares, for other approaches to this problem see refs. [8, 35–38]. The scatter parameter space for the numerical analysis in sections 4 and 5 is chosen to be

$$\begin{aligned}
 20 \text{ TeV} &\leq m_{\text{aux}} \leq 200 \text{ TeV}, \\
 0 &\leq m_0 \leq 2 \text{ TeV}, \\
 1.5 &\leq \tan \beta \leq 60, \\
 \text{sign } \mu &= \pm 1.
 \end{aligned}
 \tag{2.6}$$

The upper bound on  $m_0$  has been chosen in agreement with the CMSSM scenario. Concerning  $m_{\text{aux}}$ , being linked to the SUSY-breaking scale, we have chosen the upper bound of 200 TeV, which should be sufficient to cover the essential features of the low-energy spectrum of mAMSB.

The low-energy spectra for all soft SUSY-breaking scenarios have been evaluated with the program `SoftSUSY` [39] (version 2.0), taking into account the experimental constraints from SUSY particle searches [33]. The parameter ranges have been sampled by a random scan over the four- (three-)dimensional space of the free parameters in the CMSSM and mGMSB (in mAMSB). The sign of  $\mu$  has been treated as another free parameter. For each soft SUSY-breaking scenario about  $\sim 10^5$  random points have been generated. This large number ensures that all regions of the four- (three-)dimensional hypercube of free parameters are reached.

### 3. The precision observables

The considered data set includes four EWPO [40]: the mass of the  $W$  boson,  $M_W$ , the effective leptonic weak mixing angle,  $\sin^2 \theta_{\text{eff}}$ , the anomalous magnetic moment of the muon,  $(g-2)_\mu$ , and the mass of the lightest  $\mathcal{CP}$ -even MSSM Higgs boson,  $M_h$ . Another EWPO, the total  $Z$  boson width,  $\Gamma_Z$ , has shown to have little sensitivity to SUSY corrections [13, 41]. In addition, we include two BPO: the branching ratios  $\text{BR}(b \rightarrow s\gamma)$  and  $\text{BR}(B_s \rightarrow \mu^+\mu^-)$ . Other BPO such as  $\text{BR}(B_u \rightarrow \tau\nu_\tau)$  and the  $B_s$  mass-mixing parameter  $\Delta M_{B_s}$  with their current experimental and theoretical precision have only a small sensitivity to SUSY corrections [13].

In this section we start our analysis by recalling the current precisions of the experimental results and the theoretical predictions for all these observables. In the following, we refer to the theoretical uncertainties from unknown higher-order corrections as ‘intrinsic’ theoretical uncertainties and to the uncertainties induced by the experimental errors of the SM input parameters as ‘parametric’ theoretical uncertainties. We do not discuss here the theoretical uncertainties in the renormalization-group running between the high-scale input parameters and the weak scale. At present, these uncertainties are less important than the experimental and theoretical uncertainties in the precision observables.

Assuming that the six observables listed above are uncorrelated, a  $\chi^2$  fit has been performed with

$$\chi^2 \equiv \sum_{n=1}^4 \left( \frac{R_n^{\text{exp}} - R_n^{\text{theo}}}{\sigma_n} \right)^2 + \chi_{M_h}^2 + \chi_{B_s}^2. \quad (3.1)$$

Here  $R_n^{\text{exp}}$  denotes the experimental central value of the  $n$ th observable ( $M_W$ ,  $\sin^2 \theta_{\text{eff}}$ ,  $(g-2)_\mu$  and  $\text{BR}(b \rightarrow s\gamma)$ ),  $R_n^{\text{theo}}$  is the corresponding MSSM prediction and  $\sigma_n$  denotes the combined error, as specified below.  $\chi_{M_h}^2$  and  $\chi_{B_s}^2$  denote the  $\chi^2$  contribution coming from the experimental limits on the lightest  $\mathcal{CP}$ -even MSSM Higgs boson mass and on  $\text{BR}(B_s \rightarrow \mu^+ \mu^-)$ , respectively, which are also described below. In section 5 we assume a future measurement of  $M_h$  and use  $\chi_{M_h}^2 = ((M_h^{\text{exp}} - M_h^{\text{theo}})/\sigma_{M_h})^2$ .

We also list below the parametric uncertainties in the predictions on the observables induced by the experimental uncertainties of all relevant SM input parameters. These parametric uncertainties are then added to the other errors (intrinsic and experimental) of the observables as described in the text below. A particularly important input parameter in this respect is the top-quark mass. We evaluate the SUSY spectrum and the observables for each data point for the nominal value,  $m_t = 171.4$  GeV [42] but include the error induced by the experimental uncertainty of  $\delta m_t^{\text{exp}} = 2.1$  GeV.<sup>2</sup>

### 3.1 The $W$ boson mass

The  $W$  boson mass can be evaluated from

$$M_W^2 \left( 1 - \frac{M_W^2}{M_Z^2} \right) = \frac{\pi\alpha}{\sqrt{2}G_F} (1 + \Delta r), \quad (3.2)$$

where  $\alpha$  is the fine structure constant and  $G_F$  the Fermi constant. The radiative corrections are summarized in the quantity  $\Delta r$  [44]. The prediction for  $M_W$  within the SM or the MSSM is obtained by evaluating  $\Delta r$  in these models and solving eq. (3.2) for  $M_W$ .

We include the complete one-loop result in the MSSM [45, 46] as well as higher-order QCD corrections of SM type that are of  $\mathcal{O}(\alpha\alpha_s)$  [47, 48] and  $\mathcal{O}(\alpha\alpha_s^2)$  [49, 50]. Furthermore, we incorporate supersymmetric corrections of  $\mathcal{O}(\alpha\alpha_s)$  [51] and of  $\mathcal{O}(\alpha_t^2)$  [52, 53] to the quantity  $\Delta\rho$ , which involves the leading universal corrections induced by the mass splitting between fields in an isospin doublet [54].<sup>3</sup>

The remaining intrinsic theoretical uncertainty in the prediction for  $M_W$  within the MSSM is still significantly larger than in the SM. For typical parameters (based on ref. [53]) we estimate the current and future intrinsic uncertainties to

$$\Delta M_W^{\text{intr,current}} \lesssim 10 \text{ MeV}, \quad \Delta M_W^{\text{intr,future}} = 2 \text{ MeV}, \quad (3.3)$$

depending on the mass scale of the supersymmetric particles. The parametric uncertainties are dominated by the experimental error of the top-quark mass and the hadronic contribution to the shift in the fine structure constant. Their current errors induce the following

---

<sup>2</sup>Using the most recent experimental value,  $m_t = 172.6$  GeV, including the experimental error of  $\delta m_t^{\text{exp}} = 1.4$  GeV [43], see below, would have a relatively small impact on our analysis, see also the discussion at the end of section 4.2.

<sup>3</sup>A recent re-evaluation of  $M_W$  [55] shows good agreement with the values used here.

parametric uncertainties [13, 40]

$$\delta m_t^{\text{current}} = 2.1 \text{ GeV} \quad \Rightarrow \quad \Delta M_W^{\text{para}, m_t, \text{current}} \approx 13 \text{ MeV}, \quad (3.4)$$

$$\delta(\Delta\alpha_{\text{had}}^{\text{current}}) = 35 \times 10^{-5} \quad \Rightarrow \quad \Delta M_W^{\text{para}, \Delta\alpha_{\text{had}}, \text{current}} \approx 6.3 \text{ MeV}. \quad (3.5)$$

At the ILC, the top-quark mass will be measured with an accuracy of about 100 MeV [56, 57]. The parametric uncertainties induced by the future experimental errors of  $m_t$  and  $\Delta\alpha_{\text{had}}$  [58] will then be [59]

$$\delta m_t^{\text{future}} = 0.1 \text{ GeV} \quad \Rightarrow \quad \Delta M_W^{\text{para}, m_t, \text{future}} \approx 1 \text{ MeV}, \quad (3.6)$$

$$\delta(\Delta\alpha_{\text{had}}^{\text{future}}) = 5 \times 10^{-5} \quad \Rightarrow \quad \Delta M_W^{\text{para}, \Delta\alpha_{\text{had}}, \text{future}} \approx 1 \text{ MeV}. \quad (3.7)$$

The present experimental value of  $M_W$  is [60–64], see also ref. [65].

$$M_W^{\text{exp}, \text{current}} = 80.398 \pm 0.025 \text{ GeV}. \quad (3.8)$$

With the GigaZ option of the ILC (i.e. high-luminosity running at the  $Z$  resonance and the  $WW$  threshold) the  $W$ -boson mass will be determined with an accuracy of about [66, 67]

$$\delta M_W^{\text{exp}, \text{future}} = 7 \text{ MeV}. \quad (3.9)$$

We add the experimental and theoretical errors for  $M_W$  (for the current situation as well as for the future estimates) in quadrature in our analysis.

The predictions for  $M_W$  in the three scenarios are compared with each other in figure 1 (for  $\mu > 0$ , see section 3.3), where the  $W$  boson mass is shown as a function of the lighter scalar top quark mass,  $m_{\tilde{t}_1}$ . The shown areas are obtained as the borders of the scan over the parameters as specified in eqs. (2.2), (2.4) and (2.6). The upper limit of  $m_{\tilde{t}_1}$  reached in the three scenarios is similar in the CMSSM and in mAMSB (related to the upper bounds on  $m_{1/2}$  and  $m_{\text{aux}}$ ), whereas the allowed area for  $m_{\tilde{t}_1}$  is somewhat larger in mGMSB. Since these upper bounds depend on the chosen ranges for the high-energy scale parameters, they should be considered to be artificial and it does not make sense to compare the three soft SUSY-breaking scenarios in these terms. Consequently, we have truncated the plot at  $m_{\tilde{t}_1} = 3 \text{ TeV}$ . The range of the  $M_W$  prediction is very similar in the three scenarios. The solid (dashed) lines represent the currently allowed  $1\sigma$  interval from the experimental uncertainty (including also theoretical uncertainties). This indicates that at the current level of accuracy all three models agree similarly well with the experimental measurement. A preference for relatively low values of  $m_{\tilde{t}_1}$  is visible, which is most prominent in mGMSB.

### 3.2 The effective leptonic weak mixing angle

The effective leptonic weak mixing angle at the  $Z$  boson peak can be written as

$$\sin^2 \theta_{\text{eff}} = \frac{1}{4} \left( 1 - \text{Re} \frac{v_{\text{eff}}}{a_{\text{eff}}} \right), \quad (3.10)$$

where  $v_{\text{eff}}$  and  $a_{\text{eff}}$  denote the effective vector and axial couplings of the  $Z$  boson to charged leptons. Our theoretical prediction for  $\sin^2 \theta_{\text{eff}}$  contains the same class of higher-order contributions as described in section 3.1, supplemented with a small correction based on ref. [41], see the evaluation in ref. [13].



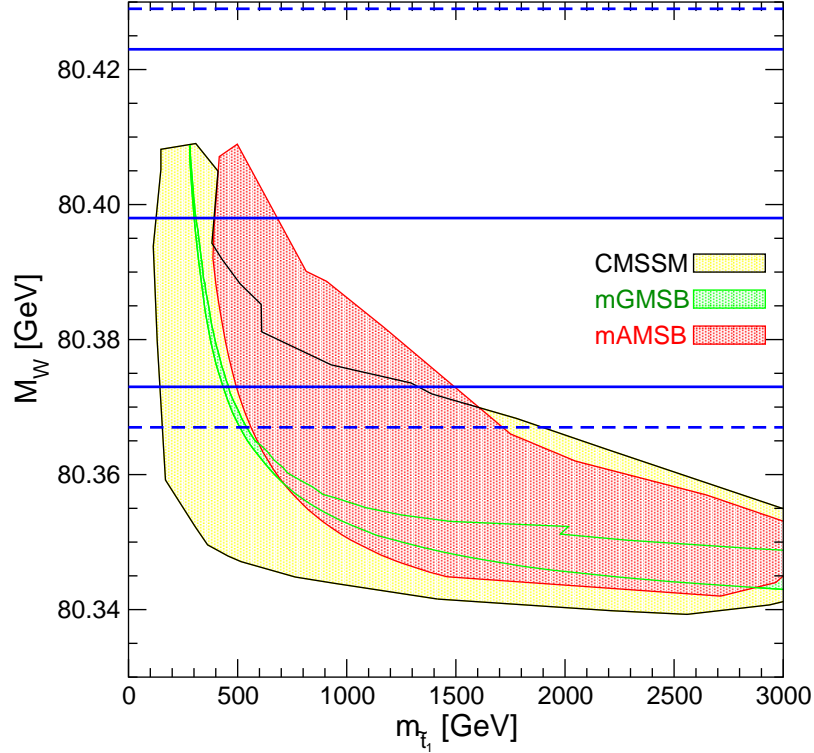


**Figure 1:** The predictions for  $M_W$  as obtained from the parameter scan are shown as a function of  $m_{\tilde{t}_1}$  for the three soft SUSY-breaking scenarios for  $\mu > 0$ . The top quark mass has been fixed to  $m_t = 171.4$  GeV. The solid (dashed) lines indicate the currently allowed  $1\sigma$  interval from the experimental uncertainty (including also theoretical uncertainties).

For the intrinsic theoretical uncertainty in the prediction for  $\sin^2 \theta_{\text{eff}}$  we use an estimate (based on refs. [53, 13, 68]) of

$$\Delta \sin^2 \theta_{\text{eff}}^{\text{intr,current}} \lesssim 12 \times 10^{-5}, \quad \Delta \sin^2 \theta_{\text{eff}}^{\text{intr,future}} \lesssim 2 \times 10^{-5}. \quad (3.11)$$

The experimental errors of  $m_t$  and  $\Delta\alpha_{\text{had}}$  induce the following parametric uncertainties [41]

$$\delta m_t^{\text{current}} = 2.1 \text{ GeV} \quad \Rightarrow \quad \Delta \sin^2 \theta_{\text{eff}}^{\text{para},m_t,\text{current}} \approx 6.3 \times 10^{-5}, \quad (3.12)$$

$$\delta(\Delta\alpha_{\text{had}}^{\text{current}}) = 35 \times 10^{-5} \quad \Rightarrow \quad \Delta \sin^2 \theta_{\text{eff}}^{\text{para},\Delta\alpha_{\text{had}},\text{current}} \approx 12 \times 10^{-5}. \quad (3.13)$$

For the future accuracies we assume

$$\delta m_t^{\text{future}} = 0.1 \text{ GeV} \quad \Rightarrow \quad \Delta \sin^2 \theta_{\text{eff}}^{\text{para},m_t,\text{future}} \approx 0.4 \times 10^{-5}, \quad (3.14)$$

$$\delta(\Delta\alpha_{\text{had}}^{\text{future}}) = 5 \times 10^{-5} \quad \Rightarrow \quad \Delta \sin^2 \theta_{\text{eff}}^{\text{para},\Delta\alpha_{\text{had}},\text{future}} \approx 1.8 \times 10^{-5}. \quad (3.15)$$

The experimental value is [60, 61]<sup>4</sup>

$$\sin^2 \theta_{\text{eff}}^{\text{exp,current}} = 0.23153 \pm 0.00016. \quad (3.16)$$

<sup>4</sup>It should be noted that this value is determined mostly by two measurements that are only marginally compatible: the forward-backward asymmetry for  $b$  quarks  $A_{\text{FB}}^b$ , and the left-right asymmetry for electrons  $A_{\text{LR}}^e$  [60].

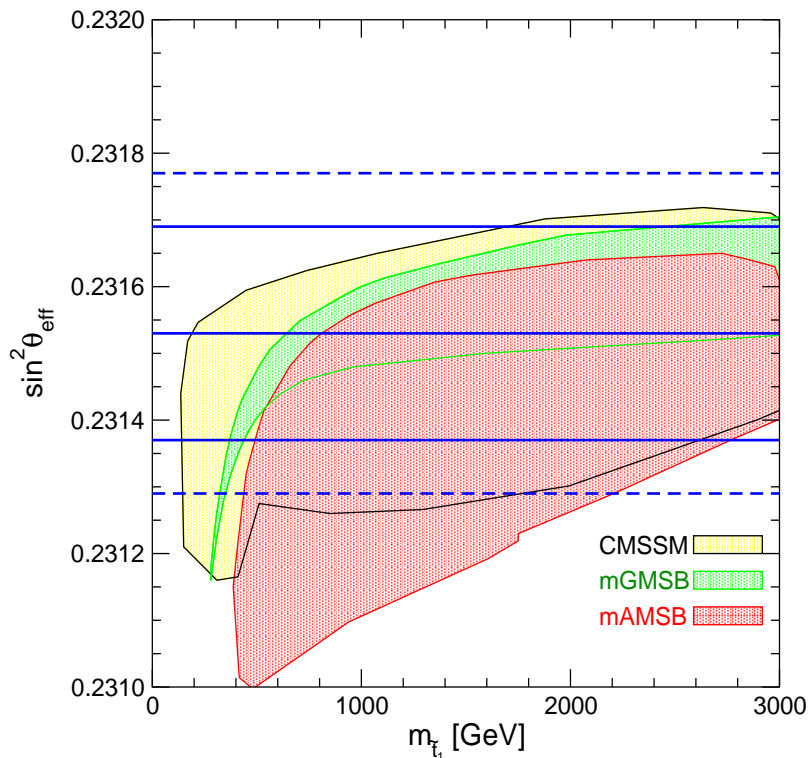


**Figure 2:** The predictions for  $\sin^2 \theta_{\text{eff}}$  as obtained from the parameter scan are shown as a function of  $m_{\tilde{t}_1}$  for the three soft SUSY-breaking scenarios for  $\mu > 0$ . The top quark mass has been fixed to  $m_t = 171.4$  GeV. The solid (dashed) lines indicate the currently allowed  $1\sigma$  interval from the experimental uncertainty (including also theoretical uncertainties).

The experimental accuracy will improve to about

$$\delta \sin^2 \theta_{\text{eff}}^{\text{exp, future}} = 1.3 \times 10^{-5}. \quad (3.17)$$

at GigaZ [69] (see also ref. [70] for a corresponding discussion). We add the experimental and theoretical errors for  $\sin^2 \theta_{\text{eff}}$  in quadrature in our analysis.

The predictions for  $\sin^2 \theta_{\text{eff}}$  in the three scenarios are compared with each other in figure 2 (for  $\mu > 0$ , see section 3.3), where the effective weak mixing angle is shown as a function of the lighter scalar top quark mass,  $m_{\tilde{t}_1}$  (truncated at  $m_{\tilde{t}_1} = 3$  TeV). As for  $M_W$ , the range of the  $\sin^2 \theta_{\text{eff}}$  prediction is very similar in the three scenarios. Smallest values are reached in mAMSB. The solid (dashed) lines indicate the currently allowed  $1\sigma$  interval from the experimental uncertainty (including also theoretical uncertainties). This indicates, as for  $M_W$ , that at the current level of accuracy all three models agree equally well with the experimental data, where no preference for  $m_{\tilde{t}_1}$  can be deduced.

### 3.3 The anomalous magnetic moment of the muon

The SM prediction for the anomalous magnetic moment of the muon,  $a_\mu = \frac{1}{2}(g - 2)_\mu$ , (see refs. [71 – 76] for reviews) depends in particular on the evaluation of QED contributions

(see refs. [77–79] for recent updates), the hadronic vacuum polarization and light-by-light (LBL) contributions. The former have been evaluated in refs. [75, 80–85] and the latter in refs. [86–89]. The evaluations of the hadronic vacuum polarization contributions using  $e^+e^-$  and  $\tau$  decay data give somewhat different results. In view of the fact that recent  $e^+e^-$  measurements tend to confirm earlier results, whereas the correspondence between previous  $\tau$  data and preliminary data from BELLE [90] is not so clear, and also in view of the additional uncertainties associated with the isospin transformation from  $\tau$  decay (see ref. [91]), we use here the latest estimate based on  $e^+e^-$  data [85]:

$$a_\mu^{\text{theo}} = (11\,659\,180.5 \pm 4.4_{\text{had}} \pm 3.5_{\text{LBL}} \pm 0.2_{\text{QED+EW}}) \times 10^{-10}, \quad (3.18)$$

where the source of each error is labeled. We note that the more recent  $e^+e^-$  data sets of refs. [92–95] have been partially included in the updated estimate of  $(g-2)_\mu$ .

The SM prediction is to be compared with the final result of the Brookhaven  $(g-2)_\mu$  experiment E821 [96, 97], namely:

$$a_\mu^{\text{exp}} = (11\,659\,208.0 \pm 6.3) \times 10^{-10}, \quad (3.19)$$

leading to an estimated discrepancy [85, 98]

$$a_\mu^{\text{exp}} - a_\mu^{\text{theo}} = (27.5 \pm 8.4) \times 10^{-10}, \quad (3.20)$$

equivalent to a  $3.3\text{-}\sigma$  effect.<sup>5</sup> While it would be premature to regard this deviation as a firm evidence for new physics, within the context of SUSY, it does indicate a preference for a non-zero contribution from superpartners.

Concerning the MSSM contribution, the complete one-loop result was evaluated over a decade ago [99]. In view of the correlation between the signs of  $(g-2)_\mu$  and of  $\mu$  [100], variants of the MSSM with  $\mu < 0$  (or more precisely a positive  $\mu \cdot M_2$ , where we use the convention of positive  $M_2$  for the three scenarios) are already severely challenged by the present data on  $a_\mu$ . However, as indicated in section 2, we have analyzed both signs of  $\mu$ , and correspondingly find a strong preference for  $\mu > 0$ , see figure 3 below. Therefore, in the other plots shown here we focus on the case  $\mu > 0$ .

In addition to the full one-loop contributions, the leading QED two-loop corrections have also been evaluated [101]. Further corrections at the two-loop level have been obtained more recently [102, 103], leading to corrections to the one-loop result that are  $\lesssim 10\%$ . These corrections are taken into account in our analysis according to the approximate formulas given in refs. [102, 103].

The current intrinsic uncertainties in the SUSY contributions to  $a_\mu$  can be estimated to be  $\lesssim 1 \times 10^{-10}$  [73]. We assume that in the future the uncertainty in eq. (3.20) will be reduced by a factor two. All errors are added in quadrature.

The predictions for  $\Delta a_\mu^{\text{SUSY}}$  in the three scenarios are compared with each other in figure 3, where the anomalous magnetic moment of the muon is shown as a function of the

---

<sup>5</sup>Three other recent evaluations yield slightly different numbers [75, 82, 74], but similar discrepancies with the SM prediction.

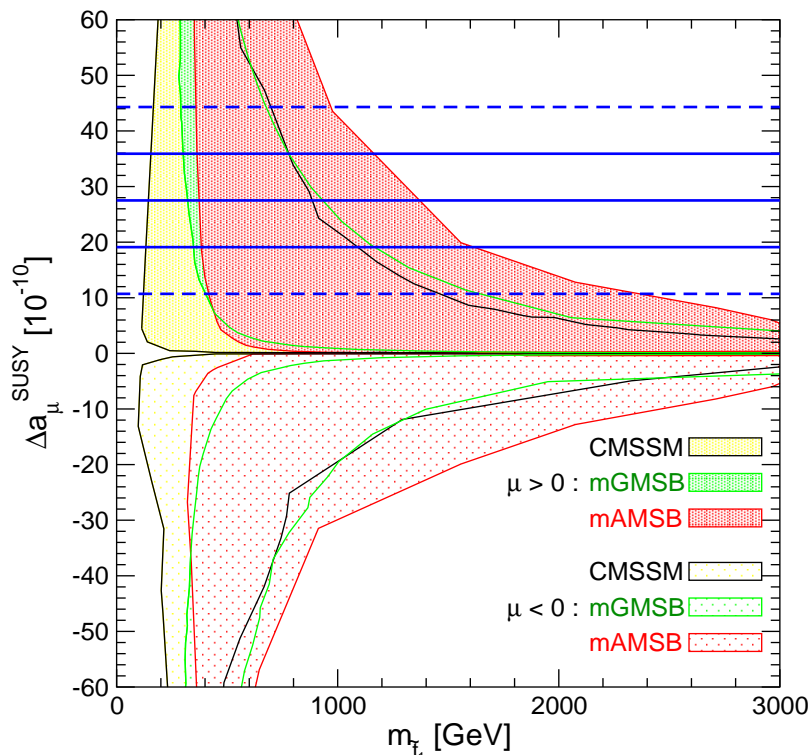


**Figure 3:** The predictions for  $\Delta a_\mu^{\text{SUSY}}$  as obtained from the parameter scan are shown as a function of  $m_{\tilde{t}_1}$  for the three soft SUSY-breaking scenarios. The full (dot) shaded areas are obtained for  $\mu > (<)0$ , resulting in  $\Delta a_\mu^{\text{SUSY}} > (<)0$ . The top quark mass has been fixed to  $m_t = 171.4$  GeV. The solid (dashed) lines indicate the currently allowed  $1(2)\sigma$  intervals of the experimental uncertainty.

lighter scalar top quark mass,  $m_{\tilde{t}_1}$  (truncated at  $m_{\tilde{t}_1} = 3$  TeV). The full (dot) shaded areas are obtained for  $\mu > (<)0$ , resulting in  $\Delta a_\mu^{\text{SUSY}} > (<)0$ . The range of the  $a_\mu$  prediction is very similar in the three scenarios. The solid (dashed) lines indicate the currently allowed  $1(2)\sigma$  intervals of the experimental uncertainty. It becomes apparent that points with  $\mu < 0$  are strongly disfavored by the analysis of  $(g-2)_\mu$ . Furthermore, at the  $2\sigma$  level stop masses heavier than  $\sim 2$  TeV are clearly disfavored.

### 3.4 The mass of the lightest $\mathcal{CP}$ -even MSSM Higgs boson

The mass of the lightest  $\mathcal{CP}$ -even MSSM Higgs boson can be predicted in terms of the other MSSM parameters. At the tree level, the two  $\mathcal{CP}$ -even Higgs boson masses are obtained as functions of  $M_Z$ , the  $\mathcal{CP}$ -odd Higgs boson mass  $M_A$ , and  $\tan\beta$ , whereas other parameters enter into the loop corrections. We employ the Feynman-diagrammatic method [104, 105] for the theoretical prediction of  $M_h$ , using the code `FeynHiggs` [106–109], which includes all numerically relevant known higher-order corrections. The status of these results can be summarized as follows. For the one-loop part, the complete result within the MSSM is known [110, 104, 111]. Computation of the two-loop effects is quite advanced: see ref. [108] and references therein. These include the strong corrections at  $\mathcal{O}(\alpha_t\alpha_s)$  and Yukawa cor-

rections at  $\mathcal{O}(\alpha_t^2)$  to the dominant one-loop  $\mathcal{O}(\alpha_t)$  term, and the strong corrections from the bottom/sbottom sector at  $\mathcal{O}(\alpha_b\alpha_s)$ . In the case of the  $b/\tilde{b}$  sector corrections, an all-order resummation of the  $\tan\beta$ -enhanced terms,  $\mathcal{O}(\alpha_b(\alpha_s \tan\beta)^n)$ , is also known [112, 113]. More recently, the  $\mathcal{O}(\alpha_t\alpha_b)$  and  $\mathcal{O}(\alpha_b^2)$  corrections have been derived [114].<sup>6</sup>The current and future intrinsic error of  $M_h$  due to unknown higher-order corrections has been estimated to be [108, 118, 40, 119]

$$\Delta M_h^{\text{intr,current}} = 3 \text{ GeV}, \quad \Delta M_h^{\text{intr,future}} = 0.5 \text{ GeV}. \quad (3.21)$$

The current uncertainty we interpret effectively as a  $\sim 95\%$  confidence level limit in the evaluation of the  $\chi^2$  contribution, see below.

The by far largest parametric uncertainty is induced by the error in  $m_t$  [42] (also slightly depending on the SUSY parameters) see refs. [40, 120] for details,

$$\begin{aligned} \text{CMSSM} : \quad \delta m_t^{\text{current}} = 2.1 (1.4) \text{ GeV} &\Rightarrow \Delta M_h^{\text{para},m_t,\text{current}} = 1.4 (0.9) \text{ GeV}, \\ \text{mGMSB} : \quad \delta m_t^{\text{current}} = 2.1 (1.4) \text{ GeV} &\Rightarrow \Delta M_h^{\text{para},m_t,\text{current}} = 1.5 (1.0) \text{ GeV}, \\ \text{mAMSB} : \quad \delta m_t^{\text{current}} = 2.1 (1.4) \text{ GeV} &\Rightarrow \Delta M_h^{\text{para},m_t,\text{current}} = 1.2 (0.8) \text{ GeV}. \end{aligned} \quad (3.22)$$

This is already substantially below the current intrinsic uncertainty. The numbers in brackets correspond to the latest  $m_t$  measurement [43] and are given for the sake of comparison.

It should be noted that, for the unconstrained MSSM with small values of  $M_A$  and values of  $\tan\beta$  which are not too small, a significant suppression of the  $hZZ$  coupling can occur compared to the SM value, in which case the experimental lower bound on  $M_h$  may be more than 20 GeV below the SM value [121] (for the MSSM with real parameters). However, it had been checked that within the CMSSM, mGMSB and mAMSB the  $hZZ$  coupling is always very close to the SM value. Accordingly, the bounds from the SM Higgs search at LEP [122] can be taken over directly (see refs. [123, 124]).

Concerning the  $\chi^2$  analysis, we use the complete likelihood information available from LEP. We evaluate the  $M_h$  contribution to the overall  $\chi^2$  function exactly as outlined in section 2.6 of ref. [13]. This evaluation takes into account the intrinsic uncertainty given in eq. (3.21). The  $\chi^2$  contribution is then combined with the corresponding quantities for the other observables we consider, see eq. (3.1).

For the analysis of future sensitivities, see section 5, we assume a measurement of the lightest MSSM Higgs boson mass with a precision of [125–128]

$$\Delta M_h^{\text{exp,future}} = 50 \text{ MeV}. \quad (3.23)$$

The future parametric uncertainties are expected to be

$$\delta m_t^{\text{future}} = 0.1 \text{ GeV} \quad \Rightarrow \quad \Delta M_h^{\text{para},m_t,\text{future}} \approx 0.1 \text{ GeV}, \quad (3.24)$$

$$\delta \alpha_s^{\text{future}} = 0.001 \quad \Rightarrow \quad \Delta M_h^{\text{para},\alpha_s,\text{future}} \approx 0.1 \text{ GeV}. \quad (3.25)$$

---

<sup>6</sup>A two-loop effective potential calculation has been presented in ref. [115], including now even the leading three-loop corrections [116], but no public code based on this result is currently available. Most recently another leading three-loop calculation, valid for certain SUSY mass combinations, became available [117].

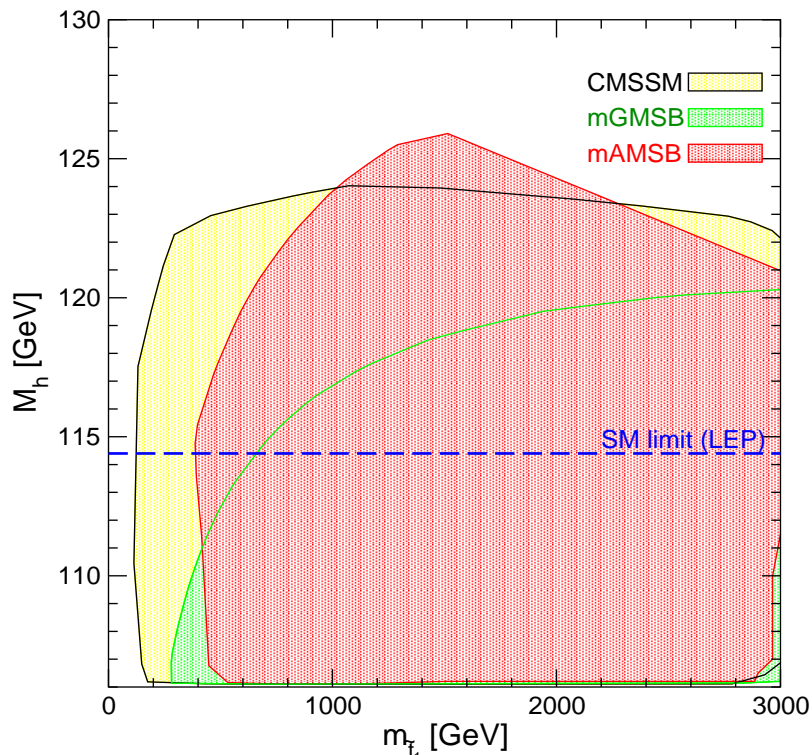


**Figure 4:** The predictions for  $M_h$  as obtained from the parameter scan are shown as a function of  $m_{\tilde{t}_1}$  for the three soft SUSY-breaking scenarios for  $\mu > 0$ . The top quark mass has been fixed to  $m_t = 171.4$  GeV. The SM lower limit of 114.4 GeV obtained at LEP is indicated with a dashed (blue) line.

Thus, the intrinsic error, eq. (3.21), would be the dominant source of uncertainty in the future. The errors are added in quadrature, yielding  $\sigma_{M_h}$ , and we use for the analysis of the future sensitivities  $\chi_{M_h}^2 = ((M_h^{\text{exp}} - M_h^{\text{theo}})/\sigma_{M_h})^2$ .

The predictions for  $M_h$  in the three scenarios are compared with each other in figure 4 (for  $\mu > 0$ , see section 3.3), where the lightest  $\mathcal{CP}$ -even Higgs boson mass is shown as a function of the lighter scalar top quark mass,  $m_{\tilde{t}_1}$  (truncated at  $m_{\tilde{t}_1} = 3$  TeV). The SM limit of 114.4 GeV obtained at LEP is indicated with a dashed (blue) line. In each scenario the SM bound from Higgs searches at LEP of  $M_h > 114.4$  GeV results in important constraints. On the other hand, the bound is still fulfilled for large parts of the parameter space. No preference for any  $m_{\tilde{t}_1}$  can be found.

### 3.5 The decay $b \rightarrow s\gamma$

Since this decay occurs at the loop level in the SM, the MSSM contribution might *a priori* be of similar magnitude. A recent theoretical estimate of the SM contribution to the branching ratio at the NNLO QCD level is [129]

$$\text{BR}(b \rightarrow s\gamma) = (3.15 \pm 0.23) \times 10^{-4} . \quad (3.26)$$

We record that the error estimate for  $\text{BR}(b \rightarrow s\gamma)$  is still under debate [130], and that other SM contributions to  $b \rightarrow s\gamma$  have been calculated [131]. These corrections are small compared with the theoretical uncertainty quoted in eq. (3.26).

For comparison, the present experimental value estimated by the Heavy Flavour Averaging Group (HFAG) is [132, 3]

$$\text{BR}(b \rightarrow s\gamma) = (3.55 \pm 0.24 \begin{smallmatrix} +0.09 \\ -0.10 \end{smallmatrix} \pm 0.03) \times 10^{-4}, \quad (3.27)$$

where the first error is the combined statistical and uncorrelated systematic uncertainty, and the other two errors are correlated systematic theoretical uncertainties and corrections, respectively.

Our numerical results have been derived with the  $\text{BR}(b \rightarrow s\gamma)$  evaluation provided in refs. [133–135], incorporating also the latest SM corrections provided in ref. [129]. The calculation has been checked against other codes [136–138]. For the evaluation of the  $\text{BR}(b \rightarrow s\gamma)$ , we assume minimal flavor violation (MFV) at the electroweak scale and neglect NMFV effects that can be induced by RGE running from the high scale, see e.g. ref. [28], that may amount to  $\sim 10\%$  of the SUSY corrections.

Concerning the total error in a conservative approach we add linearly the errors of eqs. (3.26) and (3.27) as well an intrinsic SUSY error of  $0.15 \times 10^{-4}$  [13], except the statistical error that is then added in quadrature. For the analysis of the future sensitivities in section 5 we assume that the total error will be reduced by a factor of 3.

The predictions for  $\text{BR}(b \rightarrow s\gamma)$  in the three scenarios are compared with each other in figure 5 (for  $\mu > 0$ , see section 3.3), where the branching ratio is shown as a function of the lighter scalar top quark mass,  $m_{\tilde{t}_1}$  (truncated at  $m_{\tilde{t}_1} = 3$  TeV). The solid (dashed) lines indicate the currently allowed  $1\sigma$  interval from the experimental uncertainty (including also theoretical uncertainties, which are added linearly, see above). In all three scenarios large parts of the parameter space lie within the  $1\sigma$  interval. However, for small mass scales  $\text{BR}(b \rightarrow s\gamma)$  provides important constraints on the three models. While the CMSSM and mGMSB can have very small values of  $\text{BR}(b \rightarrow s\gamma)$  for small  $m_{\tilde{t}_1}$ ,<sup>7</sup> mAMSB has typically large values of the BR. The reason can be traced back to the fact that the sign of the stop mixing angle  $\theta_{\tilde{t}}$  comes out with a positive sign in mAMSB, whereas it is negative in the CMSSM and mGMSB (as output and in the conventions of `SoftSUSY`). This different sign, in combination with a positive  $\mu$ , results in a positive SUSY contribution to  $\text{BR}(b \rightarrow s\gamma)$  within mAMSB and (for most values of the other parameters) a negative contribution in the CMSSM and mGMSB, see also the discussion in the beginning of section 4.

### 3.6 The branching ratio for $B_s \rightarrow \mu^+\mu^-$

The SM prediction for this branching ratio is  $(3.4 \pm 0.5) \times 10^{-9}$  [139], and the present experimental upper limit from the Fermilab Tevatron collider is  $5.8 \times 10^{-8}$  at the 95% C.L. [140], still providing room for the MSSM to dominate the SM contribution. The

---

<sup>7</sup>Where the  $\text{BR}(b \rightarrow s\gamma)$  becomes close to zero the calculation of the SUSY corrections is not reliable anymore. However, these parts of the parameter space anyhow result in an experimentally excluded value for  $\text{BR}(b \rightarrow s\gamma)$ .

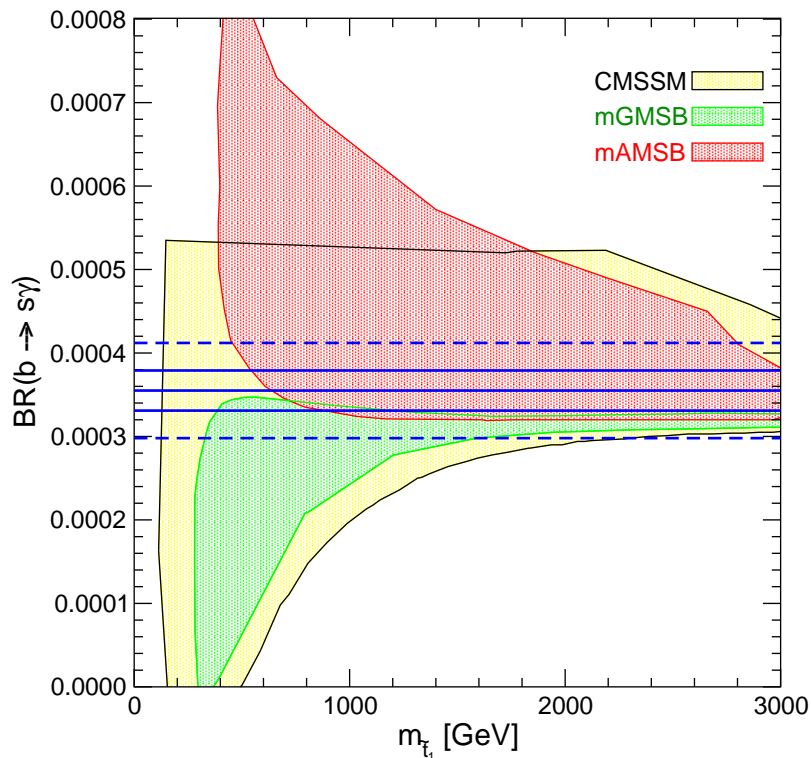


**Figure 5:** The predictions for  $\text{BR}(b \rightarrow s\gamma)$  as obtained from the parameter scan are shown as a function of  $m_{\tilde{t}_1}$  for the three soft SUSY-breaking scenarios for  $\mu > 0$ . The top quark mass has been fixed to  $m_t = 171.4$  GeV. The solid (dashed) lines indicate the currently allowed  $1\sigma$  interval from the experimental uncertainty (including also theoretical uncertainties, which are added linearly).

current Tevatron sensitivity is based on an integrated luminosity of about  $2 \text{ fb}^{-1}$  collected at CDF. For the  $\chi^2$  contribution, in order to incorporate the latest Tevatron bound, we use a smoothed step function, penalizing data points with  $\text{BR}(B_s \rightarrow \mu^+\mu^-) > 5.8 \times 10^{-8}$  and preferring lower BRs.

The Tevatron sensitivity is expected to improve significantly in the future. The limit that could be reached at the end of Run II is  $\sim 2 \times 10^{-8}$  assuming  $8 \text{ fb}^{-1}$  collected with each detector [141]. A sensitivity even down to the SM value can be expected at the LHC. Assuming the SM value, i.e.  $\text{BR}(B_s \rightarrow \mu^+\mu^-) \approx 3.4 \times 10^{-9}$ , it has been estimated [142] that LHCb can observe 33 signal events over 10 background events within 3 years of low-luminosity running. Therefore this process offers good prospects for probing the MSSM.

For the theoretical prediction we use results from ref. [143], which are in good agreement with ref. [144]. This calculation includes the full one-loop evaluation and the leading two-loop QCD corrections. As in section 3.5, we neglect any NMFV effects from RGE running. We do not include  $\text{BR}(B_s \rightarrow \mu^+\mu^-)$  in our analysis of the future sensitivities (but still require agreement with the current bound), because its impact will strongly depend on the value realized in Nature.

The predictions for  $\text{BR}(B_s \rightarrow \mu^+\mu^-)$  in the three scenarios are compared with each



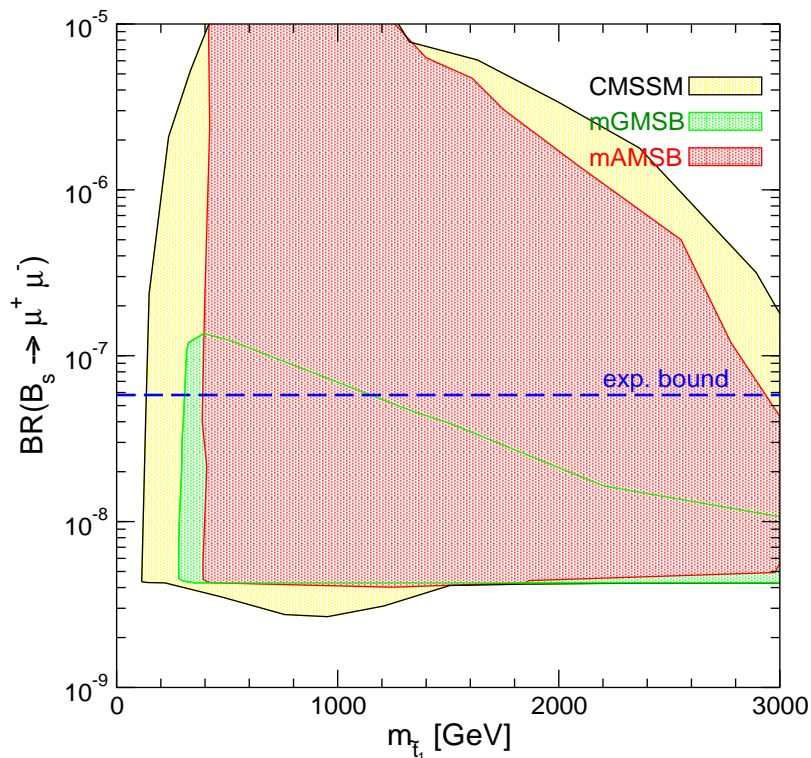


**Figure 6:** The predictions for  $\text{BR}(B_s \rightarrow \mu^+ \mu^-)$  as obtained from the parameter scan are shown as a function of  $m_{\tilde{t}_1}$  for the three soft SUSY-breaking scenarios for  $\mu > 0$ . The top quark mass has been fixed to  $m_t = 171.4$  GeV. The current upper limit of  $5.8 \times 10^{-8}$  is indicated by a dashed (blue) line.

other in figure 6 (for  $\mu > 0$ , see section 3.3), where the BR is shown as a function of the lighter scalar top quark mass,  $m_{\tilde{t}_1}$  (truncated at  $m_{\tilde{t}_1} = 3$  TeV). The current experimental limit of  $5.8 \times 10^{-8}$  is indicated by a dashed (blue) line. Each scenario has large parts of the parameter space with  $\text{BR}(B_s \rightarrow \mu^+ \mu^-) < 5.8 \times 10^{-8}$ , where no limit on  $m_{\tilde{t}_1}$  is provided by the upper limit on the BR. Within the mGMSB scenario, due to its generally larger  $M_A$  values (see below), hardly any points are ruled out by the current upper bound on the BR, while for the other two scenarios  $\text{BR}(B_s \rightarrow \mu^+ \mu^-)$  is already a strong constraint on the parameter space. We have checked that including the CDM constraint and restricting to values of  $\tan \beta \leq 50$  the results for  $\text{BR}(B_s \rightarrow \mu^+ \mu^-)$  in refs. [11–13] are reproduced.

#### 4. $\chi^2$ analysis for CMSSM, mGMSB, mAMSB

In this section we present our numerical analysis, based on the  $\chi^2$  evaluation as given in eq. (3.1). The best fit point is given by the lowest  $\chi^2$  value. The sensitivities are shown as  $\Delta\chi^2 = 1, 4, 9$ , referred to as  $\Delta_1$ ,  $\Delta_4$  and  $\Delta_9$ , respectively. They give an indication of the precision that has been reached so far for the observables under investigation. Sometimes we refer to the  $\Delta_4$  areas as ‘preferred’ regions. The lowest  $\chi^2$  values for the three scenarios are

	CMSSM	mGMSB	mAMSB
$\chi_{\min}^2$	4.6	5.1	2.9
$M_W$	1.7	2.1	0.6
$\sin^2 \theta_{\text{eff}}$	0.1	0.0	0.8
$(g - 2)_\mu$	0.6	0.9	0.0
$\text{BR}(b \rightarrow s\gamma)$	1.1	2.0	1.5
$M_h$	1.1	0.1	0.0
$\text{BR}(B_s \rightarrow \mu^+ \mu^-)$	$4.5 \times 10^{-8}$	$3.2 \times 10^{-8}$	$0.4 \times 10^{-8}$
$M_A$ [GeV] (best-fit)	394	547	616
$\tan \beta$ (best-fit)	54	55	9

**Table 1:** Minimum  $\chi^2$  values for the three soft SUSY-breaking scenarios using today’s accuracies for the experimental and theoretical precisions. We also show the individual contributions for  $M_W$ ,  $\sin^2 \theta_{\text{eff}}$ ,  $(g - 2)_\mu$ ,  $\text{BR}(b \rightarrow s\gamma)$  and  $M_h$ , as well as the value of  $\text{BR}(B_s \rightarrow \mu^+ \mu^-)$ . Shown in the last two rows are the best-fit values for the low-energy parameters,  $M_A$  and  $\tan \beta$ , as analyzed in section 4.2.

given in table 1. Also shown are the individual contributions from the precision observables.  $\text{BR}(B_s \rightarrow \mu^+ \mu^-)$  always gives a zero contribution, and we list the BR itself.

It is interesting to note that despite mAMSB has one parameter less, the minimum  $\chi^2$  value is lower by  $\sim 1.5$ – $2$  compared to the CMSSM and mGMSB. The reason for the low  $\chi^2$  values is a combination of two effects. First, there is a good agreement of mAMSB with  $(g - 2)_\mu$  and  $\text{BR}(b \rightarrow s\gamma)$ . The anomalous magnetic moment of the muon requires a positive  $\mu$  (or more precisely a positive  $\mu \cdot M_2$ , where we use the convention of positive  $M_2$  for the three scenarios, see the discussion above).  $\text{BR}(b \rightarrow s\gamma)$  on the other hand depends on the combinations of the stop masses, mixing angle and  $\mu$ . The sign of the stop mixing angle  $\theta_{\tilde{t}}$  comes out with a positive sign in mAMSB, whereas it is negative in the CMSSM and mGMSB (as output and in the convention of `SoftSUSY`). This different sign, in combination with a positive  $\mu$ , results in a positive SUSY contribution to  $\text{BR}(b \rightarrow s\gamma)$  within mAMSB and a (usually) negative contribution in the CMSSM and mGMSB. In this way mAMSB can fulfill the  $\text{BR}(b \rightarrow s\gamma)$  constraint as well as the other two scenarios (but with a best-fit value *above* the experimental value). Second, due to the structure of the soft SUSY-breaking parameters in the chargino/neutralino sector relatively light charginos are present in mAMSB (where the lightest one is nearly mass degenerate with the lightest neutralino). Thus a large contribution to  $(g - 2)_\mu$  and also to  $M_W$  [55] can be obtained for a relatively heavier spectrum otherwise, resulting in an  $M_h$  value above  $\sim 116$  GeV. The overall effect of this interplay is a total minimum  $\chi^2$  value of 2.9.

In the analysis presented below, in the first step we show the three soft SUSY-breaking scenarios separately in terms of their high-scale parameters. In a second step we compare

their respective predictions in terms of the low-scale parameters  $M_A$  and  $\tan\beta$  and other SUSY mass scales. In the final step in section 5 we assume future precisions for the measurements and theory evaluations and compare the sensitivities the precision observables will offer in the three scenarios.

#### 4.1 Analysis of high-scale parameters

In the following subsections we analyze the CMSSM, mGMSB and mAMSB in terms of their respective high-energy parameters, see section 2.

##### 4.1.1 CMSSM

In figure 7 we show the results for the  $\Delta_{1,4,9}$  areas in terms of the high-energy parameters, using the current experimental and theoretical precisions as described in section 3. The  $\Delta_1$  area is medium shaded (green), the  $\Delta_4$  area is dark shaded (red), and the  $\Delta_9$  area is light shaded (yellow). The rest of the scanned parameter space is given in black shading. The best-fit point is marked with a circle. Because of the contribution to  $(g-2)_\mu$  only very few points with  $\mu < 0$  have  $\Delta\chi^2 < 9$ , and we concentrate here on the data with  $\mu > 0$ . For this sign of  $\mu$  the  $\Delta_9$  area nearly covers the whole parameter space (in agreement with the results presented in ref. [13]). In terms of  $m_{1/2}$  relatively low values are favored around  $m_{1/2} = 500$  GeV, with the  $\Delta_4$  region extending up to  $m_{1/2} = 1000$  GeV. For  $m_0$ , on the other hand, hardly any bound is obtained, and values up to 2000 GeV are possible. Only at the  $\Delta_1$  level a preference of the allowed values for a light  $m_0$  can be found. For  $A_0$  a slight preference for positive values can be observed (note the different sign convention here in comparison with refs. [11–15]), and the  $\Delta_4$  region extends from  $-1000$  GeV to about  $+2500$  GeV. The apparent differences to existing analyses [11, 12, 18] are due to the fact that the CDM constraint has not been applied here, see the discussion below.

##### 4.1.2 mGMSB

In figures 8, 9 we show the results for the  $\Delta_{1,4,9}$  areas in terms of the high-energy parameters, using the current experimental and theoretical precisions as described in section 3. The color coding is as in figure 7. As in the CMSSM, because of the contribution to  $(g-2)_\mu$  only very few points with  $\mu < 0$  have  $\Delta\chi^2 < 9$ , and we concentrate here on the data with  $\mu > 0$ .

The plots in figure 8 show the  $\Lambda$ - $M_{\text{mess}}$  plane for  $N_{\text{mess}} = 1 \dots 8$  separately. The  $\Delta\chi^2$  values are obtained with respect to the overall best fit point, which is reached for  $N_{\text{mess}} = 8$  (marked with a circle). The ‘preferred’  $\Lambda$  values depend on the choice of  $N_{\text{mess}}$ , going from  $\sim 10^5$  GeV at low  $N_{\text{mess}}$  down to  $\sim 2 \times 10^4$  GeV for large  $N_{\text{mess}}$ . However, the  $\Delta_9$  region extend over large parts of the whole parameter space. Furthermore no bound on  $M_{\text{mess}}$  can be set. Similar results are found in figure 9, where we show the  $N_{\text{mess}}$ - $\Lambda$  plane. The lower  $N_{\text{mess}}$ , the higher are the possible values for  $\Lambda$ .

In order to analyze the compatibility of the various  $N_{\text{mess}}$  values with the precision data, we show in table 2 the lowest  $\chi^2_{\text{min}, N_{\text{mess}}}$  values reached for each  $N_{\text{mess}}$ . It can be seen that  $\chi^2_{\text{min}, N_{\text{mess}}}$  increases monotonically with decreasing  $N_{\text{mess}}$ . In agreement with figures 8 and 9 the difference in the minimum  $\chi^2$  between  $N_{\text{mess}} = 8$  and  $N_{\text{mess}} > 1$  is smaller than

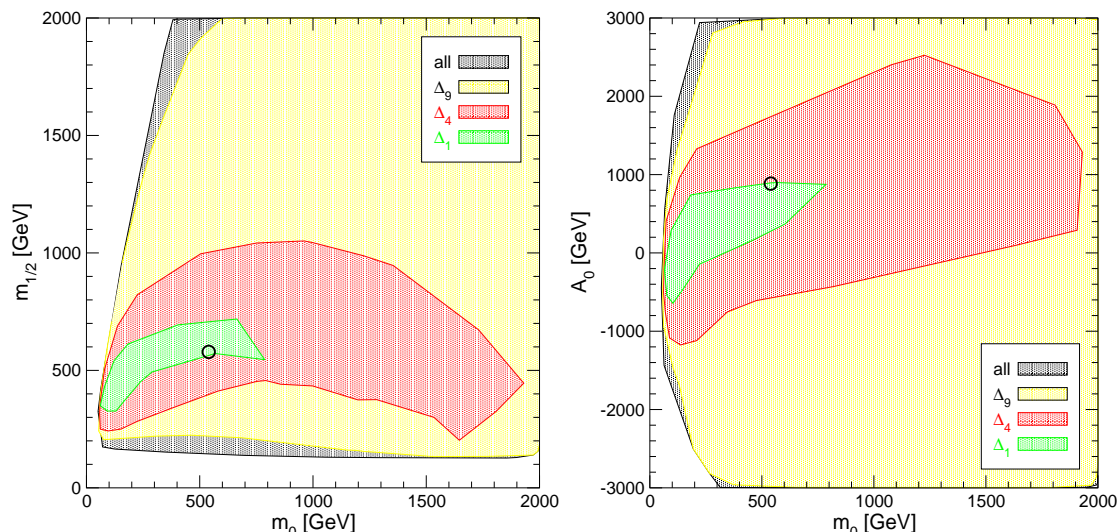


**Figure 7:** The  $\Delta_{1,4,9}$  regions in the  $m_0$ - $m_{1/2}$  plane (left) and in the  $m_0$ - $A_0$  plane (right) in the CMSSM for  $\mu > 0$ . The  $\Delta_1$  area is medium shaded (green), the  $\Delta_4$  area is dark shaded (red), and the  $\Delta_9$  area is light shaded (yellow). The rest of the scanned parameter space is given in black shading. The best-fit point is marked with a circle.

$N_{\text{mess}}$	1	2	3	4	5	6	7	8
$\chi^2_{\text{min}, N_{\text{mess}}}$	6.17	5.53	5.45	5.25	5.25	5.20	5.16	5.13

**Table 2:** Minimum  $\chi^2$  values reached for each  $N_{\text{mess}}$ .

one, and only for  $N_{\text{mess}} = 1$  the difference exceeds one by  $\sim 0.04$ . Consequently no  $\Delta_1$  region appears in the  $N_{\text{mess}} = 1$  plots.

### 4.1.3 mAMSB

In figure 10 we show the only high-energy parameter plane in the mAMSB,  $m_{\text{aux}}$  vs.  $m_0$  for  $\mu > 0$ . While nearly the whole parameter space is covered by the  $\Delta_9$  area, the  $\Delta_4$  and  $\Delta_1$  regions are located at a relatively thin strip at the lowest possible  $m_0$  values with a width  $\lesssim 300$  GeV. The precision observables clearly show a preference for a relatively small scalar soft SUSY-breaking parameter  $m_0$ . This can be traced back to the  $\chi^2$  contribution to  $(g - 2)_\mu$  that requires relatively light sleptons of the second generation. Since  $m_0$  is needed to prevent the tachyon problem within mAMSB, it controls to a large extent the slepton masses. The strong bound from  $(g - 2)_\mu$  then translates into a relatively strong bound on  $m_0$ . On the other hand,  $m_{\text{aux}}$  is only mildly restricted. The lower absolute bound on  $m_{\text{aux}}$  is mainly due to the lower experimental bound on the lightest chargino of  $\sim 70$  GeV [33].

### 4.2 Low-energy analysis

We now turn to the comparison of the three soft SUSY-breaking scenarios. In figure 11 we

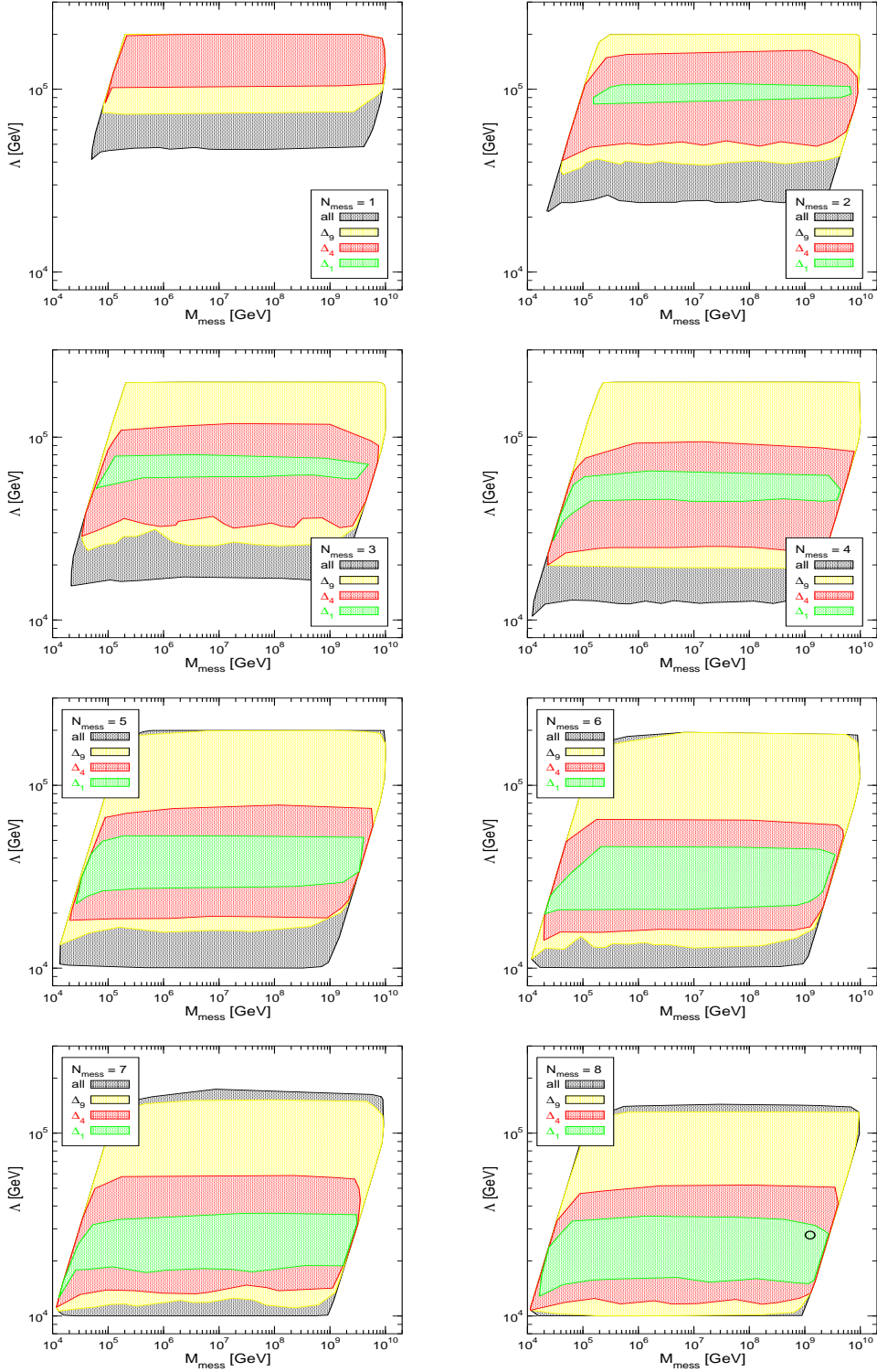


**Figure 8:** The  $\Delta_{1,4,9}$  regions in the  $M_{\text{mess}} - \Lambda$  plane for  $N = 1 \dots 8$  in the mGMSB for  $\mu > 0$ . The color coding is as in figure 7. The best fit point is realized for  $N_{\text{mess}} = 8$  and marked with a circle.

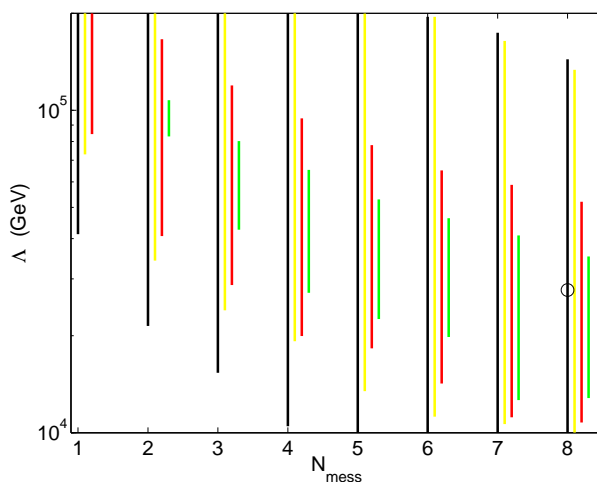


**Figure 9:** The  $\Delta_{1,4,9}$  regions in the  $N_{\text{mess}}-\Lambda$  plane in the mGMSB for  $\mu > 0$ . The color coding is as in figure 7. Marked with a circle is the current best-fit point.

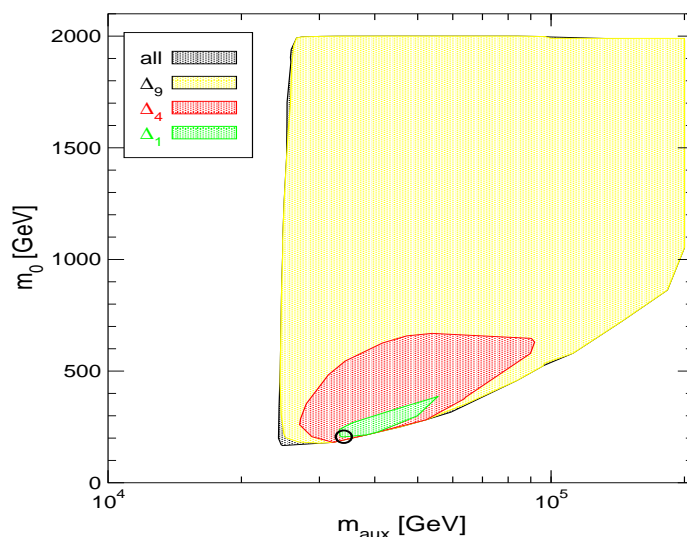


**Figure 10:** The  $\Delta_{1,4,9}$  regions in the  $m_{\text{aux}}-m_0$  plane in the mAMSB for  $\mu > 0$ . The color coding is as in figure 7. The best-fit point is marked with a circle.

show the  $M_A-\tan\beta$  plane for the CMSSM (top), mGMSB (middle) and mAMSB (bottom) with the same color coding as in figure 7. As in section 4.1 we restrict ourselves to  $\mu > 0$ . The allowed  $M_A-\tan\beta$  parameter space is somewhat different in the three scenarios. While in mAMSB the parameters are restricted to  $M_A \lesssim 4$  TeV and  $\tan\beta \lesssim 50$ , this extends to  $M_A \lesssim 4$  TeV and  $\tan\beta \lesssim 60$  (where we stopped our  $\tan\beta$  scan) in the CMSSM, and within mGMSB  $M_A$  values up to 6 TeV are possible (not shown in the plot). The qualitative features of the  $\Delta_{9,4,1}$  areas are very similar for the three scenarios. The  $\Delta_9$  area extends over large parts of the whole parameter space. On the other hand, within

all three scenarios, the  $\Delta_4$  and even more the  $\Delta_1$  areas are located at relatively low  $M_A$ , extending up to  $M_A \lesssim 1000$  GeV at the  $\Delta_4$  level in all three scenarios. The ‘preferred’  $\tan\beta$  regions, on the other hand, nearly span the full possible range in the CMSSM and mGMSB, whereas in the mAMSB scenario the  $\chi^2$  ‘preferred’ areas are located at lower  $\tan\beta$  values, reaching up to  $\tan\beta \lesssim 35$ . The low value of  $\text{BR}(B_s \rightarrow \mu^+\mu^-)$  at the best-fit point in mAMSB is due to the relatively low  $\tan\beta$  value. However, in view of these ranges, the actual values of the best-fit points for  $\tan\beta$  are not very significant, in accordance with earlier analyses [11–14, 16]. In conclusion a preference for not too large  $M_A$  values is clearly visible as a common feature in all three scenarios. Depending on the actual combination of  $M_A$  and  $\tan\beta$ , the LHC can cover a large part of the ‘preferred’ parameter space by searches for the heavy Higgs bosons [145–150].

We now turn to the analysis of various mass values in the three soft SUSY-breaking scenarios. We start with the mass of the lightest  $\mathcal{CP}$ -even Higgs boson, see section 3.4, presented in figure 12.  $M_h$  is shown in the CMSSM (top), mGMSB (middle) and mAMSB (bottom) scenarios for  $\mu > 0$  with the corresponding  $\chi^2$ , where the  $\chi^2$  contribution of  $M_h$  itself has been left out. In this way the plot shows the indirect predictions for  $M_h$  without imposing the bounds from the Higgs boson searches at LEP. In the CMSSM and in mGMSB the impact of dropping the  $\chi^2$  contribution from  $M_h$  leads to a drastically lower total  $\chi^2$  as compared to the case when the  $M_h$  bound is included, see table 1. In these two scenarios the best-fit point changes to new points with substantially lower  $M_h$  values (as discussed below). These new best-fit points can also accommodate the other precision observables better, thus leading to a reduction of  $\chi_{\text{min}}^2$  by more than  $\sim 3$  in the CMSSM and mGMSB. In the mAMSB scenario, on the other hand, the effect is small, and the best-fit point changes only slightly. The color coding is as in figure 7.

In all three scenarios a shallow minimum can be observed. The  $\Delta_1$  regions are in the intervals of  $M_h = 98 \dots 111$  GeV (CMSSM),  $97 \dots 112$  GeV (mGMSB) and  $104 \dots 122$  GeV (mAMSB). In all three scenarios the  $\Delta_4$  regions extend beyond the LEP limit of  $M_h > 114.4$  GeV at the 95% C.L. shown as dashed (blue) line in figure 12 (which is valid for the three soft SUSY-breaking scenarios, see refs. [123, 124]). The analysis for the CMSSM can be compared with refs. [13, 18], where (among other contributions) also the cold dark matter constraint had been included in the analysis. In refs. [13, 18] best fit values of  $M_h = 110 \dots 115$  GeV (depending on  $\tan\beta$ ) had been observed, which is at the border of the  $\Delta_1$  region here. These results are well compatible with each other. The inclusion of the CDM constraint yields the effect of cutting out a (thin) band in the  $M_h$ - $\chi_{\text{tot}}^2$  plane. In conclusion all three scenarios have a significant part of the parameter space with a relatively low total  $\chi^2$  that is in agreement with the bounds from Higgs-boson searches at LEP. Especially within the mAMSB scenario the  $\Delta_1$  region extends beyond the LEP bound of 114.4 GeV.

Next we turn to the prediction of the masses of various SUSY particles, starting with  $m_{\tilde{\chi}_1^0}$  (left) and  $m_{\tilde{\chi}_2^0}$  (right) in figure 13. The masses are shown in the CMSSM (top), mGMSB (middle) and mAMSB (bottom) scenarios for  $\mu > 0$  with their respective total  $\chi^2$ , i.e. including the  $\chi^2$  contribution of  $M_h$ . The color coding is as in figure 7. The mGMSB shows for all masses (see below) a local minimum at a lower value and an absolute

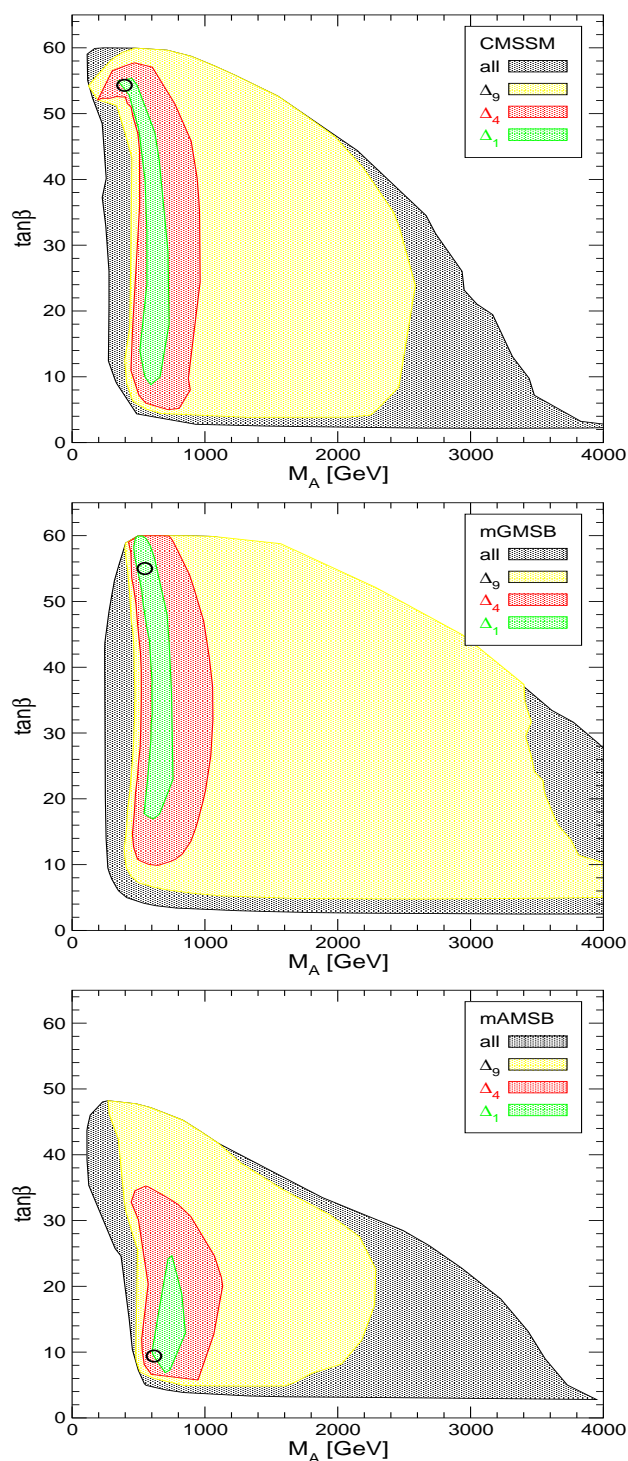


**Figure 11:** The  $\Delta_{1,4,9}$  regions in the  $M_A$ - $\tan\beta$  planes in the CMSSM (top), mGMSB (middle) and mAMSB (bottom) for  $\mu > 0$ . The color coding is as in figure 7. In each plot the best-fit point is marked with a circle.



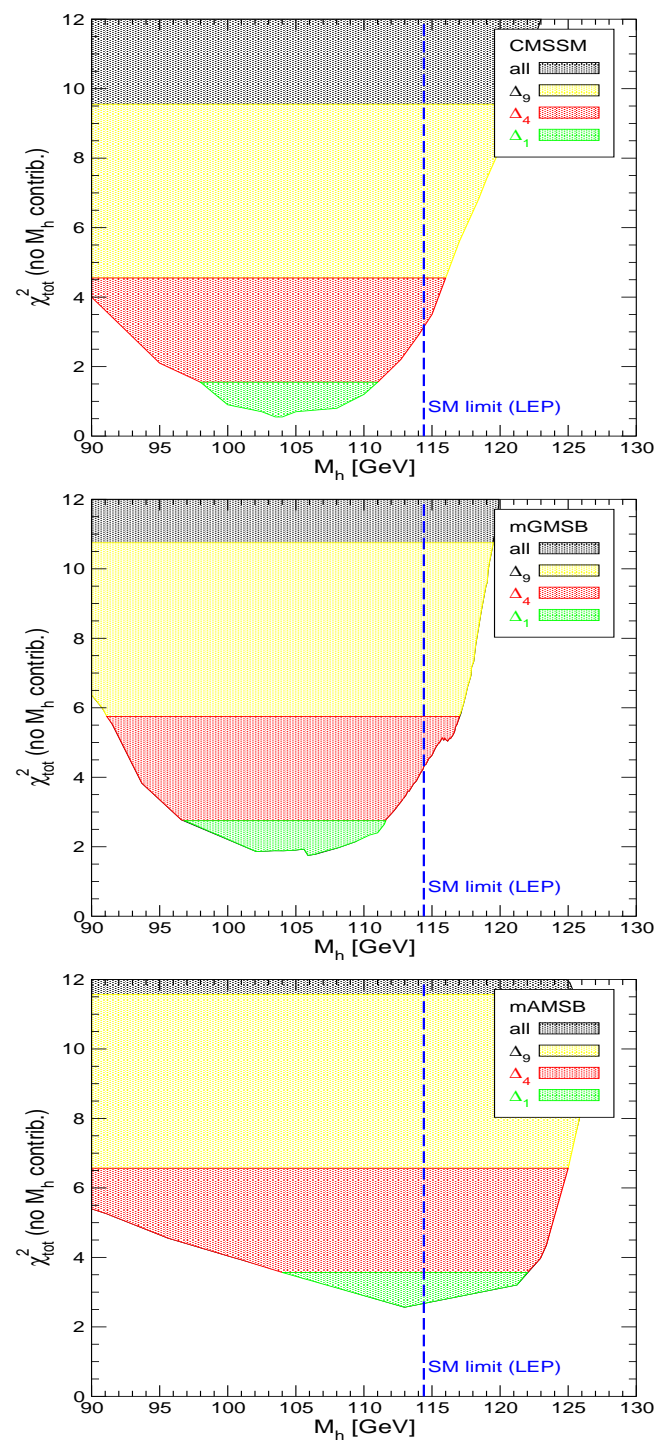


**Figure 12:** The  $M_h$  values in the CMSSM (top), mGMSB (middle) and mAMSB (bottom) scenarios for  $\mu > 0$  with their respective  $\chi^2$ , where the  $\chi^2$  contribution of the  $M_h$  itself has been left out. The color coding is as in figure 7. The SM limit of 114.4 GeV obtained at LEP is indicated with a dashed (blue) line.

minimum at a somewhat higher mass value. The effect of having a minimum in the  $\chi^2$  plot can in general be understood by investigating the  $\chi^2$  contribution of  $M_h$  and of  $(g - 2)_\mu$ . While the former penalizes strongly a light spectrum (especially for the stops), the latter penalizes a heavy spectrum (especially sleptons and charginos/neutralinos). The appearance of the second local minimum at lower mass values is a result from the interplay of several observables, especially  $M_W$  and  $M_h$ . Going to a lighter spectrum improves  $\chi^2(M_W)$  more than it worsens  $\chi^2(M_h)$ , while a very light spectrum results in a very large  $\chi^2$  contribution from  $M_h$ , yielding the local minimum in between.

In the three scenarios limited ranges can be observed for the  $\Delta_1$  and  $\Delta_4$  regions, whereas the  $\Delta_9$  regions extend to the highest possible mass values. For the CMSSM and mAMSB the truncation of the parameter space at high  $m_{1/2}$ ,  $m_{\text{aux}}$  and  $m_0$  is clearly visible for some particle masses, e.g. in the left column of figure 13. The mass of the lightest neutralino (the LSP) has ‘preferred’ values,  $\Delta\chi^2 < 4$ , ranging from about 100 GeV to values up to 500 GeV, depending on the scenario. Within the CMSSM and mAMSB the lightest neutralino, being stable, cannot be observed via a decay to other particles, so that its detection has to rely on a ‘missing energy’ signature. In mGMSB the LSP is the gravitino,  $\tilde{G}$ , leading to distinctive decay patterns of the  $\tilde{\chi}_1^0$  if it decays within the detector. The decay BRs depend largely on the mass pattern of the  $\tilde{\chi}_1^0$ ,  $\tilde{\tau}_1$  and  $\tilde{G}$ . The ‘preferred’ mass values thus offer good prospects for the detection at the LHC and excellent prospects for the ILC(1000) (i.e. with  $\sqrt{s}$  up to 1 TeV) in the case where the decay happens in the detector. At the ILC also the process  $e^+e^- \rightarrow \tilde{\chi}_1^0\tilde{\chi}_1^0\gamma$  can in principle be observed, permitting in this case the observation of the  $\tilde{\chi}_1^0$  in all the three scenarios in the ‘preferred’ mass ranges.

The second lightest neutralino, see the right column of figure 13, can in principle be observed via its decay to a SM particle and the LSP (or another SUSY particle if it is lighter than the  $\tilde{\chi}_2^0$ , as e.g. the  $\tilde{\chi}_1^\pm$  in the case of the mAMSB). The best fit values vary around 300 GeV to values above 550 GeV, depending on the scenario. With these mass ranges the observation at the LHC will be very challenging for the direct production, but might be better (depending on SUSY mass patterns) for the production in cascades. At the ILC(1000) one could search for the associated production of  $e^+e^- \rightarrow \tilde{\chi}_1^0\tilde{\chi}_2^0$ . The three soft SUSY-breaking scenarios show similar prospects for the discovery, although mGMSB results in overall somewhat higher mass scales.

The predictions of the lightest chargino mass,  $m_{\tilde{\chi}_1^\pm}$  (left), and the gluino mass,  $m_{\tilde{g}}$  (right), are shown in figure 14. As before, the masses are shown in the CMSSM (top), mGMSB (middle) and mAMSB (bottom) scenarios for  $\mu > 0$  with their respective total  $\chi^2$ . The color coding is as in figure 7. In the three scenarios limited ranges can be observed for the  $\Delta_1$  and  $\Delta_4$  regions, whereas the  $\Delta_9$  regions extend to the highest possible mass values. Within the CMSSM and mGMSB the light chargino mass ranges from about 100 GeV up to  $\sim 900$  GeV in the  $\Delta_4$  area, whereas somewhat higher masses are reached in mGMSB. Consequently only a part of the ‘preferred’ parameter space can be accessed at the LHC or the ILC(1000). Within the CMSSM and mGMSB the  $\tilde{\chi}_1^\pm$  and the  $\tilde{\chi}_2^0$  are nearly mass degenerate, resulting in very similar results for the two particles as can be seen in figures 13 and 14. The situation concerning the observation of the  $\tilde{\chi}_1^\pm$  is much more favorable in mAMSB, where much lighter masses, only up to about 300 GeV are preferred.

This offers very good perspectives for its production at the LHC and the ILC. However, it should be kept in mind that in the mAMSB scenario the lightest chargino is only a few hundred MeV heavier than the LSP, which poses certain problems for its detection [151].

The ‘preferred’ gluino masses, as shown in the right column of figure 14, range from a few hundred GeV up to about 3 TeV in mGMSB, exhausting the accessible range at the LHC. In the other two scenarios the  $\Delta_4$  regions end at  $\sim 2$  TeV (mAMSB) and  $\sim 2.5$  TeV (CMSSM), making them more easily accessible at the LHC than in the mGMSB scenario.

We now turn to the scalar fermion sector. The predictions for the two scalar tau masses,  $m_{\tilde{\tau}_1}$  (left) and  $m_{\tilde{\tau}_2}$  (right), are shown in figure 15. As before, the masses are shown in the CMSSM (top), mGMSB (middle) and mAMSB (bottom) scenarios for  $\mu > 0$  with their respective total  $\chi^2$ . The color coding is as in figure 7. The light  $\tilde{\tau}$  has its best-fit values at very low masses, and even the  $\Delta_4$  regions hardly exceed  $\sim 500$  GeV in mGMSB and mAMSB. Therefore in these scenarios there are good prospects for the ILC(1000). Also the LHC can be expected to cover large parts of the  $\Delta_4$  mass intervals. In the CMSSM scenario, on the other hand, the  $\Delta_4$  region exceeds  $\sim 1$  TeV such that only parts can be probed at the ILC(1000) and the LHC. The ‘preferred’  $m_{\tilde{\tau}_2}$  values, by construction larger than  $m_{\tilde{\tau}_1}$ , stay mostly below 500, 1000, 1500 GeV for mAMSB, mGMSB and the CMSSM, respectively.

In figure 16 we show the predictions for the two scalar top masses,  $m_{\tilde{t}_1}$  (left) and  $m_{\tilde{t}_2}$  (right). As before, the masses are shown in the CMSSM (top), mGMSB (middle) and mAMSB (bottom) scenarios for  $\mu > 0$  with their respective total  $\chi^2$ . The color coding is as in figure 7. The ‘preferred’ mass ranges, i.e.  $\Delta\chi^2 < 4$ , range from about 300 GeV up to about 2300 GeV, depending somewhat on the scenario. Finally, the predictions for the sbottom masses are shown in figure 17. The sbottom masses follow the same pattern as the stop masses. Taking these values as representative scalar quark mass values, the LHC should have no problem to discover the SUSY partners of the quarks, whereas for the ILC(1000) only the lower part of the ‘preferred’ values could be in the kinematic reach. However, it should be kept in mind that the  $\Delta_9$  regions extend beyond  $\sim 3$  TeV, which could exceed even the discovery reach of the SLHC [152].

Apart from the values of the various SUSY and Higgs particle masses, also the ‘preferred’ values of  $|\mu|$  and of  $B$  (with  $\mu B$  being the prefactor of the Higgs mixing term in the potential) are of interest. In table 3 we list the current best fit points and the  $\Delta_{1,4}$  ranges for  $\mu$  (with  $\mu > 0$ , see section 3.3) and  $B$ . The ‘preferred’ values for  $\mu$  range between 130 GeV and 1420 GeV in the mAMSB and somewhat smaller intervals within in the two other scenarios. The ‘preferred’ values of  $B$  are bounded from above by  $\sim 540$  GeV in mAMSB, where also negative values down to  $-275$  GeV are reached in the  $\Delta_4$  area. In the other two scenarios the intervals are substantially smaller, and only in the CMSSM negative values down to  $-75$  GeV are reached.

The results for the SUSY masses in the CMSSM can be compared with previous analyses taking into account the CDM constraint [11–13, 16, 18]. We focus here on refs. [11–13], since similar sets of precision observables and very similar  $\chi^2$  analyses had been used. Qualitative agreement can be found in the observed ‘preferred’ mass values. In our analysis the lower mass values in the  $\Delta_1$  and  $\Delta_4$  regions are obtained for low  $\tan\beta$ , where these masses are similar to to the ones in refs. [11–13] obtained for  $\tan\beta = 10$ . Higher mass values in

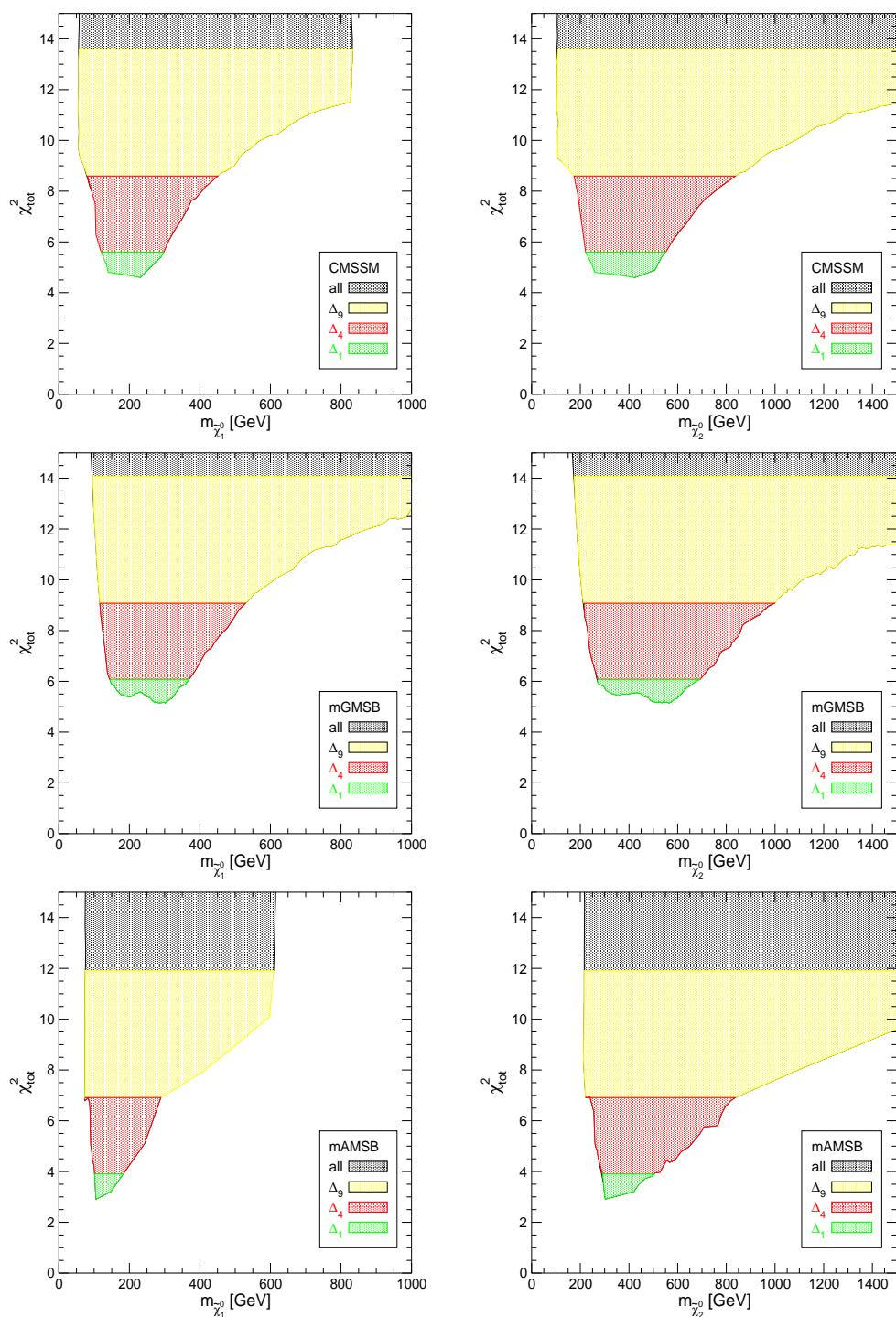


**Figure 13:**  $m_{\tilde{\chi}_1^0}$  (left) and  $m_{\tilde{\chi}_2^0}$  (right) are shown in the CMSSM (top), mGMSB (middle) and mAMSB (bottom) scenarios for  $\mu > 0$  with their respective total  $\chi^2$ , i.e. including the  $\chi^2$  contribution of  $M_h$ . The color coding is as in figure 7.

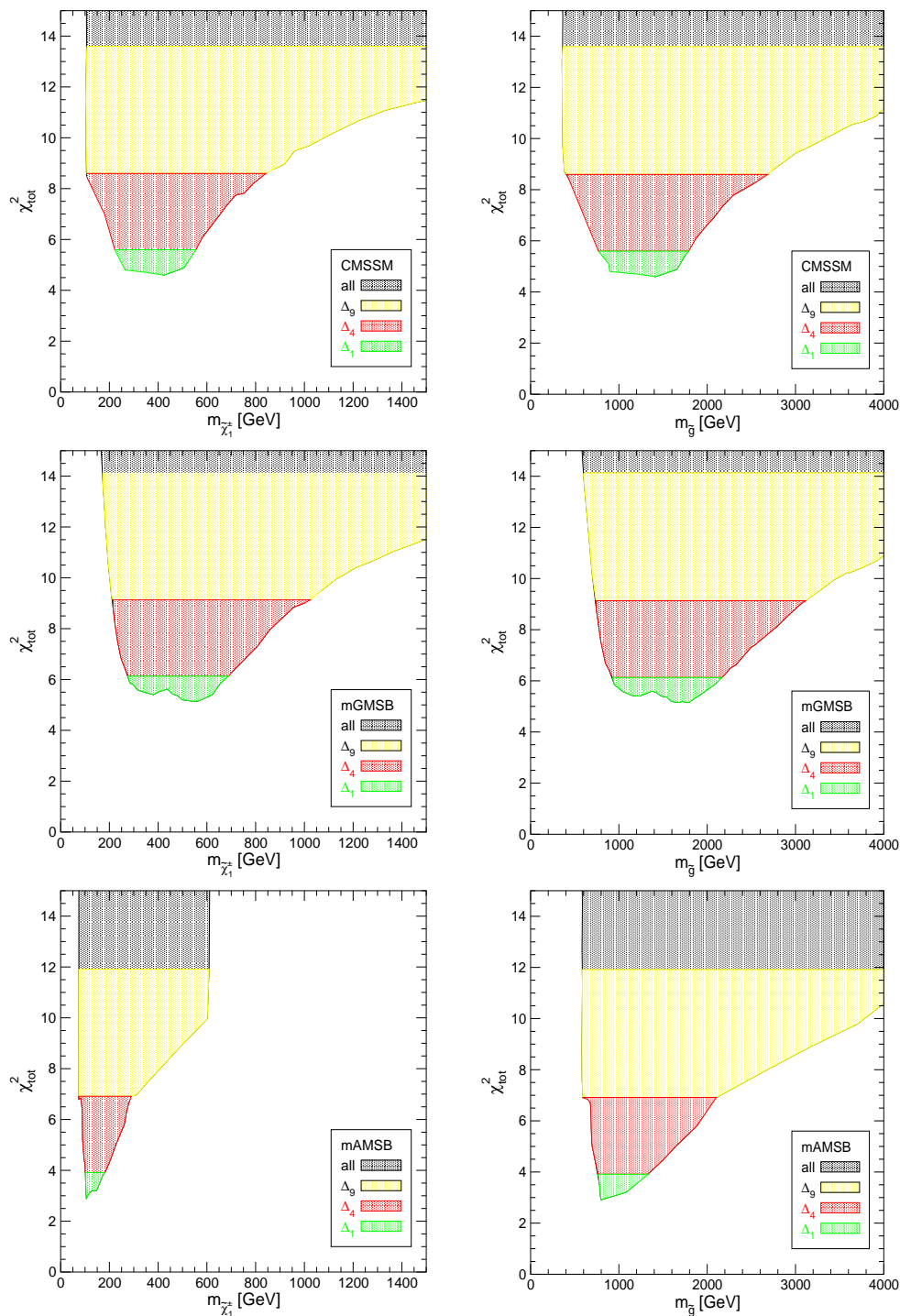


**Figure 14:**  $m_{\tilde{\chi}_1^\pm}$  (left) and  $m_{\tilde{g}}$  (right) are shown in the CMSSM (top), mGMSB (middle) and mAMSB (bottom) scenarios for  $\mu > 0$  with their respective total  $\chi^2$ . The color coding is as in figure 7.

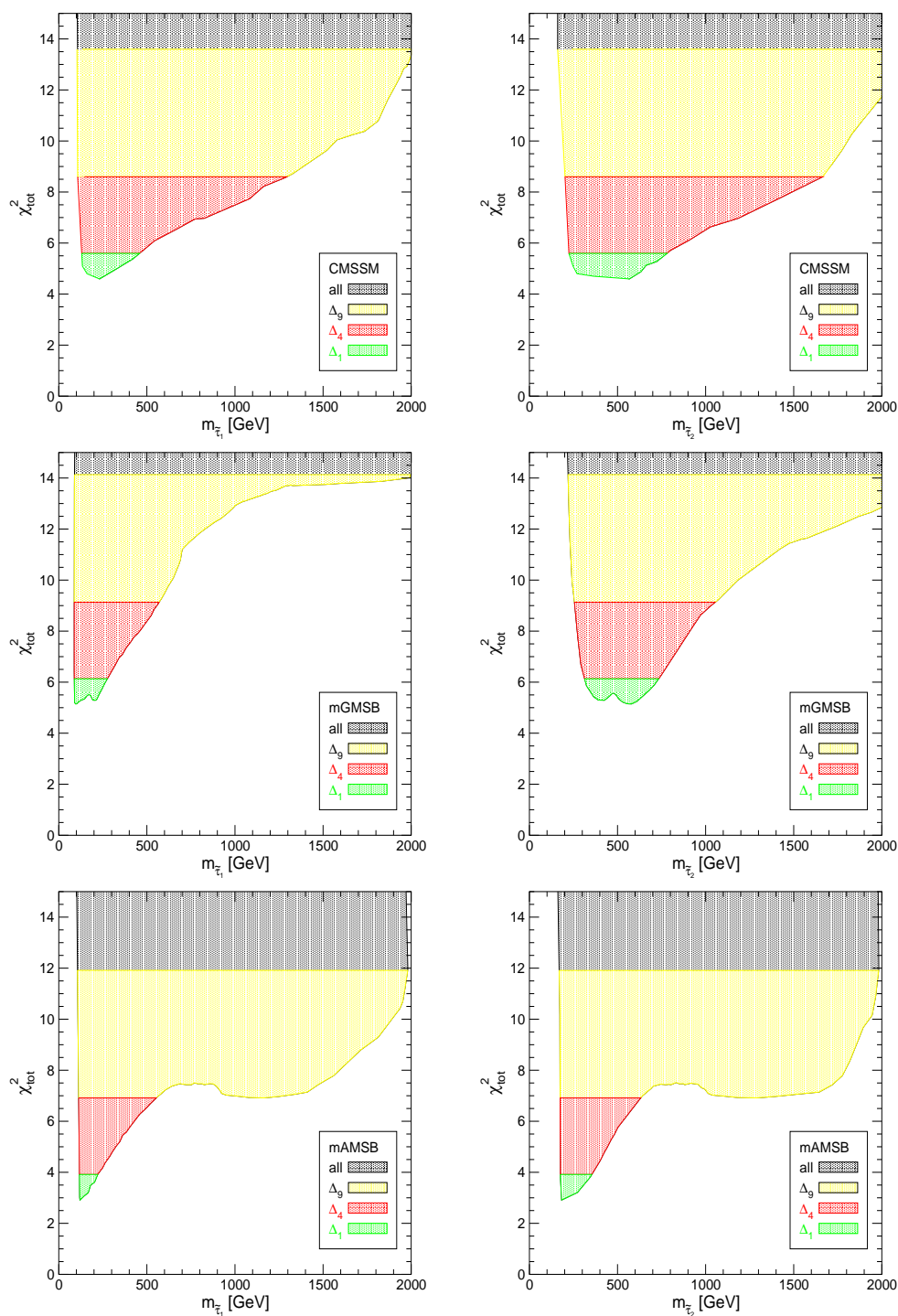


**Figure 15:**  $m_{\tilde{\tau}_1}$  (left) and  $m_{\tilde{\tau}_2}$  (right) are shown in the CMSSM (top), mGMSB (middle) and mAMSB (bottom) scenarios for  $\mu > 0$  with their respective total  $\chi^2$ . The color coding is as in figure 7.

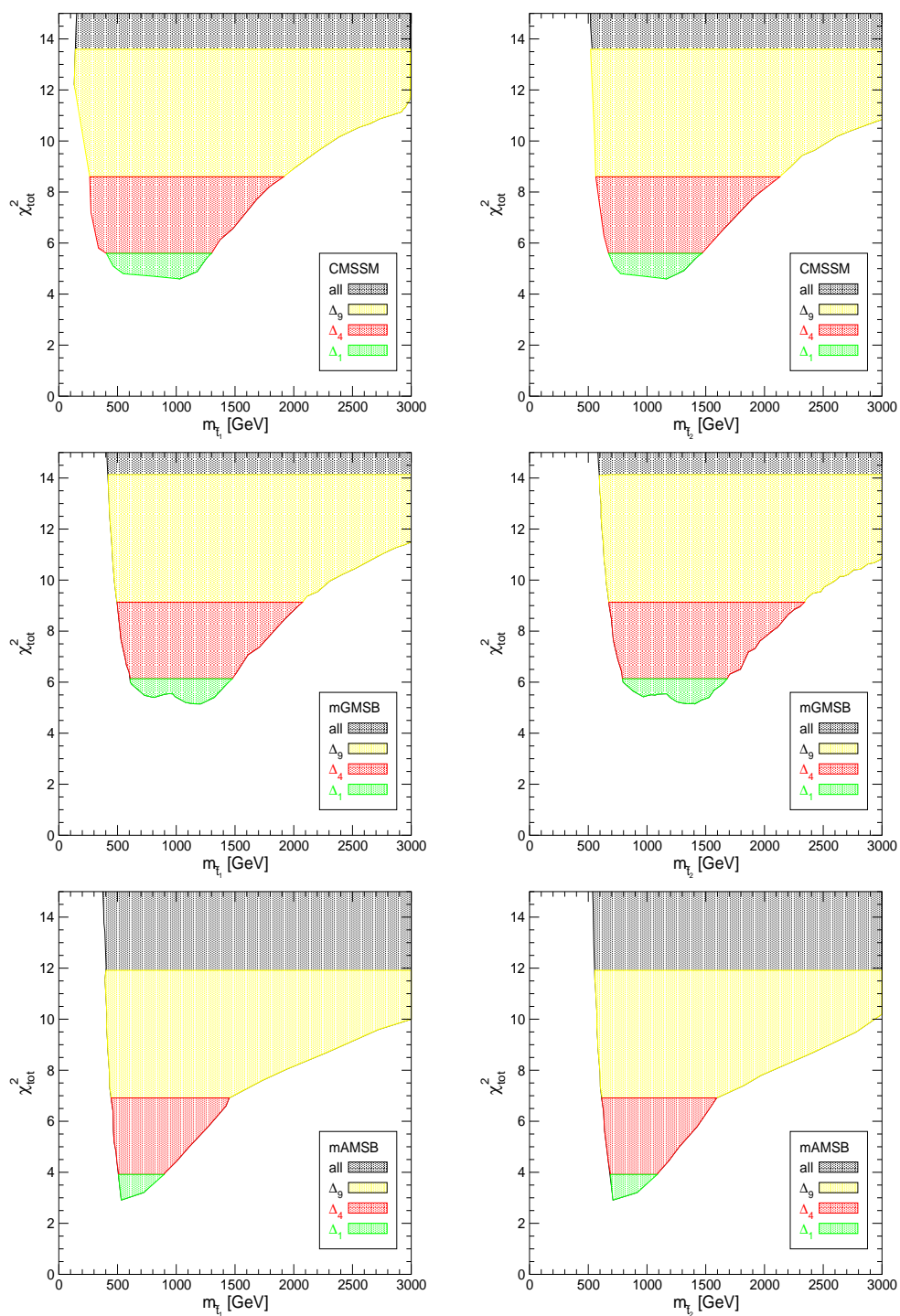


**Figure 16:**  $m_{\tilde{t}_1}$  (left) and  $m_{\tilde{t}_2}$  (right) are shown in the CMSSM (top), mGMSB (middle) and mAMSB (bottom) scenarios for  $\mu > 0$  with their respective total  $\chi^2$ . The color coding is as in figure 7.

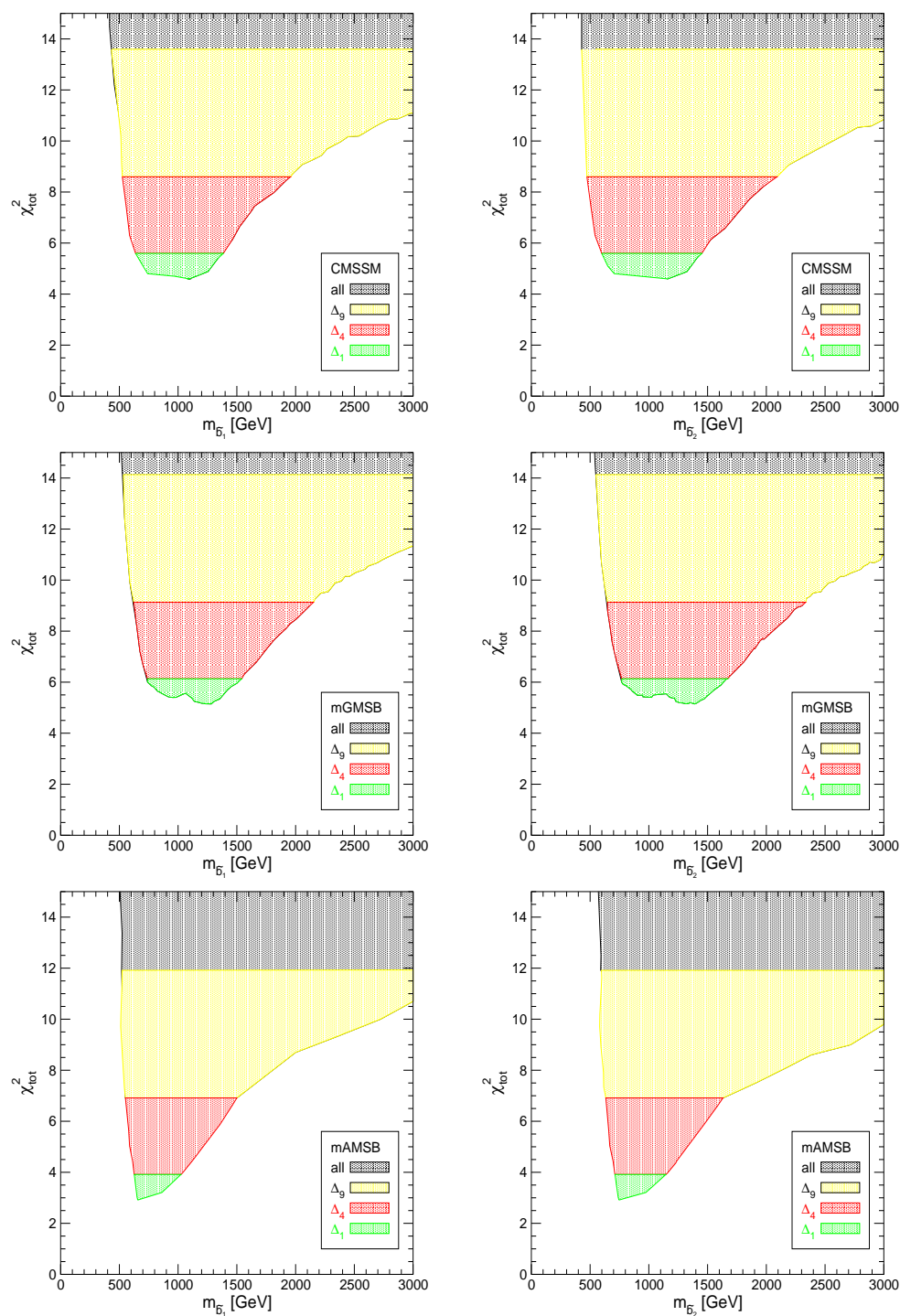


**Figure 17:**  $m_{\tilde{b}_1}$  (left) and  $m_{\tilde{b}_2}$  (right) are shown in the CMSSM (top), mGMSB (middle) and mAMSB (bottom) scenarios for  $\mu > 0$  with their respective total  $\chi^2$ . The color coding is as in figure 7.



	CMSSM	mGMSB	mAMSB
$\mu$ (best fit)	588	810	604
$\mu$ in $\Delta_1$	510–730	460–995	560–980
$\mu$ in $\Delta_4$	160–1100	390–1400	130–1420
$B$ (best fit)	94	151	28
$B$ in $\Delta_1$	65–155	75–210	-105–50
$B$ in $\Delta_4$	-75–250	65–330	-275–540

**Table 3:** ‘Preferred’ values of  $\mu$  and  $B$  (with  $\mu B$  being the prefactor of the Higgs mixing term in the potential). Shown are the best-fit points as well as the intervals covered for  $\Delta\chi^2 < 1, 4$ . All values are in GeV.

the  $\Delta_1$  and  $\Delta_4$  regions, on the other hand, are obtained for large  $\tan\beta$ , where these masses are similar to the ones in refs. [11–13] obtained for  $\tan\beta = 50$ . On the other hand, the following difference can be observed: while the fit results obtained for the particle masses in refs. [11–13] are ‘parabola shaped’, whereas the mass plots presented in figures 13–17 show ‘full’ areas. This can easily be understood as an effect of taking the CDM constraint into account in refs. [11–13], while at the same time  $\tan\beta$  had been restricted to the two discrete values  $\tan\beta = 10$  and  $50$ . The CDM constraint cuts out thin strips, for instance, in the  $m_0$ – $m_{1/2}$  plane (for fixed  $A_0$  and  $\tan\beta$ ) [153, 154]. This yields naturally strips in the mass vs.  $\chi_{\text{tot}}^2$  plots. Incorporating all  $\tan\beta$  values by scanning over all allowed values simultaneously in our analysis (where low (high)  $\tan\beta$  values yield lower (higher) best-fit masses), broadens and fills automatically the  $\Delta_1$  and  $\Delta_4$  regions. Another difference in our analysis compared to the ones in refs. [11–13] is the lower value of  $m_t$  that has been used here. Lowering the experimental value of  $m_t$  in the  $\chi^2$  analysis yields an increase in the minimum total  $\chi^2$ , as has been analyzed for  $\tan\beta = 10$  in ref. [12]. The minimum  $\chi^2$  values reached in refs. [11–13] and in our analysis roughly follow the results presented in ref. [12]. However, it should be kept in mind that the latest value of  $m_t$  that has been published recently [43] has moved upwards to  $m_t^{\text{exp}} = 172.6 \pm 1.4$  GeV.

## 5. Future sensitivities

We now turn to the analysis of the future sensitivities. In a first step we take the current best-fit point in each scenario and assume that the future measurements exactly agree with this point. The experimental and theory uncertainties are set to their ‘future’ values as discussed in section 3. Also for  $M_h$  we assume that its value is measured and include it into the  $\chi^2$  fit with the future uncertainties given in section 3.4. In a second step, in order to compare the sensitivities in the three scenarios, we have chosen one hypothetical best-fit point in each scenario, where the low-energy spectrum is “similar” in all three scenarios.

In more detail, we have demanded that

$$M_A \approx 800 \text{ GeV}, \quad \tan \beta \approx 40, \quad m_{\tilde{t}_1} \approx 1225 \text{ GeV}, \quad m_{\tilde{t}_2} \approx 1400 \text{ GeV}, \quad \mu > 0. \quad (5.1)$$

These masses are somewhat higher than the current best-fit values and thus illustrate a future scenario that is somewhat more in the decoupling regime (i.e. where SUSY masses are heavy and loop corrections are correspondingly smaller) than what is currently favored. Furthermore the combination of  $M_A$  and  $\tan \beta$ , according to current analyses [125–128, 145–150, 152], is not in the discovery reach of the LHC or the ILC. In such a scenario without experimental information on  $M_A$  and  $\tan \beta$  from the observation of the heavy Higgs bosons any sensitivity to these parameters would constitute information *in addition* to the direct collider data. The three points are defined in terms of high-energy parameters as

$$\text{CMSSM :} \quad m_0 = 640 \text{ GeV} \quad (5.2)$$

$$m_{1/2} = 720 \text{ GeV}$$

$$A_0 = 500 \text{ GeV}$$

$$\tan \beta = 41$$

$$\text{mGMSB :} \quad \Lambda = 33200 \text{ GeV} \quad (5.3)$$

$$M_{\text{mess}} = 580000 \text{ GeV}$$

$$N_{\text{mess}} = 7$$

$$\tan \beta = 41$$

$$\text{mAMSB :} \quad m_{\text{aux}} = 50500 \text{ GeV} \quad (5.4)$$

$$m_0 = 1600 \text{ GeV}$$

$$\tan \beta = 40$$

The choices in eq. (5.1) ensure a “similar” behavior in the Higgs and in the scalar top sector and their contributions to the EWPO and BPO. This allows a comparison of the future sensitivities of the EWPO and BPO in the three scenarios. The values for the lightest Higgs boson mass at the three hypothetical best-fit points are 116.8 GeV (CMSSM), 117.5 GeV (mGMSB) and 119.1 GeV (mAMSB). The spread of  $\sim 2.3$  GeV has only a minor direct impact on the predictions of the EWPO and BPO.

## 5.1 Analysis of high-scale parameters

We start by analyzing the CMSSM, mGMSB and mAMSB in terms of their respective high-energy parameters, see section 2.

### 5.1.1 CMSSM

In figure 18 we show the results for the  $\Delta_{1,4,9}$  areas in terms of the high-energy parameters, using the  $\chi^2$  result based on the assumed future experimental and theoretical precisions as described in section 3. As can be seen, the areas of the parameter space with  $\Delta\chi^2 < 1, 4, 9$  shrink substantially in comparison with figure 7. At the  $\Delta\chi^2 = 9$  level  $m_{1/2}$  is

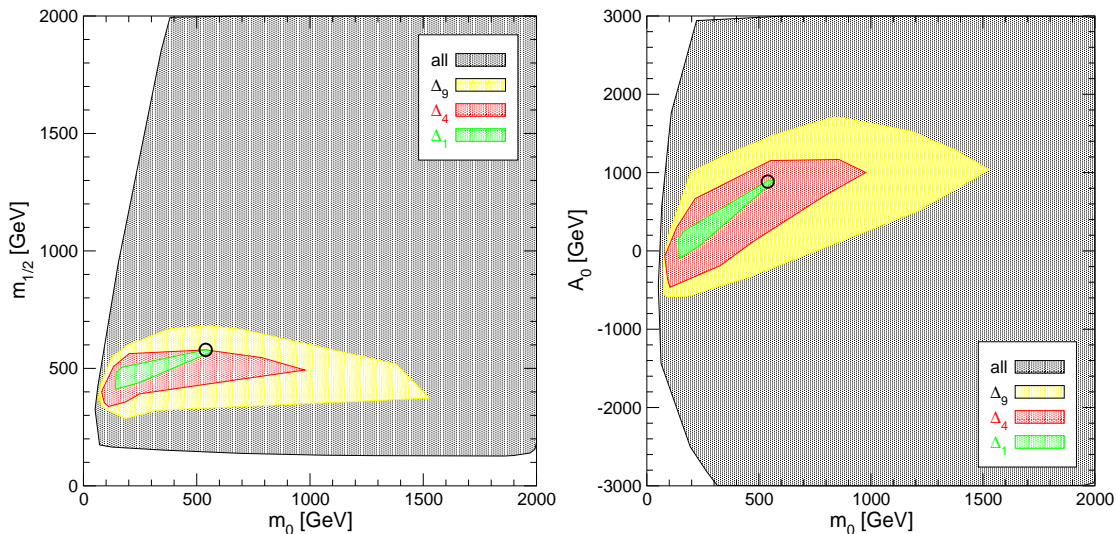


**Figure 18:** Future projection for the  $\Delta_{1,4,9}$  regions in the  $m_0$ - $m_{1/2}$  plane (left) and in the  $m_0$ - $A_0$  plane (right) in the CMSSM assuming that the future experimental data agree exactly with the current best-fit point. The color code is as in figure 7.

determined up to  $\pm 200$  GeV for the assumed best-fit point. For  $m_0$ , on the other hand, still values up to  $\sim 1500$  GeV are permitted. The  $\Delta_9$  interval for  $A_0$  shrinks to  $\pm 1000$  GeV.

The reduction of the preferred parameter region with the assumed higher precision in the future is so substantial because the currently favored best-fit parameters are relatively small, where smaller SUSY mass scales lead to larger loop effects in the precision observables. This effect is less pronounced for larger GUT scale parameters. To illustrate this effect we have chosen a CMSSM point as defined in eq. (5.2). We assume that the future experimental values agree exactly with the low-energy parameters resulting from eq. (5.2). The reduction of the preferred parameter region as shown in figure 19 compared to the present situation is still visible, but much weaker than for the current best-fit point in figure 18. Similar results (including the CDM constraint) had been found in ref. [11].

### 5.1.2 mGMSB

In figure 20 we show the results for the  $\Delta_{1,4,9}$  areas in terms of the high-energy parameters, using the future experimental and theoretical precisions as described in section 3. The color coding is as in figure 7. The plots in figure 20 show the  $\Lambda$ - $M_{\text{mess}}$  plane for  $N_{\text{mess}} = 1 \dots 8$ . For each  $N_{\text{mess}}$  a small  $\Lambda$  interval is singled out, but hardly any limit on  $M_{\text{mess}}$  is obtained even with the future precisions.

The results look similar in figure 22, where we show the  $N_{\text{mess}}$ - $\Lambda$  plane. For each  $N_{\text{mess}}$  value a relatively small range of  $\Lambda$  is favored, even at the  $\Delta\chi^2 = 9$  level. If  $N_{\text{mess}}$  could be determined in an independent way, the precision observables could give a relatively precise determination of  $\Lambda$ . On the other hand, if  $\Lambda$  could be determined, e.g. from the measurement of SUSY masses, the precision observables would give a preference for certain  $N_{\text{mess}}$  values.

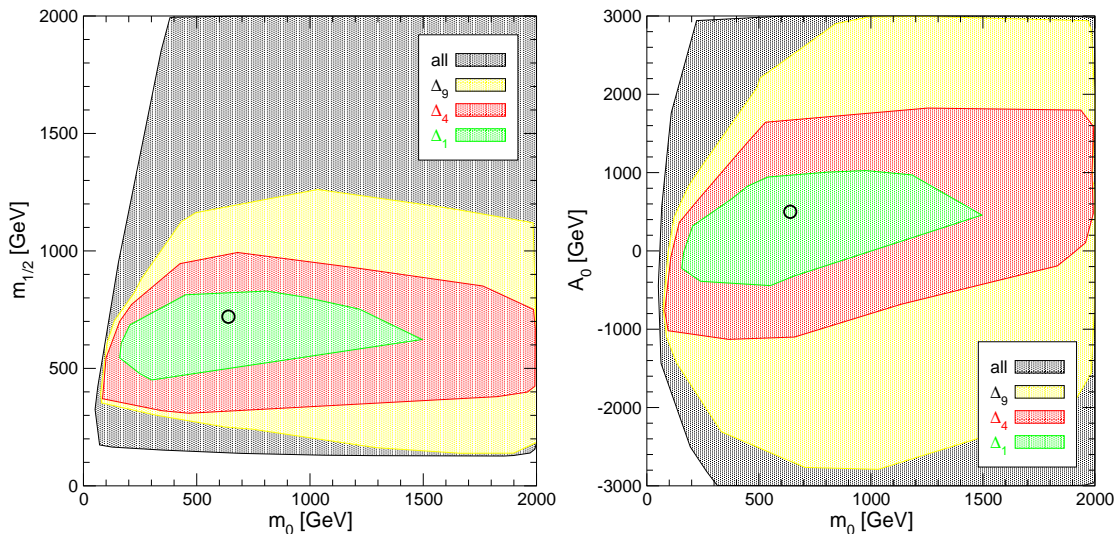


**Figure 19:** Future projection for the  $\Delta_{1,4,9}$  regions in the  $m_0$ - $m_{1/2}$  plane (left) and in the  $m_0$ - $A_0$  plane (right) in the CMSSM assuming that the future experimental data agree exactly with a hypothetical best-fit point as specified in eq. (5.2). The color code is as in figure 7.

As for the CMSSM scenario also in mGMSB we have chosen a hypothetical future best-fit point with higher mass scales, defined by eq. (5.3). As for the CMSSM, we assume that the future experimental values agree exactly with the low-energy parameters corresponding to eq. (5.3). The reduction of the  $\Delta_{1,4,9}$  regions can be observed in figure 21. It is at the same level as for the current best-fit point in figure 20. These results are also shown in the  $N_{\text{mess}}-\Lambda$  plane in figure 23, where the same sensitivity is found as for the current best-fit point displayed in figure 22.

### 5.1.3 mAMSB

In figure 24 we show the only high-energy parameter plane in the mAMSB,  $m_{\text{aux}}$  vs.  $m_0$ , with the same color coding as in figure 7. Within this scenario the precision observables will allow an extremely precise determination of the high-energy parameters. For the case that the current best-fit point agrees exactly with the future measurements, at the  $\Delta\chi^2 = 9$  level  $m_{\text{aux}}$  is determined to  $\pm 3 \times 10^3$  GeV, i.e. to  $\sim 10\%$ . The absolute precision for  $m_0$  is  $\pm 100$  GeV, whereas the relative precision reaches only  $\sim 30\%$ . (The  $\Delta_4$  and  $\Delta_1$  regions are very small and nearly invisible inside (by definition) the  $\Delta_9$  region.) This result is to a large extent due to the fact that the  $\tan\beta$  value for the current best-fit point is relatively low (see also the discussion of the hypothetical best-fit point below).

As for the other two scenarios, also in mAMSB we have chosen a hypothetical future best-fit point with higher mass scales, defined by eq. (5.4). It should be noted that for mAMSB the increase in  $M_A$  from the current best-fit point to the hypothetical best-fit point is a bit smaller than in the other two scenarios, while the shift in  $\tan\beta$  is substantially larger. Again we assume that the future experimental values agree exactly with the low-energy parameters corresponding to eq. (5.4). We show the preferred parameter space for

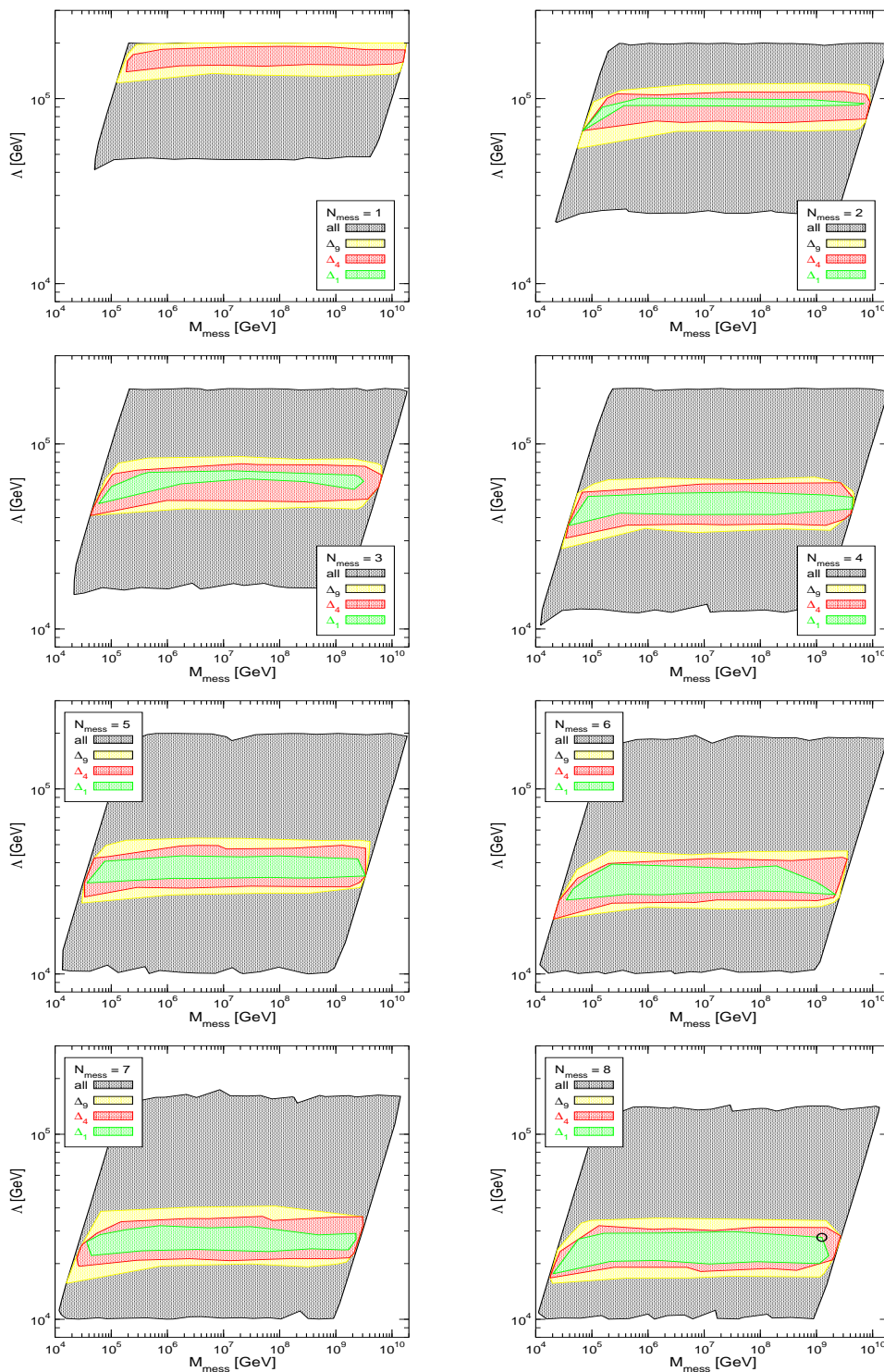


**Figure 20:** Future projection for the  $\Delta_{1,4,9}$  regions in the  $\Lambda$ - $M_{\text{mess}}$  plane for the  $N_{\text{mess}} = 1 \dots 8$  in the mGMSB assuming that the future experimental data agree exactly with the current best-fit point (marked by a circle). The color coding is as in figure 7.

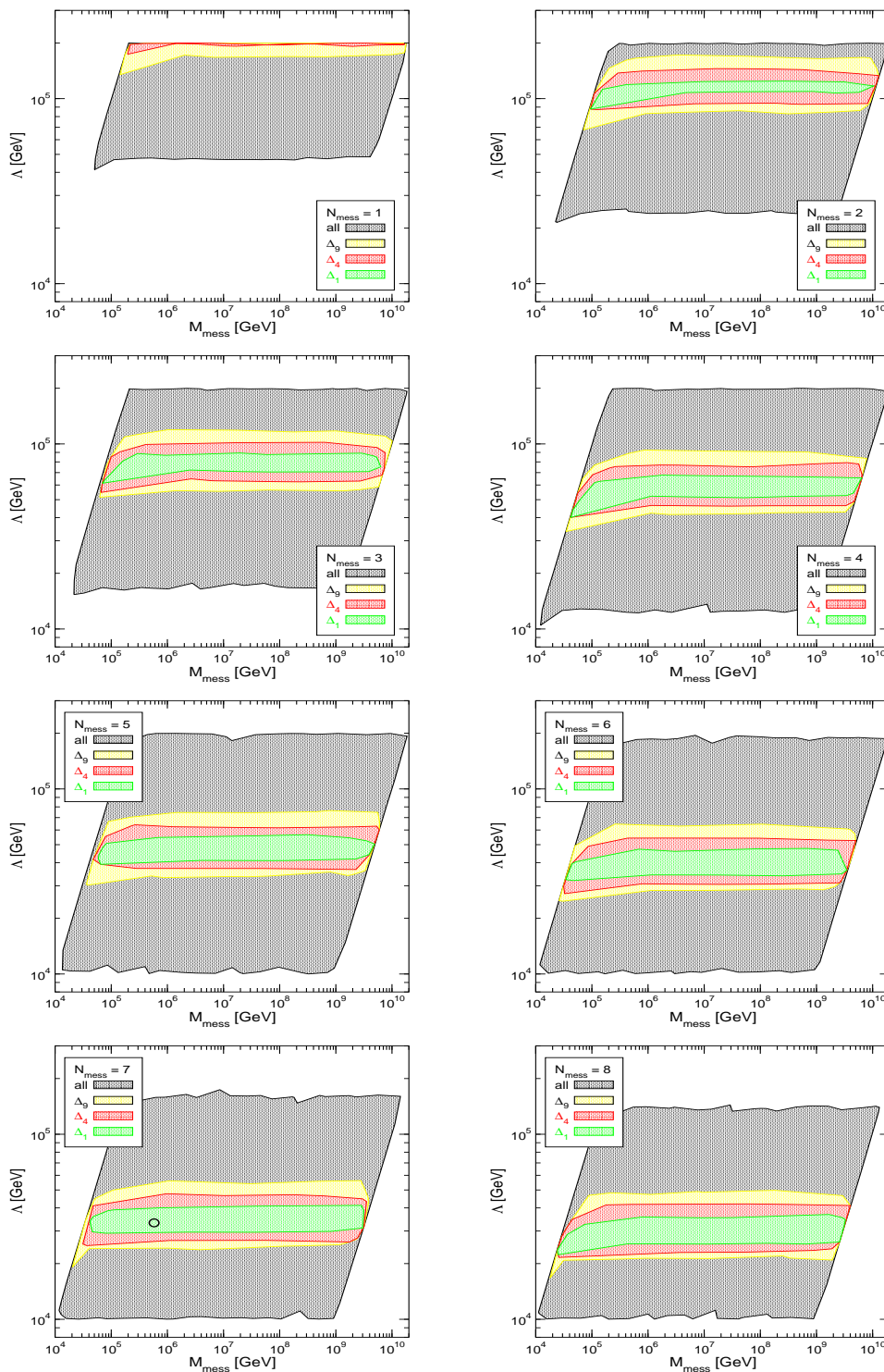


**Figure 21:** Future projection for the  $\Delta_{1,4,9}$  regions in the  $\Lambda$ - $M_{\text{mess}}$  plane for the  $N_{\text{mess}} = 1 \dots 8$  in the mGMSB assuming that the future experimental data agree exactly with the hypothetical best-fit point as defined in eq. (5.3) (marked by a circle). The color coding is as in figure 7.

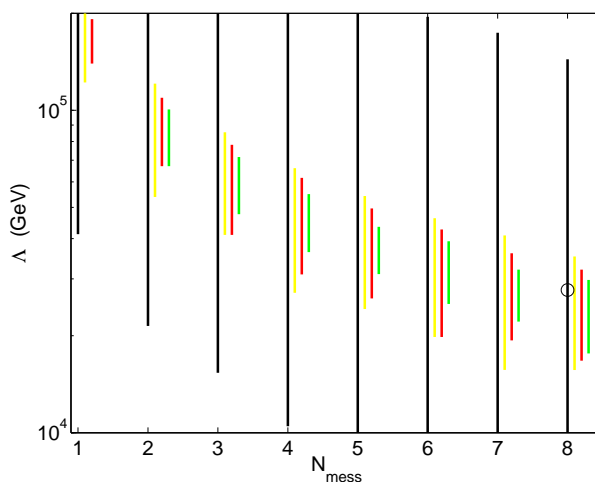


**Figure 22:** Future projection for the  $\Delta_{1,4,9}$  regions in the  $N_{\text{mess}}-\Lambda$  plane in the mGMSB assuming that the future experimental data agree exactly with the current best-fit point (marked by a circle). The color coding is as in figure 7.

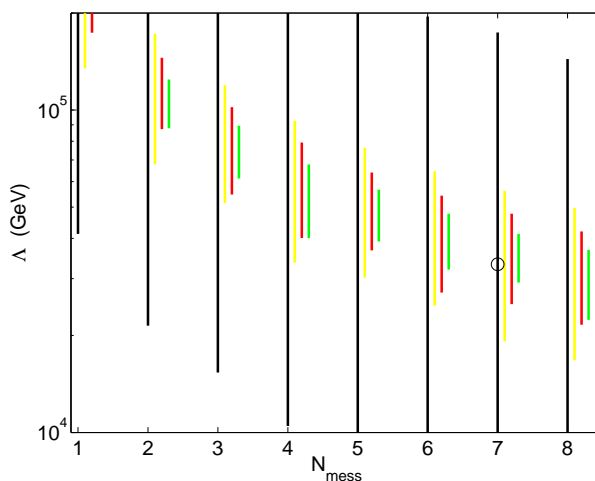


**Figure 23:** Future projection for the  $\Delta_{1,4,9}$  regions in the  $N_{\text{mess}}-\Lambda$  plane in the mGMSB assuming that the future experimental data agree exactly with the hypothetical best-fit point as defined in eq. (5.3) (marked by a circle). The color coding is as in figure 7.

this hypothetical point in figure 25. The reduction in the size of the  $\Delta_{1,4,9}$  regions compared to the present situation is much weaker than for the current best-fit point in figure 24. At the  $\Delta_9$  level no limit on  $m_0$  can be set. This shows that the very high precision obtainable with the current best-fit point is not generally valid in the mAMS scenario.

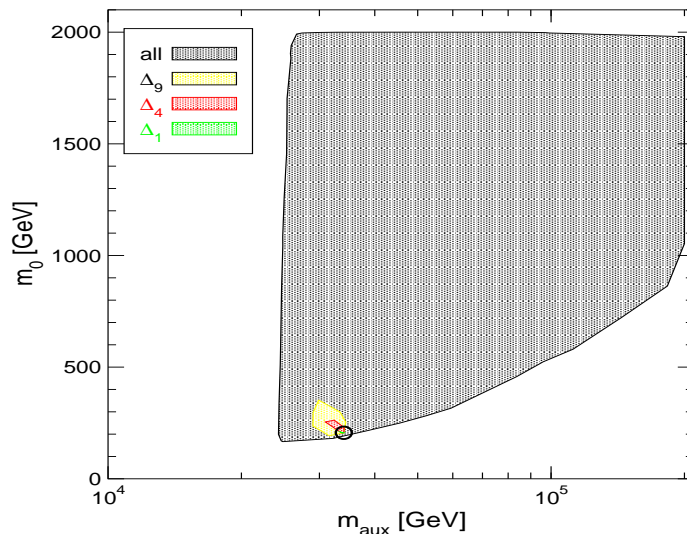


**Figure 24:** Future projection for the  $\Delta_{1,4,9}$  regions in the  $m_{\text{aux}}-m_0$  plane in the mAMSB assuming that the future experimental data agree exactly with the current best-fit point. The color coding is as in figure 7.

## 5.2 Low-energy analysis

We now turn to the comparison of the three soft SUSY-breaking scenarios in terms of  $M_A$  and  $\tan\beta$ , assuming the future experimental and theory precisions as discussed in section 3. In figure 26 we show the  $M_A-\tan\beta$  plane for the CMSSM (top), mGMSB (middle) and mAMSB (bottom) with the same color coding as in figure 7. In each scenario we assume that the future measurements will agree exactly with the current best-fit point.

A drastic improvement compared to the present situation can be observed in all three scenarios. However, also for the low-energy parameters the quality of the improvement going to the future sensitivities depends on the fact that currently relatively low mass scales are favored, see below. The results look quite different in mAMSB as compared to the CMSSM and mGMSB. Within the latter two the  $\Delta_9$  region is confined to  $M_A \lesssim 1000$  GeV with a width of 300(400) GeV for the CMSSM (mGMSB), whereas  $\tan\beta$  is only weakly restricted,  $10(20) \lesssim \tan\beta \lesssim 60$ . Within mAMSB, as for the high-energy parameters, a very precise indirect determination of  $M_A$  and  $\tan\beta$  can be performed. At the  $\Delta\chi^2 = 9$  level  $M_A$  is confined to  $\pm 50$  GeV, i.e. to about 6%.  $\tan\beta$  is determined to  $\pm 3$ , corresponding to a precision of  $\sim 8\%$ . However, as discussed in section 5.1.3, this is largely due to the relatively small value of  $\tan\beta$  within the mAMSB scenario at the current best-fit point.

We finally investigate the future sensitivity of the three soft SUSY-breaking scenarios for the hypothetical best-fit point. In figure 27 we show the results for the hypothetical best-fit points as defined in eqs. (5.2), (5.3), (5.4) for the CMSSM, mGMSB and mAMSB, respectively. By definition, see eq. (5.1), the hypothetical best-fit values for  $M_A$  and  $\tan\beta$  are very similar in the three scenarios,  $M_A \approx 800$  GeV and  $\tan\beta \approx 40$ . These  $M_A$  values are somewhat larger than the current best-fit values, see table 1. In combination with  $\tan\beta \approx$



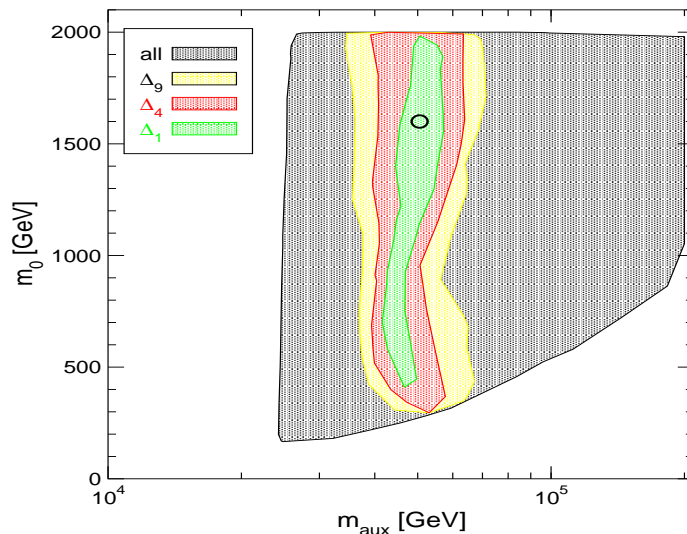


**Figure 25:** Future projection for the  $\Delta_{1,4,9}$  regions in the  $m_{\text{aux}}-m_0$  plane in the mAMSB assuming that the future experimental data agree exactly with the hypothetical best-fit point as defined in eq. (5.4) The color coding is as in figure 7.

40 such heavy MSSM Higgs bosons could not be detected at the LHC [145–150, 152] or the ILC [125–128]. Despite the fact that these values are already in the decoupling regime (i.e. where SUSY masses are large and loop effects are correspondingly small), the precision observables are still able to provide upper (and lower) limits on  $M_A$  and  $\tan\beta$  with similar results in the three soft SUSY-breaking scenarios. The upper limit at the  $\Delta\chi^2 = 9$  level on  $M_A$  varies between  $\sim 2000$  GeV in the CMSSM and  $\sim 1400$  GeV in mGMSB. This means that the limits obtainable for  $M_A$  and  $\tan\beta$  depend only to a small extent on the details of the underlying physics scenario and can thus be viewed as a more general result for scenarios resulting from a high-scale theory. In conclusion, the precision observables could allow one to set an indirect bound on  $M_A$  (and mildly also on  $\tan\beta$ ) beyond the direct collider reach. This sensitivity would improve even more if the future collider data (SUSY masses etc.) would be included (see e.g. ref. [155]). Such an analysis, however, would at the present state be highly speculative and is beyond the scope of our paper.

## 6. Conclusions

We investigated the constraints arising from electroweak precision observables (EWPO) and  $B$ -physics observables (BPO) providing a comparison of the CMSSM, the mGMSB and the mAMSB. We performed a  $\chi^2$  analysis based on the mass of the  $W$  boson,  $M_W$ , the effective weak leptonic mixing angle,  $\sin^2\theta_{\text{eff}}$ , the anomalous magnetic moment of the muon  $(g-2)_\mu$ , the mass of the lightest  $\mathcal{CP}$ -even MSSM Higgs boson,  $M_h$ , as well as on  $\text{BR}(b \rightarrow s\gamma)$  and  $\text{BR}(B_s \rightarrow \mu^+\mu^-)$ . Our analysis should be viewed as an exploratory study for the comparison of the scenarios, providing a starting point for a more refined investigation using more precision data and an elaborate  $\chi^2$  analysis [18].

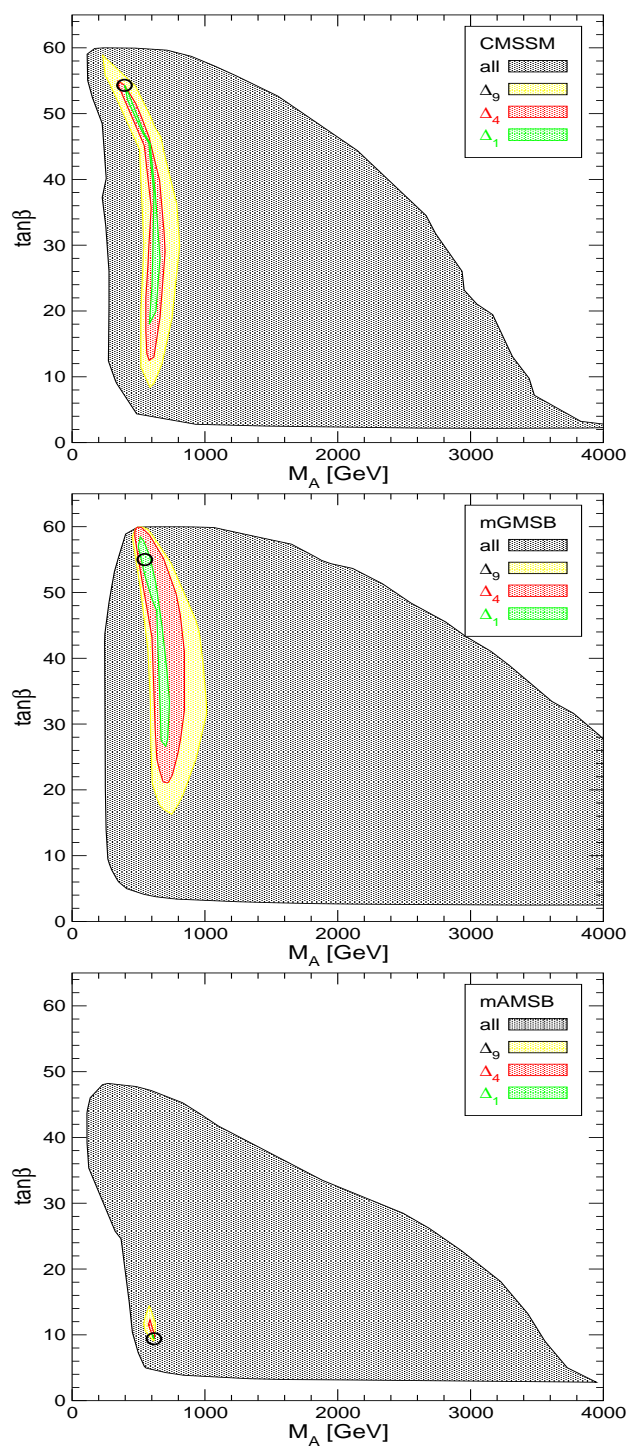


**Figure 26:** Future projection for the  $\Delta_{1,4,9}$  regions in the  $M_A$ - $\tan\beta$  planes in the CMSSM (top), mGMSB (middle) and mAMSB (bottom) assuming that the future measurements will agree exactly with the current best-fit point. The color coding is as in figure 7.

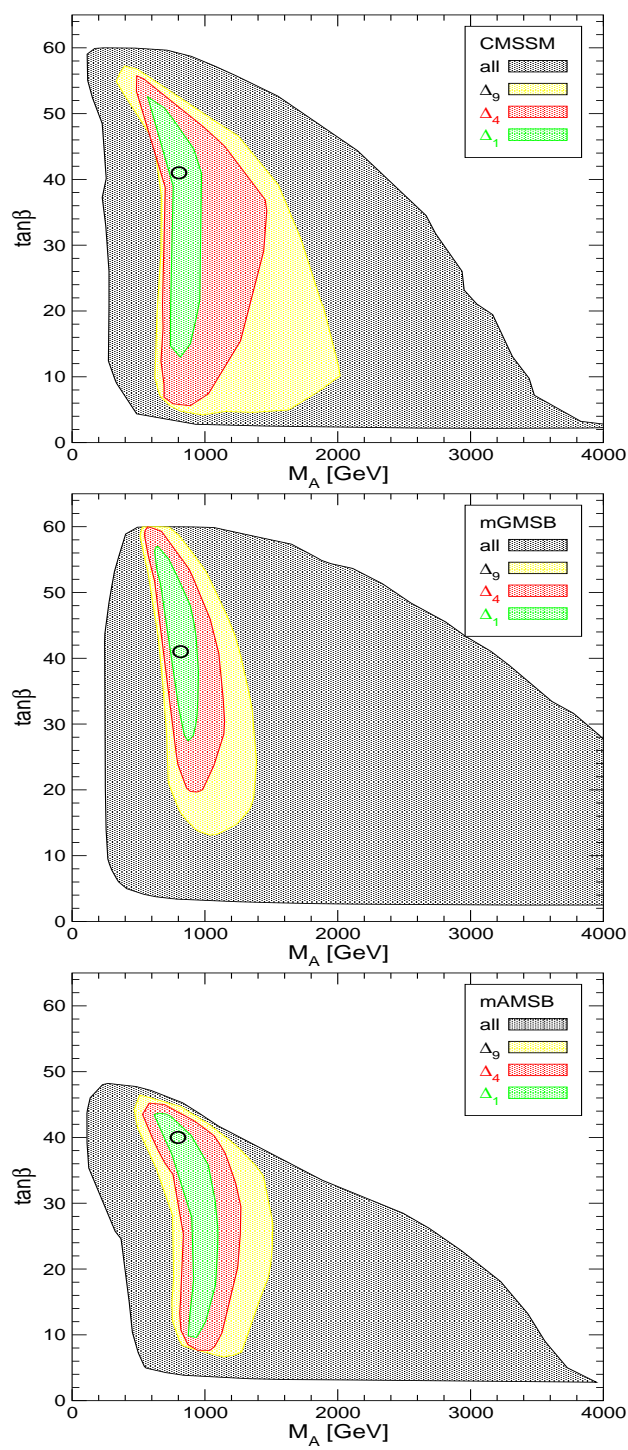


**Figure 27:** Future projection for the  $\Delta_{1,4,9}$  regions in the  $M_A$ - $\tan\beta$  planes in the CMSSM (top), mGMSB (middle) and mAMSB (bottom) assuming the hypothetical future best fit points defined eqs. (5.2), (5.3), (5.4) for the CMSSM, mGMSB and mAMSB, respectively. The color coding is as in figure 7.

Our results are analyzed separately in terms of the high-scale parameters of the respective model as well as in terms of low-energy parameters such as  $M_A$ ,  $\tan\beta$  and SUSY particle masses. Using today's measurements, uncertainties and exclusion bounds, we find that relatively low mass scales in all three scenarios are favored at the level of  $\Delta\chi^2 < 1$  or 4. However, the current data of EWPO and BPO can hardly set any upper bound on the SUSY mass scales at the level of  $\Delta\chi^2 = 9$ . The best fit-values for  $M_A$  range from  $\sim 400$  GeV in the CMSSM up to  $\sim 600$  GeV in mAMSB, whereas the  $\tan\beta$  values are only weakly constrained. Remarkably the mAMSB scenario, despite having one free GUT scale parameter less than the other two scenarios, has a somewhat lower total minimum  $\chi^2$ . This can be traced back to a better agreement with the combination of the  $\text{BR}(b \rightarrow s\gamma)$  and  $(g-2)_\mu$  measurements (with some help from  $M_W$ ) for a heavier scalar quark spectrum and a corresponding slightly larger value of  $M_h$ .

We presented predictions for the lightest  $\mathcal{CP}$ -even Higgs boson mass, based on the current  $\chi^2$  data, but without imposing the current LEP bound from Higgs boson searches and its corresponding  $\chi^2$  contribution. Best-fit values of  $M_h \sim 105$  GeV are found for the CMSSM and mGMSB, and  $M_h \sim 113$  GeV for mAMSB. In all three scenarios a relatively good compatibility with the direct bounds from the Higgs searches at LEP is found. Within mAMSB the  $\Delta\chi^2 < 1$  region extends up to  $M_h \lesssim 122$  GeV.

We also presented the predictions for the masses of various SUSY particles such as  $m_{\tilde{t}_1}$ ,  $m_{\tilde{t}_2}$ ,  $m_{\tilde{b}_1}$ ,  $m_{\tilde{b}_2}$ ,  $m_{\tilde{\tau}_1}$ ,  $m_{\tilde{\tau}_2}$ ,  $m_{\tilde{\chi}_1^0}$ ,  $m_{\tilde{\chi}_2^0}$ ,  $m_{\tilde{\chi}_1^\pm}$  and  $m_{\tilde{g}}$  in the three soft SUSY-breaking scenarios. As a general feature lowest masses are found in the mAMSB and heaviest in mGMSB. All three scenarios offer good prospects for the discovery of some color-neutral particles at the ILC (with a center-of-mass energy up to  $\sqrt{s} = 1$  TeV) and for colored particles at the LHC. There are also good prospects for the discovery of uncolored particles such as charginos, neutralinos and light sleptons, especially if they are produced in cascade decays. Some part of the preferred parameter space in the three scenarios is currently probed at the Tevatron. Within the CMSSM qualitative agreement in the preferred mass ranges with previous analyses [11–13] has been found.

Finally, we explored the projection for the future sensitivities of the EWPO and BPO in the three soft SUSY-breaking scenarios. Here we also assumed a measurement of the lightest MSSM Higgs boson mass. In a first step we analyzed the future sensitivities assuming that the future measurements agree with the current best-fit results. We found a strong improvement with respect to the current sensitivity. Within the mAMSB scenario  $M_A$  and  $\tan\beta$  can be determined indirectly with very high precision, largely due to the fact that the current best-fit point has a relatively low  $\tan\beta$  value. On the other hand, in the CMSSM and mGMSB the  $\tan\beta$  determination remains relatively weak, where the current best-fit points have very large  $\tan\beta$  values. In a second step we assumed that the future measurements will agree in each scenario with a certain hypothetical point. These three points were defined for each scenario such that they result in a similar Higgs and SUSY spectrum with  $M_A \approx 800$  GeV and  $\tan\beta \approx 40$ . In general the Higgs and SUSY mass scales are somewhat higher than for the current best-fit points, i.e. loop corrections are correspondingly somewhat smaller. These points would not permit a direct determination of the heavy Higgs-boson mass scale. We find that the EWPO and BPO exhibit a similar future sensi-

tivity in the CMSSM, mGMSB and mAMSB giving rise to an upper limit on the high-scale parameters at the  $\Delta\chi^2 = 9$  level. The future EWPO and BPO sensitivities depend only mildly on the underlying physics scenario. The precision observables could allow one to constrain the Higgs sector parameters even beyond the direct reach of the LHC or the ILC.

Once LHC (and ILC) data on SUSY masses will be available, the assumption about the underlying scenario itself will be investigated. While information from the direct production of SUSY particles will obviously be crucial for disentangling the underlying scenario of SUSY-breaking, also the EWPO and BPO will certainly play an important role in this context.

## Acknowledgments

We thank B. Allanach for help with in the use of `SoftSUSY`. We thank A. Dedes and C.E.M. Wagner for helpful discussions. The work of S.H. was partially supported by CICYT (grant FPA 2007-66387). X.M. and S.S. are supported under U.S. Department of Energy contract # DE-FG02-04ER-41298. Work supported in part by the European Community's Marie-Curie Research Training Network under contract MRTN-CT-2006-035505 'Tools and Precision Calculations for Physics Discoveries at Colliders'.

## References

- [1] H.P. Nilles, *Supersymmetry, supergravity and particle physics*, *Phys. Rept.* **110** (1984) 1.
- [2] H.E. Haber and G.L. Kane, *The search for supersymmetry: probing physics beyond the standard model*, *Phys. Rept.* **117** (1985) 75;  
R. Barbieri, *Looking beyond the standard model: the supersymmetric option*, *Riv. Nuovo Cim.* **11N4** (1988) 1.
- [3] HEAVY FLAVOR ANALYSIS GROUP collaboration, *Heavy flavor averaging group homepage*, <http://www.slac.stanford.edu/xorg/hfag/>.
- [4] J.R. Ellis, S. Kelley and D.V. Nanopoulos, *Probing the desert using gauge coupling unification*, *Phys. Lett.* **B 260** (1991) 131;  
U. Amaldi, W. de Boer and H. Furstenuau, *Comparison of grand unified theories with electroweak and strong coupling constants measured at LEP*, *Phys. Lett.* **B 260** (1991) 447;  
C. Giunti, C.W. Kim and U.W. Lee, *Running coupling constants and grand unification models*, *Mod. Phys. Lett.* **A 6** (1991) 1745.
- [5] M. Dine, W. Fischler and M. Srednicki, *Supersymmetric technicolor*, *Nucl. Phys.* **B 189** (1981) 575;  
S. Dimopoulos and S. Raby, *Supercolor*, *Nucl. Phys.* **B 192** (1981) 353;  
M. Dine and W. Fischler, *A phenomenological model of particle physics based on supersymmetry*, *Phys. Lett.* **B 110** (1982) 227;  
M. Dine and M. Srednicki, *More supersymmetric technicolor*, *Nucl. Phys.* **B 202** (1982) 238;  
M. Dine and W. Fischler, *A supersymmetric GUT*, *Nucl. Phys.* **B 204** (1982) 346;  
L. Álvarez-Gaumé, M. Claudson and M.B. Wise, *Low-energy supersymmetry*, *Nucl. Phys.* **B 207** (1982) 96;  
C.R. Nappi and B.A. Ovrut, *Supersymmetric extension of the  $SU(3) \times SU(2) \times U(1)$  model*, *Phys. Lett.* **B 113** (1982) 175;

- S. Dimopoulos and S. Raby, *Geometric hierarchy*, *Nucl. Phys. B* **219** (1983) 479.
- [6] M. Dine and A.E. Nelson, *Dynamical supersymmetry breaking at low-energies*, *Phys. Rev. D* **48** (1993) 1277 [[hep-ph/9303230](#)];  
M. Dine, A. Nelson and Y. Shirman, *Low-energy dynamical supersymmetry breaking simplified*, *Phys. Rev. D* **51** (1995) 1362 [[hep-ph/9408384](#)];  
M. Dine, A. Nelson, Y. Nir and Y. Shirman, *New tools for low-energy dynamical supersymmetry breaking*, *Phys. Rev. D* **53** (1996) 2658 [[hep-ph/9507378](#)].
- [7] For a review see G.F. Giudice and R. Rattazzi, *Theories with gauge-mediated supersymmetry breaking*, *Phys. Rept.* **322** (1999) 419 [[hep-ph/9801271](#)].
- [8] L. Randall and R. Sundrum, *Out of this world supersymmetry breaking*, *Nucl. Phys. B* **557** (1999) 79 [[hep-th/9810155](#)].
- [9] G.F. Giudice, M.A. Luty, H. Murayama and R. Rattazzi, *Gaugino mass without singlets*, *JHEP* **12** (1998) 027 [[hep-ph/9810442](#)].
- [10] T. Gherghetta, G.F. Giudice and J.D. Wells, *Phenomenological consequences of supersymmetry with anomaly-induced masses*, *Nucl. Phys. B* **559** (1999) 27 [[hep-ph/9904378](#)].
- [11] J.R. Ellis, S. Heinemeyer, K.A. Olive and G. Weiglein, *Indirect sensitivities to the scale of supersymmetry*, *JHEP* **02** (2005) 013 [[hep-ph/0411216](#)].
- [12] J.R. Ellis, S. Heinemeyer, K.A. Olive and G. Weiglein, *Phenomenological indications of the scale of supersymmetry*, *JHEP* **05** (2006) 005 [[hep-ph/0602220](#)].
- [13] J.R. Ellis, S. Heinemeyer, K.A. Olive, A.M. Weber and G. Weiglein, *The supersymmetric parameter space in light of B-physics observables and electroweak precision data*, *JHEP* **08** (2007) 083 [[arXiv:0706.0652](#)].
- [14] J. Ellis, T. Hahn, S. Heinemeyer, K.A. Olive and G. Weiglein, *WMAP-compliant benchmark surfaces for MSSM Higgs bosons*, *JHEP* **10** (2007) 092 [[arXiv:0709.0098](#)].
- [15] J.R. Ellis, S. Heinemeyer, K.A. Olive and G. Weiglein, *Light heavy MSSM Higgs bosons at large  $\tan\beta$* , *Phys. Lett. B* **653** (2007) 292 [[arXiv:0706.0977](#)].
- [16] J.R. Ellis, K.A. Olive, Y. Santoso and V.C. Spanos, *Likelihood analysis of the CMSSM parameter space*, *Phys. Rev. D* **69** (2004) 095004 [[hep-ph/0310356](#)];  
B.C. Allanach and C.G. Lester, *Multi-dimensional mSUGRA likelihood maps*, *Phys. Rev. D* **73** (2006) 015013 [[hep-ph/0507283](#)];  
B.C. Allanach, *Naturalness priors and fits to the constrained minimal supersymmetric standard model*, *Phys. Lett. B* **635** (2006) 123 [[hep-ph/0601089](#)];  
R.R. de Austri, R. Trotta and L. Roszkowski, *A Markov chain Monte Carlo analysis of the CMSSM*, *JHEP* **05** (2006) 002 [[hep-ph/0602028](#)];  
L. Roszkowski, R.R. de Austri and R. Trotta, *On the detectability of the CMSSM light Higgs boson at the Tevatron*, *JHEP* **04** (2007) 084 [[hep-ph/0611173](#)];  
L. Roszkowski et al., *Implications for the constrained MSSM from a new prediction for  $b \rightarrow s\gamma$* , *JHEP* **07** (2007) 075 [[arXiv:0705.2012](#)];  
B.C. Allanach, C.G. Lester and A.M. Weber, *The dark side of mSUGRA*, *JHEP* **12** (2006) 065 [[hep-ph/0609295](#)];  
B.C. Allanach, K. Cranmer, C.G. Lester and A.M. Weber, *Natural priors, CMSSM fits and LHC weather forecasts*, *JHEP* **08** (2007) 023 [[arXiv:0705.0487](#)];

- S. Heinemeyer, *Electroweak precision data and gravitino dark matter*, *Pramana* **69** (2007) 947 [[hep-ph/0611372](#)].
- [17] G. Isidori, F. Mescia, P. Paradisi and D. Temes, *Flavour physics at large  $\tan\beta$  with a Bino-like LSP*, *Phys. Rev. D* **75** (2007) 115019 [[hep-ph/0703035](#)];  
M. Carena, A. Menon and C. Wagner, *Challenges for MSSM Higgs searches at hadron colliders*, *Phys. Rev. D* **76** (2007) 035004 [[arXiv:0704.1143](#)].
- [18] O. Buchmueller et al., *Prediction for the lightest Higgs boson mass in the CMSSM using indirect experimental constraints*, *Phys. Lett. B* **657** (2007) 87 [[arXiv:0707.3447](#)].
- [19] S. Heinemeyer, M. Mondragón and G. Zoupanos, *Confronting finite unified theories with low-energy phenomenology*, *JHEP* **07** (2008) 135 [[arXiv:0712.3630](#)];  
A. Djouadi, S. Heinemeyer, M. Mondragón and G. Zoupanos, *Finite unified theories and the Higgs mass prediction*, *Springer Proc. Phys.* **98** (2005) 273 [[hep-ph/0404208](#)].
- [20] F. Mahmoudi, *New constraints on supersymmetric models from  $b \rightarrow s\gamma$* , *JHEP* **12** (2007) 026 [[arXiv:0710.3791](#)].
- [21] F. Domingo and U. Ellwanger, *Updated constraints from B physics on the MSSM and the NMSSM*, *JHEP* **12** (2007) 090 [[arXiv:0710.3714](#)].
- [22] J. Kasahara, K. Freese and P. Gondolo, *Dark matter in the MSSM golden region*, [arXiv:0805.0999](#).
- [23] WMAP collaboration, C.L. Bennett et al., *First year Wilkinson Microwave Anisotropy Probe (WMAP) observations: preliminary maps and basic results*, *Astrophys. J. Suppl.* **148** (2003) 1 [[astro-ph/0302207](#)];  
WMAP collaboration, D.N. Spergel et al., *First year Wilkinson Microwave Anisotropy Probe (WMAP) observations: determination of cosmological parameters*, *Astrophys. J. Suppl.* **148** (2003) 175 [[astro-ph/0302209](#)]; *Wilkinson Microwave Anisotropy Probe (WMAP) three year results: implications for cosmology*, *Astrophys. J. Suppl.* **170** (2007) 377 [[astro-ph/0603449](#)].
- [24] A. Arbey and F. Mahmoudi, *SUSY constraints from relic density: high sensitivity to pre-BBN expansion rate*, [arXiv:0803.0741](#).
- [25] H.K. Dreiner, *An introduction to explicit R-parity violation*, [hep-ph/9707435](#);  
G. Bhattacharyya, *A brief review of R-parity-violating couplings*, [hep-ph/9709395](#);  
B.C. Allanach, A. Dedes and H.K. Dreiner, *Bounds on R-parity violating couplings at the weak scale and at the GUT scale*, *Phys. Rev. D* **60** (1999) 075014 [[hep-ph/9906209](#)].
- [26] D.H. Lyth and E.D. Stewart, *Thermal inflation and the moduli problem*, *Phys. Rev. D* **53** (1996) 1784 [[hep-ph/9510204](#)].
- [27] G.B. Gelmini and P. Gondolo, *Neutralino with the right cold dark matter abundance in (almost) any supersymmetric model*, *Phys. Rev. D* **74** (2006) 023510 [[hep-ph/0602230](#)].
- [28] G. Degrandi, P. Gambino and P. Slavich, *QCD corrections to radiative B decays in the MSSM with minimal flavor violation*, *Phys. Lett. B* **635** (2006) 335 [[hep-ph/0601135](#)];  
E. Lunghi, W. Porod and O. Vives, *Analysis of enhanced  $\tan\beta$  corrections in MFV GUT scenarios*, *Phys. Rev. D* **74** (2006) 075003 [[hep-ph/0605177](#)].
- [29] H.P. Nilles, *Dynamically broken supergravity and the hierarchy problem*, *Phys. Lett. B* **115** (1982) 193; *Supergravity generates hierarchies*, *Nucl. Phys. B* **217** (1983) 366;

- A.H. Chamseddine, R.L. Arnowitt and P. Nath, *Locally supersymmetric grand unification*, *Phys. Rev. Lett.* **49** (1982) 970;
- R. Barbieri, S. Ferrara and C.A. Savoy, *Gauge models with spontaneously broken local supersymmetry*, *Phys. Lett.* **B 119** (1982) 343;
- H.P. Nilles, M. Srednicki and D. Wyler, *Weak interaction breakdown induced by supergravity*, *Phys. Lett.* **B 120** (1983) 346;
- E. Cremmer, P. Fayet and L. Girardello, *Gravity induced supersymmetry breaking and low-energy mass spectrum*, *Phys. Lett.* **B 122** (1983) 41;
- S. Ferrara, L. Girardello and H.P. Nilles, *Breakdown of local supersymmetry through gauge fermion condensates*, *Phys. Lett.* **B 125** (1983) 457;
- L.J. Hall, J.D. Lykken and S. Weinberg, *Supergravity as the messenger of supersymmetry breaking*, *Phys. Rev.* **D 27** (1983) 2359;
- S.K. Soni and H.A. Weldon, *Analysis of the supersymmetry breaking induced by  $N = 1$  supergravity theories*, *Phys. Lett.* **B 126** (1983) 215;
- P. Nath, R.L. Arnowitt and A.H. Chamseddine, *Gauge hierarchy in supergravity guts*, *Nucl. Phys.* **B 227** (1983) 121;
- For more details see S. Weinberg, *The quantum theory of fields. Vol. 3: supersymmetry*, Cambridge University Press, Cambridge U.K. (2000).
- [30] A.B. Lahanas and D.V. Nanopoulos, *The road to no scale supergravity*, *Phys. Rept.* **145** (1987) 1;  
S.P. Martin, *A supersymmetry primer*, [hep-ph/9709356](#).
- [31] H. Murayama and Y. Nomura, *Gauge mediation simplified*, *Phys. Rev. Lett.* **98** (2007) 151803 [[hep-ph/0612186](#)]; *Simple scheme for gauge mediation*, *Phys. Rev.* **D 75** (2007) 095011 [[hep-ph/0701231](#)].
- [32] S.A. Abel, C. Durnford, J. Jaeckel and V.V. Khoze, *Patterns of gauge mediation in metastable SUSY breaking*, *JHEP* **02** (2008) 074 [[arXiv:0712.1812](#)].
- [33] PARTICLE DATA GROUP collaboration, W.M. Yao et al., *Review of particle physics*, *J. Phys.* **G 33** (2006) 1.
- [34] P. Fayet, *Mixing between gravitational and weak interactions through the massive gravitino*, *Phys. Lett.* **B 70** (1977) 461; *Scattering cross-sections of the photino and the goldstino (gravitino) on matter*, *Phys. Lett.* **B 86** (1979) 272; *Lower limit on the mass of a light gravitino from  $e^+e^-$  annihilation experiments*, *Phys. Lett.* **B 175** (1986) 471;  
*Supersymmetry, particle physics and gravitation*, in *Unification of the fundamental particle interactions*, S. Ferrara, J. Ellis and P. van Nieuwenhuizen eds., Plenum, New York U.S.A. (1980) pg. 587 [*Ettore Majorana Int. Sci. Ser. Phys. Sci.* **7** (1980) 587].
- [35] A. Pomarol and R. Rattazzi, *Sparticle masses from the superconformal anomaly*, *JHEP* **05** (1999) 013 [[hep-ph/9903448](#)].
- [36] Z. Chacko, M.A. Luty, I. Maksymyk and E. Ponton, *Realistic anomaly-mediated supersymmetry breaking*, *JHEP* **04** (2000) 001 [[hep-ph/9905390](#)].
- [37] E. Katz, Y. Shadmi and Y. Shirman, *Heavy thresholds, slepton masses and the  $\mu$  term in anomaly mediated supersymmetry breaking*, *JHEP* **08** (1999) 015 [[hep-ph/9906296](#)].
- [38] I. Jack, D.R.T. Jones and R. Wild, *Fayet-Iliopoulos D-terms, neutrino masses and anomaly mediated supersymmetry breaking*, *Phys. Lett.* **B 535** (2002) 193 [[hep-ph/0202101](#)].



- [39] B.C. Allanach, *SOFTSUSY: a C++ program for calculating supersymmetric spectra*, *Comput. Phys. Commun.* **143** (2002) 305 [[hep-ph/0104145](#)].
- [40] S. Heinemeyer, W. Hollik and G. Weiglein, *Electroweak precision observables in the minimal supersymmetric standard model*, *Phys. Rept.* **425** (2006) 265 [[hep-ph/0412214](#)].
- [41] S. Heinemeyer, W. Hollik, A.M. Weber and G. Weiglein, *Z pole observables in the MSSM*, *JHEP* **04** (2008) 039 [[arXiv:0710.2972](#)].
- [42] TEVATRON ELECTROWEAK WORKING GROUP collaboration, E. Brubaker et al., *Combination of CDF and D0 results on the mass of the top quark*, [hep-ex/0608032](#); TEVATRON ELECTROWEAK WORKING GROUP collaboration, *Top subgroup homepage*, <http://tevewwg.fnal.gov/top/>.
- [43] CDF collaboration, *A combination of CDF and D0 results on the mass of the top quark*, [arXiv:0803.1683](#); TEVATRON ELECTROWEAK WORKING GROUP collaboration, *Top subgroup homepage*, <http://tevewwg.fnal.gov/top/>.
- [44] A. Sirlin, *Radiative corrections in the  $SU(2)_L \times U(1)$  theory: a simple renormalization framework*, *Phys. Rev.* **D 22** (1980) 971; W.J. Marciano and A. Sirlin, *Radiative corrections to neutrino induced neutral current phenomena in the  $SU(2)_L \times U(1)$  theory*, *Phys. Rev.* **D 22** (1980) 2695 [*Erratum ibid.* **D 31** (1985) 213].
- [45] P.H. Chankowski et al.,  *$\Delta R$  in the MSSM*, *Nucl. Phys.* **B 417** (1994) 101.
- [46] D. Garcia and J. Solà, *Full one loop supersymmetric quantum effects on  $M_W$* , *Mod. Phys. Lett.* **A 9** (1994) 211.
- [47] A. Djouadi and C. Verzegnassi, *Virtual very heavy top effects in LEP/SLC precision measurements*, *Phys. Lett.* **B 195** (1987) 265; A. Djouadi,  *$O(\alpha_s)$  vacuum polarization functions of the standard model gauge bosons*, *Nuovo Cim.* **A100** (1988) 357.
- [48] B. Kniehl, *Two-loop corrections to the vacuum polarizations in perturbative QCD*, *Nucl. Phys.* **B 347** (1990) 86; F. Halzen and B.A. Kniehl,  *$\Delta r$  beyond one loop*, *Nucl. Phys.* **B 353** (1991) 567; B.A. Kniehl and A. Sirlin, *Dispersion relations for vacuum polarization functions in electroweak physics*, *Nucl. Phys.* **B 371** (1992) 141; *On the effect of the  $t\bar{t}$  threshold on electroweak parameters*, *Phys. Rev.* **D 47** (1993) 883.
- [49] K.G. Chetyrkin, J.H. Kühn and M. Steinhauser, *QCD corrections from top quark to relations between electroweak parameters to order  $\alpha_s^2$* , *Phys. Rev. Lett.* **75** (1995) 3394 [[hep-ph/9504413](#)]; L. Avdeev, J. Fleischer, S. Mikhailov and O. Tarasov,  *$O(\alpha_s^2)$  correction to the electroweak  $\rho$  parameter*, *Phys. Lett.* **B 336** (1994) 560 [*Erratum ibid.* **B 349** (1995) 597] [[hep-ph/9406363](#)].
- [50] K.G. Chetyrkin, J.H. Kühn and M. Steinhauser, *Three-loop polarization function and  $O(\alpha_s^2)$  corrections to the production of heavy quarks*, *Nucl. Phys.* **B 482** (1996) 213 [[hep-ph/9606230](#)].

- [51] A. Djouadi et al., *Supersymmetric contributions to electroweak precision observables: QCD corrections*, *Phys. Rev. Lett.* **78** (1997) 3626 [[hep-ph/9612363](#)]; *Leading QCD corrections to scalar quark contributions to electroweak precision observables*, *Phys. Rev. D* **57** (1998) 4179 [[hep-ph/9710438](#)].
- [52] S. Heinemeyer and G. Weiglein, *Leading electroweak two loop corrections to precision observables in the MSSM*, *JHEP* **10** (2002) 072 [[hep-ph/0209305](#)]; *Precision observables in the MSSM: status and perspectives*, [hep-ph/0301062](#).
- [53] J. Haestier, S. Heinemeyer, D. Stöckinger and G. Weiglein, *Electroweak precision observables: two-loop Yukawa corrections of supersymmetric particles*, *JHEP* **12** (2005) 027 [[hep-ph/0508139](#)]; *Two-loop contributions to electroweak precision observables in the MSSM*, [hep-ph/0506259](#).
- [54] M.J.G. Veltman, *Limit on mass differences in the Weinberg model*, *Nucl. Phys. B* **123** (1977) 89.
- [55] S. Heinemeyer, W. Hollik, D. Stöckinger, A.M. Weber and G. Weiglein, *Precise prediction for  $M_W$  in the MSSM*, *JHEP* **08** (2006) 052 [[hep-ph/0604147](#)]; *Testing the MSSM with the mass of the  $W$  boson*, *Pramana* **69** (2007) 783 [[hep-ph/0611371](#)].
- [56] A.H. Hoang et al., *Top-antitop pair production close to threshold: synopsis of recent NNLO results*, *Eur. Phys. J. Direct.* **C 2** (2000) 1 [[hep-ph/0001286](#)].
- [57] M. Martinez and R. Miquel, *Multi-parameter fits to the  $t\bar{t}$  threshold observables at a future  $e^+e^-$  linear collider*, *Eur. Phys. J. C* **27** (2003) 49 [[hep-ph/0207315](#)].
- [58] F. Jegerlehner, *Introduction to problems of very precise cross-sections at DAFNE energies*, talk presented at the *LNFSpring School*, Frascati Italy April 12–17 1999, see <http://www-com.physik.hu-berlin.de/~fjeger/Frascati99.ps.gz>; *The effective fine structure constant at TESLA energies*, [hep-ph/0105283](#).
- [59] S. Heinemeyer, S. Kraml, W. Porod and G. Weiglein, *Physics impact of a precise determination of the top quark mass at an  $e^+e^-$  linear collider*, *JHEP* **09** (2003) 075 [[hep-ph/0306181](#)].
- [60] ALEPH, DELPHI, L3, OPAL, SLD collaborations, the LEP Electroweak Working Group, the SLD Electroweak and Heavy Flavour Groups, *Precision electroweak measurements on the  $Z$  resonance*, *Phys. Rept.* **427** (2006) 257 [[hep-ex/0509008](#)]; LEP collaborations: ALEPH, DELPHI, L3, OPAL, the LEP Electroweak Working Group *A combination of preliminary electroweak measurements and constraints on the standard model*, [hep-ex/0612034](#).
- [61] LEP ELECTROWEAK WORKING GROUP collaboration, *The LEP electroweak working group homepage*, <http://lepewwg.web.cern.ch/LEPEWWG/Welcome.html>.
- [62] TEVATRON ELECTROWEAK WORKING GROUP collaboration, *Tevatron Electroweak Working Group TEV-EWWG homepage*, <http://tevewwg.fnal.gov>.
- [63] CDF collaboration, T. Aaltonen et al., *First measurement of the  $W$  boson mass in run II of the Tevatron*, *Phys. Rev. Lett.* **99** (2007) 151801 [[arXiv:0707.0085](#)]; *CDF run 2 electroweak public results*, <http://www-cdf.fnal.gov/physics/ewk/>.
- [64] M. Grünewald, private communication.

- [65] S. Brensing, S. Dittmaier, M. Krämer and A. Muck, *Radiative corrections to W-boson hadroproduction: higher-order electroweak and supersymmetric effects*, *Phys. Rev. D* **77** (2008) 073006 [[arXiv:0710.3309](#)].
- [66] G. Wilson, *Precision measurement of the w mass with a polarized threshold scan at a linear collider*, LC-PHSM-2001-009, see <http://www.desy.de/~lcnotes/>.
- [67] U. Baur et al., *Theoretical and experimental status of the indirect Higgs boson mass determination in the standard model*, *eConf C010630* (2001) P122 [[hep-ph/0111314](#)].
- [68] M. Awramik, M. Czakon, A. Freitas and G. Weiglein, *Complete two-loop electroweak fermionic corrections to  $\sin^2(\theta_{\text{eff}}^{\text{lept}})$  and indirect determination of the Higgs boson mass*, *Phys. Rev. Lett.* **93** (2004) 201805 [[hep-ph/0407317](#)].
- [69] R. Hawkings and K. Mönig, *Electroweak and CP-violation physics at a linear collider Z-factory*, *Eur. Phys. J. Direct.* **C 1** (1999) 8 [[hep-ex/9910022](#)].
- [70] J. Erler, S. Heinemeyer, W. Hollik, G. Weiglein and P.M. Zerwas, *Physics impact of GigaZ*, *Phys. Lett. B* **486** (2000) 125 [[hep-ph/0005024](#)].
- [71] A. Czarnecki and W.J. Marciano, *The muon anomalous magnetic moment: a harbinger for 'new physics'*, *Phys. Rev. D* **64** (2001) 013014 [[hep-ph/0102122](#)].
- [72] M. Knecht, *The anomalous magnetic moment of the muon: a theoretical introduction*, *Lect. Notes Phys.* **629** (2004) 37 [[hep-ph/0307239](#)];  
M. Passera, *Status of the standard model prediction of the muon g-2*, *Nucl. Phys.* **155** (Proc. Suppl.) (2006) 365 [[hep-ph/0509372](#)].
- [73] D. Stöckinger, *The muon magnetic moment and supersymmetry*, *J. Phys. G* **34** (2007) R45 [[hep-ph/0609168](#)].
- [74] J.P. Miller, E. de Rafael and B.L. Roberts, *Muon g-2: review of theory and experiment*, *Rept. Prog. Phys.* **70** (2007) 795 [[hep-ph/0703049](#)].
- [75] F. Jegerlehner, *Essentials of the muon g-2*, *Acta Phys. Polon.* **B38** (2007) 3021 [[hep-ph/0703125](#)].
- [76] M. Passera, W.J. Marciano and A. Sirlin, *The muon g-2 and the bounds on the Higgs boson mass*, *Phys. Rev. D* **78** (2008) 013009 [[arXiv:0804.1142](#)].
- [77] T. Kinoshita and M. Nio, *Improved  $\alpha^4$  term of the muon anomalous magnetic moment*, *Phys. Rev. D* **70** (2004) 113001 [[hep-ph/0402206](#)]; *The tenth-order QED contribution to the lepton g-2: evaluation of dominant  $\alpha^5$  terms of muon g-2*, *Phys. Rev. D* **73** (2006) 053007 [[hep-ph/0512330](#)].
- [78] M. Passera, *Precise mass-dependent QED contributions to leptonic g-2 at order  $\alpha^2$  and  $\alpha^3$* , *Phys. Rev. D* **75** (2007) 013002 [[hep-ph/0606174](#)].
- [79] T. Aoyama, M. Hayakawa, T. Kinoshita and M. Nio, *Revised value of the eighth-order electron g-2*, *Phys. Rev. Lett.* **99** (2007) 110406 [[arXiv:0706.3496](#)]; *Automated calculation scheme for  $\alpha^n$  contributions of QED to lepton g-2: new treatment of infrared divergence for diagrams without lepton loops*, *Nucl. Phys. B* **796** (2008) 184 [[arXiv:0709.1568](#)]; *Revised value of the eighth-order QED contribution to the anomalous magnetic moment of the electron*, *Phys. Rev. D* **77** (2008) 053012 [[arXiv:0712.2607](#)].

- [80] M. Davier, S. Eidelman, A. Höcker and Z. Zhang, *Updated estimate of the muon magnetic moment using revised results from  $e^+e^-$  annihilation*, *Eur. Phys. J. C* **31** (2003) 503 [[hep-ph/0308213](#)].
- [81] K. Hagiwara, A.D. Martin, D. Nomura and T. Teubner, *Predictions for  $g-2$  of the muon and  $\alpha_{\text{QED}}(M_Z^2)$* , *Phys. Rev. D* **69** (2004) 093003 [[hep-ph/0312250](#)].
- [82] K. Hagiwara, A. Martin, D. Nomura and T. Teubner, *Improved predictions for  $g-2$  of the muon and  $\alpha_{\text{QED}}(M_Z^2)$* , *Phys. Lett. B* **649** (2007) 173 [[hep-ph/0611102](#)].
- [83] S. Ghozzi and F. Jegerlehner, *Isospin violating effects in  $e^+e^-$  vs.  $\tau$  measurements of the pion form factor  $|F_\pi|^2(s)$* , *Phys. Lett. B* **583** (2004) 222 [[hep-ph/0310181](#)].
- [84] J.F. de Troconiz and F.J. Yndurain, *The hadronic contributions to the anomalous magnetic moment of the muon*, *Phys. Rev. D* **71** (2005) 073008 [[hep-ph/0402285](#)].
- [85] M. Davier, *The hadronic contribution to  $(g-2)_\mu$* , *Nucl. Phys.* **169** (Proc. Suppl.) (2007) 288 [[hep-ph/0701163](#)].
- [86] J. Bijnens and J. Prades, *The hadronic light-by-light contribution to the muon anomalous magnetic moment: where do we stand?*, *Mod. Phys. Lett. A* **22** (2007) 767 [[hep-ph/0702170](#)].
- [87] M. Knecht and A. Nyffeler, *Hadronic light-by-light corrections to the muon  $g-2$ : the pion-pole contribution*, *Phys. Rev. D* **65** (2002) 073034 [[hep-ph/0111058](#)];  
M. Knecht, A. Nyffeler, M. Perrottet and E. De Rafael, *Hadronic light-by-light scattering contribution to the muon  $g-2$ : an effective field theory approach*, *Phys. Rev. Lett.* **88** (2002) 071802 [[hep-ph/0111059](#)];  
I.R. Blokland, A. Czarnecki and K. Melnikov, *Pion pole contribution to hadronic light-by-light scattering and muon anomalous magnetic moment*, *Phys. Rev. Lett.* **88** (2002) 071803 [[hep-ph/0112117](#)];  
M. Ramsey-Musolf and M.B. Wise, *Hadronic light-by-light contribution to muon  $g-2$  in chiral perturbation theory*, *Phys. Rev. Lett.* **89** (2002) 041601 [[hep-ph/0201297](#)];  
J. Kühn, A. Onishchenko, A. Pivovarov and O. Veretin, *Heavy mass expansion, light by light scattering and the anomalous magnetic moment of the muon*, *Phys. Rev. D* **68** (2003) 033018 [[hep-ph/0301151](#)].
- [88] K. Melnikov and A. Vainshtein, *Hadronic light-by-light scattering contribution to the muon anomalous magnetic moment revisited*, *Phys. Rev. D* **70** (2004) 113006 [[hep-ph/0312226](#)].
- [89] M. Davier and W. Marciano, *The theoretical prediction for the muon anomalous magnetic moment*, *Ann. Rev. Nucl. Part. Sci.* **54** (2004) 115.
- [90] BELLE collaboration, H. Hayashii, *Tau lepton physics at Belle*, PoS(HEP2005)291.
- [91] M. Benayoun, P. David, L. DelBuono, O. Leitner and H.B. O'Connell, *The dipion mass spectrum in  $e^+e^-$  annihilation and  $\tau$  decay: a dynamical  $(\rho, \omega, \phi)$  mixing approach*, *Eur. Phys. J. C* **55** (2008) 199 [[arXiv:0711.4482](#)].
- [92] KLOE collaboration, A. Aloisio et al., *Measurement of  $\sigma(e^+e^- \rightarrow \pi^+\pi^-\gamma)$  and extraction of  $\sigma(e^+e^- \rightarrow \pi^+\pi^-)$  below 1 GeV with the KLOE detector*, *Phys. Lett. B* **606** (2005) 12 [[hep-ex/0407048](#)];  
KLOE collaboration, D. Leone, *Measuring the pion form factor via radiative return at large photon angles with KLOE*, *Nucl. Phys.* **162** (Proc. Suppl.) (2006) 95.

- [93] CMD-2 collaboration, R.R. Akhmetshin et al., *Reanalysis of hadronic cross section measurements at CMD-2*, *Phys. Lett.* **B 578** (2004) 285 [[hep-ex/0308008](#)]; *High-statistics measurement of the pion form factor in the rho-meson energy range with the CMD-2 detector*, *Phys. Lett.* **B 648** (2007) 28 [[hep-ex/0610021](#)].
- [94] SND collaboration, M.N. Achasov et al., *Study of the process  $e^+e^- \rightarrow \pi^+\pi^-$  in the energy region  $400 \text{ MeV} < \sqrt{s} < 1000 \text{ MeV}$* , *J. Exp. Theor. Phys.* **101** (2005) 1053 [*Zh. Eksp. Teor. Fiz.* **101** (2005) 1201] [[hep-ex/0506076](#)].
- [95] S. Müller, *Measurements of radiative processes at KLOE*, talk given at the *Europhysics Conference on High Energy Physics EPS07*, Manchester U.K. July 19–25 2007, see <http://agenda.hep.man.ac.uk/contributionDisplay.py?contribId=36&sessionId=26&confId=70>.
- [96] MUON G-2 collaboration, G.W. Bennett et al., *Measurement of the negative muon anomalous magnetic moment to 0.7 ppm*, *Phys. Rev. Lett.* **92** (2004) 161802 [[hep-ex/0401008](#)].
- [97] MUON G-2 collaboration, G.W. Bennett et al., *Final report of the muon E821 anomalous magnetic moment measurement at BNL*, *Phys. Rev.* **D 73** (2006) 072003 [[hep-ex/0602035](#)].
- [98] S. Eidelman, *Current status of muon  $g-2$* , talk given at the *ICHEP06*, Moscow Russia July 26 – August 2 2006, see [http://ic hep06.jinr.ru/reports/333\\_6s1\\_9p30\\_Eidelman.pdf](http://ic hep06.jinr.ru/reports/333_6s1_9p30_Eidelman.pdf); V. Druzhinin, *Study of  $e^+e^-$  annihilation at low energies*, talk given at *Lepton Photon 07*, Daegu Korea August 13–18 2007, see <http://chep.knu.ac.kr/lp07/htm/S5/S05-15.pdf>.
- [99] T. Moroi, *The muon anomalous magnetic dipole moment in the minimal supersymmetric standard model*, *Phys. Rev.* **D 53** (1996) 6565 [*Erratum ibid.* **56** (1997) 4424] [[hep-ph/9512396](#)].
- [100] J.L. Lopez, D.V. Nanopoulos and X. Wang, *Large  $(g-2)_\mu$  in  $SU(5) \times U(1)$  supergravity models*, *Phys. Rev.* **D 49** (1994) 366 [[hep-ph/9308336](#)]; U. Chattopadhyay and P. Nath, *Probing supergravity grand unification in the Brookhaven  $g-2$  experiment*, *Phys. Rev.* **D 53** (1996) 1648 [[hep-ph/9507386](#)].
- [101] G. Degrossi and G.F. Giudice, *QED logarithms in the electroweak corrections to the muon anomalous magnetic moment*, *Phys. Rev.* **D 58** (1998) 053007 [[hep-ph/9803384](#)].
- [102] S. Heinemeyer, D. Stöckinger and G. Weiglein, *Two-loop SUSY corrections to the anomalous magnetic moment of the muon*, *Nucl. Phys.* **B 690** (2004) 62 [[hep-ph/0312264](#)].
- [103] S. Heinemeyer, D. Stöckinger and G. Weiglein, *Electroweak and supersymmetric two-loop corrections to  $(g-2)_\mu$* , *Nucl. Phys.* **B 699** (2004) 103 [[hep-ph/0405255](#)].
- [104] A. Dabelstein, *Fermionic decays of neutral MSSM Higgs bosons at the one loop level*, *Nucl. Phys.* **B 456** (1995) 25 [[hep-ph/9503443](#)]; *The one loop renormalization of the MSSM Higgs sector and its application to the neutral scalar Higgs masses*, *Z. Physik* **C 67** (1995) 495 [[hep-ph/9409375](#)].
- [105] S. Heinemeyer, W. Hollik and G. Weiglein, *QCD corrections to the masses of the neutral CP-even Higgs bosons in the MSSM*, *Phys. Rev.* **D 58** (1998) 091701 [[hep-ph/9803277](#)]; *Precise prediction for the mass of the lightest Higgs boson in the MSSM*, *Phys. Lett.* **B 440** (1998) 296 [[hep-ph/9807423](#)].
- [106] S. Heinemeyer, W. Hollik and G. Weiglein, *FeynHiggs: a program for the calculation of the masses of the neutral CP-even Higgs bosons in the MSSM*, *Comput. Phys. Commun.* **124** (2000) 76 [[hep-ph/9812320](#)], the code is accessible via <http://www.feynhiggs.de>.

- [107] S. Heinemeyer, W. Hollik and G. Weiglein, *The masses of the neutral CP-even Higgs bosons in the MSSM: accurate analysis at the two-loop level*, *Eur. Phys. J. C* **9** (1999) 343 [[hep-ph/9812472](#)].
- [108] G. Degrandi, S. Heinemeyer, W. Hollik, P. Slavich and G. Weiglein, *Towards high-precision predictions for the MSSM Higgs sector*, *Eur. Phys. J. C* **28** (2003) 133 [[hep-ph/0212020](#)].
- [109] M. Frank et al., *The Higgs boson masses and mixings of the complex MSSM in the Feynman-diagrammatic approach*, *JHEP* **02** (2007) 047 [[hep-ph/0611326](#)].
- [110] Y. Okada, M. Yamaguchi and T. Yanagida, *Upper bound of the lightest Higgs boson mass in the minimal supersymmetric standard model*, *Prog. Theor. Phys.* **85** (1991) 1;  
 J.R. Ellis, G. Ridolfi and F. Zwirner, *Radiative corrections to the masses of supersymmetric Higgs bosons*, *Phys. Lett. B* **257** (1991) 83;  
 H.E. Haber and R. Hempfling, *Can the mass of the lightest Higgs boson of the minimal supersymmetric model be larger than  $m_Z$ ?*, *Phys. Rev. Lett.* **66** (1991) 1815.
- [111] P.H. Chankowski, S. Pokorski and J. Rosiek, *One loop corrections to the supersymmetric Higgs boson couplings and LEP phenomenology*, *Phys. Lett. B* **286** (1992) 307; *Complete on-shell renormalization scheme for the minimal supersymmetric Higgs sector*, *Nucl. Phys. B* **423** (1994) 437 [[hep-ph/9303309](#)].
- [112] M.S. Carena, D. Garcia, U. Nierste and C.E.M. Wagner, *Effective Lagrangian for the  $\bar{t}bH$  interaction in the MSSM and charged Higgs phenomenology*, *Nucl. Phys. B* **577** (2000) 88 [[hep-ph/9912516](#)];  
 H. Eberl, K. Hidaka, S. Kraml, W. Majerotto and Y. Yamada, *Improved SUSY QCD corrections to Higgs boson decays into quarks and squarks*, *Phys. Rev. D* **62** (2000) 055006 [[hep-ph/9912463](#)].
- [113] T. Banks, *Supersymmetry and the quark mass matrix*, *Nucl. Phys. B* **303** (1988) 172;  
 L.J. Hall, R. Rattazzi and U. Sarid, *The top quark mass in supersymmetric SO(10) unification*, *Phys. Rev. D* **50** (1994) 7048 [[hep-ph/9306309](#)];  
 R. Hempfling, *Yukawa coupling unification with supersymmetric threshold corrections*, *Phys. Rev. D* **49** (1994) 6168;  
 M.S. Carena, M. Olechowski, S. Pokorski and C.E.M. Wagner, *Electroweak symmetry breaking and bottom-top Yukawa unification*, *Nucl. Phys. B* **426** (1994) 269 [[hep-ph/9402253](#)].
- [114] A. Dedes, G. Degrandi and P. Slavich, *On the two-loop Yukawa corrections to the MSSM Higgs boson masses at large  $\tan\beta$* , *Nucl. Phys. B* **672** (2003) 144 [[hep-ph/0305127](#)].
- [115] S.P. Martin, *Two-loop effective potential for a general renormalizable theory and softly broken supersymmetry*, *Phys. Rev. D* **65** (2002) 116003 [[hep-ph/0111209](#)]; *Two-loop effective potential for the minimal supersymmetric standard model*, *Phys. Rev. D* **66** (2002) 096001 [[hep-ph/0206136](#)]; *Complete two-loop effective potential approximation to the lightest Higgs scalar boson mass in supersymmetry*, *Phys. Rev. D* **67** (2003) 095012 [[hep-ph/0211366](#)]; *Evaluation of two-loop self-energy basis integrals using differential equations*, *Phys. Rev. D* **68** (2003) 075002 [[hep-ph/0307101](#)]; *Two-loop scalar self-energies in a general renormalizable theory at leading order in gauge couplings*, *Phys. Rev. D* **70** (2004) 016005 [[hep-ph/0312092](#)]; *Strong and Yukawa two-loop contributions to Higgs scalar boson self-energies and pole masses in supersymmetry*, *Phys. Rev. D* **71** (2005) 016012 [[hep-ph/0405022](#)]; *Two-loop scalar self-energies and pole masses in a general renormalizable theory with massless gauge bosons*, *Phys. Rev. D* **71** (2005) 116004 [[hep-ph/0502168](#)];

- S.P. Martin and D.G. Robertson, *TSIL: a program for the calculation of two-loop self-energy integrals*, *Comput. Phys. Commun.* **174** (2006) 133 [[hep-ph/0501132](#)].
- [116] S.P. Martin, *Three-loop corrections to the lightest Higgs scalar boson mass in supersymmetry*, *Phys. Rev. D* **75** (2007) 055005 [[hep-ph/0701051](#)].
- [117] R.V. Harlander, P. Kant, L. Mihaila and M. Steinhauser, *Higgs boson mass in supersymmetry to three loops*, *Phys. Rev. Lett.* **100** (2008) 191602 [[arXiv:0803.0672](#)].
- [118] S. Heinemeyer, W. Hollik, H. Rzehak and G. Weiglein, *High-precision predictions for the MSSM Higgs sector at  $O(\alpha_b\alpha_s)$* , *Eur. Phys. J. C* **39** (2005) 465 [[hep-ph/0411114](#)]; *The MSSM Higgs sector at  $O(\alpha_b\alpha_s)$  and beyond*, [hep-ph/0506254](#).
- [119] B.C. Allanach, A. Djouadi, J.L. Kneur, W. Porod and P. Slavich, *Precise determination of the neutral Higgs boson masses in the MSSM*, *JHEP* **09** (2004) 044 [[hep-ph/0406166](#)].
- [120] S. Heinemeyer, W. Hollik and G. Weiglein, *Constraints on  $\tan\beta$  in the MSSM from the upper bound on the mass of the lightest Higgs boson*, *JHEP* **06** (2000) 009 [[hep-ph/9909540](#)].
- [121] LEP WORKING GROUP FOR HIGGS BOSON SEARCHES collaboration, S. Schael et al., *Search for neutral MSSM Higgs bosons at LEP*, *Eur. Phys. J. C* **47** (2006) 547 [[hep-ex/0602042](#)].
- [122] LEP WORKING GROUP FOR HIGGS BOSON SEARCHES collaboration, R. Barate et al., *Search for the standard model Higgs boson at LEP*, *Phys. Lett. B* **565** (2003) 61 [[hep-ex/0306033](#)].
- [123] S. Ambrosanio, A. Dedes, S. Heinemeyer, S. Su and G. Weiglein, *Implications of the Higgs boson searches on different soft SUSY-breaking scenarios*, *Nucl. Phys. B* **624** (2002) 3 [[hep-ph/0106255](#)].
- [124] J.R. Ellis, S. Heinemeyer, K.A. Olive and G. Weiglein, *Observability of the lightest CMSSM Higgs boson at hadron colliders*, *Phys. Lett. B* **515** (2001) 348 [[hep-ph/0105061](#)].
- [125] ECFA/DESY LC PHYSICS WORKING GROUP collaboration, J.A. Aguilar-Saavedra et al., *TESLA technical design report part III: physics at an  $e^+e^-$  linear collider*, [hep-ph/0106315](#).
- [126] AMERICAN LINEAR COLLIDER WORKING GROUP collaboration, T. Abe et al., *Linear collider physics resource book for Snowmass 2001. 1: introduction*, [hep-ex/0106055](#).
- [127] ACFA LINEAR COLLIDER WORKING GROUP collaboration, K. Abe et al., *Particle physics experiments at JLC*, [hep-ph/0109166](#).
- [128] S. Heinemeyer et al., *Toward high precision Higgs-boson measurements at the international linear  $e^+e^-$  collider*, *eConf C0508141* (2005) ALCPG0214 [[hep-ph/0511332](#)].
- [129] M. Misiak et al., *The first estimate of  $B(\bar{B} \rightarrow X_s\gamma)$  at  $O(\alpha_s^2)$* , *Phys. Rev. Lett.* **98** (2007) 022002 [[hep-ph/0609232](#)].
- [130] T. Hurth, E. Lunghi and W. Porod, *Untagged  $B \rightarrow X_{s+d}\gamma$  CP asymmetry as a probe for new physics*, *Nucl. Phys. B* **704** (2005) 56 [[hep-ph/0312260](#)].
- [131] M. Neubert, *Renormalization-group improved calculation of the  $B \rightarrow X_s + \gamma$  branching ratio*, *Eur. Phys. J. C* **40** (2005) 165 [[hep-ph/0408179](#)].
- [132] ALEPH collaboration, R. Barate et al., *A measurement of the inclusive  $b \rightarrow s\gamma$  branching ratio*, *Phys. Lett. B* **429** (1998) 169;  
CLEO collaboration, S. Chen et al., *Branching fraction and photon energy spectrum for  $b \rightarrow s\gamma$* , *Phys. Rev. Lett.* **87** (2001) 251807 [[hep-ex/0108032](#)];

- BELLE collaboration, P. Koppenburg et al., *An inclusive measurement of the photon energy spectrum in  $b \rightarrow s\gamma$  decays*, *Phys. Rev. Lett.* **93** (2004) 061803 [[hep-ex/0403004](#)];
- BELLE collaboration, K. Abe et al., *A measurement of the branching fraction for the inclusive  $B \rightarrow X_s\gamma$  decays with Belle*, *Phys. Lett.* **B 511** (2001) 151 [[hep-ex/0103042](#)];
- BABAR collaboration, B. Aubert et al.,  *$b \rightarrow s\gamma$  using a sum of exclusive modes*, [hep-ex/0207074](#); *Determination of the branching fraction for inclusive decays  $B \rightarrow X_s\gamma$* , [hep-ex/0207076](#).
- [133] P.L. Cho, M. Misiak and D. Wyler,  *$K_L \rightarrow \pi^0 e^+ e^-$  and  $B \rightarrow X_s \ell^+ \ell^-$  decay in the MSSM*, *Phys. Rev.* **D 54** (1996) 3329 [[hep-ph/9601360](#)];
- A.L. Kagan and M. Neubert, *QCD anatomy of  $B \rightarrow X_s\gamma$  decays*, *Eur. Phys. J.* **C 7** (1999) 5 [[hep-ph/9805303](#)];
- A. Ali, E. Lunghi, C. Greub and G. Hiller, *Improved model-independent analysis of semileptonic and radiative rare B decays*, *Phys. Rev.* **D 66** (2002) 034002 [[hep-ph/0112300](#)];
- G. Hiller and F. Krüger, *More model-independent analysis of  $b \rightarrow s$  processes*, *Phys. Rev.* **D 69** (2004) 074020 [[hep-ph/0310219](#)];
- M.S. Carena, D. Garcia, U. Nierste and C.E.M. Wagner,  *$b \rightarrow s\gamma$  and supersymmetry with large  $\tan\beta$* , *Phys. Lett.* **B 499** (2001) 141 [[hep-ph/0010003](#)];
- D.A. Demir and K.A. Olive,  *$B \rightarrow X_s\gamma$  in supersymmetry with explicit CP-violation*, *Phys. Rev.* **D 65** (2002) 034007 [[hep-ph/0107329](#)];
- T. Hurth, *Present status of inclusive rare B decays*, *Rev. Mod. Phys.* **75** (2003) 1159 [[hep-ph/0212304](#)].
- [134] K. Adel and Y.-P. Yao, *Exact  $\alpha_s$  calculation of  $b \rightarrow s + \gamma$   $b \rightarrow s + g$* , *Phys. Rev.* **D 49** (1994) 4945 [[hep-ph/9308349](#)];
- C. Greub, T. Hurth and D. Wyler, *Virtual corrections to the decay  $b \rightarrow s\gamma$* , *Phys. Lett.* **B 380** (1996) 385 [[hep-ph/9602281](#)]; *Virtual  $O(\alpha_s)$  corrections to the inclusive decay  $b \rightarrow s\gamma$* , *Phys. Rev.* **D 54** (1996) 3350 [[hep-ph/9603404](#)];
- A. Ali, *Review of heavy quark physics-theory*, talk given at ICHEP04, Beijing China August 16–22 2004, appeared in the proceedings, see <http://ichep04.ihep.ac.cn/db/paper.php>.
- [135] K.G. Chetyrkin, M. Misiak and M. Münz, *Weak radiative B-meson decay beyond leading logarithms*, *Phys. Lett.* **B 400** (1997) 206 [*Erratum ibid.* **B 425** (1998) 414] [[hep-ph/9612313](#)].
- [136] G. Bélanger, F. Boudjema, A. Pukhov and A. Semenov, *MicrOMEGAs: a program for calculating the relic density in the MSSM*, *Comput. Phys. Commun.* **149** (2002) 103 [[hep-ph/0112278](#)]; *MicrOMEGAs: version 1.3*, *Comput. Phys. Commun.* **174** (2006) 577 [[hep-ph/0405253](#)].
- [137] G. Degrandi, P. Gambino and G.F. Giudice,  *$B \rightarrow X_s\gamma$  in supersymmetry: large contributions beyond the leading order*, *JHEP* **12** (2000) 009 [[hep-ph/0009337](#)].
- [138] P. Gambino and M. Misiak, *Quark mass effects in  $\bar{B} \rightarrow X_s\gamma$* , *Nucl. Phys.* **B 611** (2001) 338 [[hep-ph/0104034](#)].
- [139] G. Buchalla and A.J. Buras, *QCD corrections to rare K and B decays for arbitrary top quark mass*, *Nucl. Phys.* **B 400** (1993) 225;
- M. Misiak and J. Urban, *QCD corrections to FCNC decays mediated by Z-penguins and W-boxes*, *Phys. Lett.* **B 451** (1999) 161 [[hep-ph/9901278](#)];
- G. Buchalla and A.J. Buras, *The rare decays  $K \rightarrow \pi\nu\bar{\nu}$ ,  $B \rightarrow X\nu\bar{\nu}$  and  $B \rightarrow \ell^+\ell^-$ : an update*, *Nucl. Phys.* **B 548** (1999) 309 [[hep-ph/9901288](#)];



- A.J. Buras, *Relations between  $\Delta(M_{s,d})$  and  $B_{s,d} \rightarrow \mu\bar{\mu}$  in models with minimal flavour violation*, *Phys. Lett.* **B 566** (2003) 115 [[hep-ph/0303060](#)].
- [140] CDF collaboration, T. Aaltonen et al., *Search for  $B_s \rightarrow \mu^+\mu^-$  and  $B_d \rightarrow \mu^+\mu^-$  decays with  $2fb^{-1}$  of  $p\bar{p}$  collisions*, *Phys. Rev. Lett.* **100** (2008) 101802 [[arXiv:0712.1708](#)];  
K. Tollefson, *Striking results from the Tevatron*, talk given at *Lepton photon 07*, Daegu Korea August 13–18 2007, see [http://chep.knu.ac.kr/lp07/htm/S4/S04\\_14.pdf](http://chep.knu.ac.kr/lp07/htm/S4/S04_14.pdf).
- [141] CDF collaboration, *Tevatron run II physics projections*, <http://www-cdf.fnal.gov/physics/projections/>.
- [142] P. Ball et al., *B decays at the LHC*, [hep-ph/0003238](#).
- [143] K.S. Babu and C.F. Kolda, *Higgs-mediated  $B^0 \rightarrow \mu^+\mu^-$  in minimal supersymmetry*, *Phys. Rev. Lett.* **84** (2000) 228 [[hep-ph/9909476](#)];  
S.R. Choudhury and N. Gaur, *Dileptonic decay of  $B_s$  meson in SUSY models with large  $\tan\beta$* , *Phys. Lett.* **B 451** (1999) 86 [[hep-ph/9810307](#)];  
C. Bobeth, T. Ewerth, F. Krüger and J. Urban, *Analysis of neutral Higgs-boson contributions to the decays  $\bar{B}_s \rightarrow \ell^+\ell^-$  and  $\bar{B} \rightarrow K\ell^+\ell^-$* , *Phys. Rev.* **D 64** (2001) 074014 [[hep-ph/0104284](#)];  
A. Dedes, H.K. Dreiner and U. Nierste, *Correlation of  $B_s \rightarrow \mu^+\mu^-$  and  $(g-2)_\mu$  in minimal supergravity*, *Phys. Rev. Lett.* **87** (2001) 251804 [[hep-ph/0108037](#)];  
G. Isidori and A. Retico, *Scalar flavour-changing neutral currents in the large- $\tan\beta$  limit*, *JHEP* **11** (2001) 001 [[hep-ph/0110121](#)];  
A. Dedes and A. Pilaftsis, *Resummed effective Lagrangian for Higgs-mediated FCNC interactions in the CP-violating MSSM*, *Phys. Rev.* **D 67** (2003) 015012 [[hep-ph/0209306](#)];  
A.J. Buras, P.H. Chankowski, J. Rosiek and L. Slawianowska,  *$\Delta(M_{d,s})$ ,  $B_{d,s}^0 \rightarrow \mu^+\mu^-$  and  $B \rightarrow X_s\gamma$  in supersymmetry at large  $\tan\beta$* , *Nucl. Phys.* **B 659** (2003) 3 [[hep-ph/0210145](#)];  
A. Dedes, *The Higgs penguin and its applications: an overview*, *Mod. Phys. Lett.* **A 18** (2003) 2627 [[hep-ph/0309233](#)].
- [144] J.R. Ellis, K.A. Olive and V.C. Spanos, *On the interpretation of  $B_s \rightarrow \mu^+\mu^-$  in the CMSSM*, *Phys. Lett.* **B 624** (2005) 47 [[hep-ph/0504196](#)].
- [145] ATLAS collaboration, *Detector and physics performance technical design report*, CERN-LHCC-99-15 (1999), see <http://atlasinfo.cern.ch/Atlas/GROUPS/PHYSICS/TDR/access.html>.
- [146] CMS collaboration, *Physics technical design report, volume 2*, CERN-LHCC-2006-021, see <http://cmsdoc.cern.ch/cms/cpt/tdr/>.
- [147] V. Büscher and K. Jakobs, *Higgs boson searches at hadron colliders*, *Int. J. Mod. Phys.* **A 20** (2005) 2523 [[hep-ph/0504099](#)].
- [148] M. Schumacher, *Investigation of the discovery potential for Higgs bosons of the minimal supersymmetric extension of the standard model (MSSM) with ATLAS*, *Czech. J. Phys.* **54** (2004) A103 [[hep-ph/0410112](#)].
- [149] S. Abdullin et al., *Summary of the CMS potential for the Higgs boson discovery*, *Eur. Phys. J.* **C 39S2** (2005) 41.
- [150] S. Gennai et al., *Search for heavy neutral MSSM Higgs bosons with CMS: reach and Higgs-mass precision*, *Eur. Phys. J.* **C 52** (2007) 383 [[arXiv:0704.0619](#)];  
M. Hashemi, S. Heinemeyer, R. Kinnunen, A. Nikitenko and G. Weiglein, *Charged Higgs bosons in the MSSM at CMS: discovery reach and parameter dependence*, [arXiv:0804.1228](#).

- [151] J.L. Feng, T. Moroi, L. Randall, M. Strassler and S.-F. Su, *Discovering supersymmetry at the Tevatron in Wino LSP scenarios*, *Phys. Rev. Lett.* **83** (1999) 1731 [[hep-ph/9904250](#)]; S. Asai, T. Moroi and T.T. Yanagida, *Test of anomaly mediation at the LHC*, *Phys. Lett. B* **664** (2008) 185 [[arXiv:0802.3725](#)].
- [152] F. Gianotti et al., *Physics potential and experimental challenges of the LHC luMINOSity upgrade*, *Eur. Phys. J. C* **39** (2005) 293 [[hep-ph/0204087](#)].
- [153] J.R. Ellis, K.A. Olive, Y. Santoso and V.C. Spanos, *Supersymmetric dark matter in light of WMAP*, *Phys. Lett. B* **565** (2003) 176 [[hep-ph/0303043](#)].
- [154] U. Chattopadhyay, A. Corsetti and P. Nath, *WMAP constraints, SUSY dark matter and implications for the direct detection of SUSY*, *Phys. Rev. D* **68** (2003) 035005 [[hep-ph/0303201](#)];  
H. Baer and C. Balázs,  *$\chi^2$  analysis of the minimal supergravity model including WMAP,  $g_\mu-2$  and  $b \rightarrow s\gamma$  constraints*, *JCAP* **05** (2003) 006 [[hep-ph/0303114](#)];  
A.B. Lahanas and D.V. Nanopoulos, *WMAPing out supersymmetric dark matter and phenomenology*, *Phys. Lett. B* **568** (2003) 55 [[hep-ph/0303130](#)];  
R.L. Arnowitt, B. Dutta and B. Hu, *Dark matter, muon  $g-2$  and other SUSY constraints*, [hep-ph/0310103](#).
- [155] K. Desch, E. Gross, S. Heinemeyer, G. Weiglein and L. Zivkovic, *LHC/LC interplay in the MSSM Higgs sector*, *JHEP* **09** (2004) 062 [[hep-ph/0406322](#)].